Hoist and boom wire dynamics during offshore heavy lifting

R. van der Valk

TUDelft
Delft
University of
Technology

Challenge the future
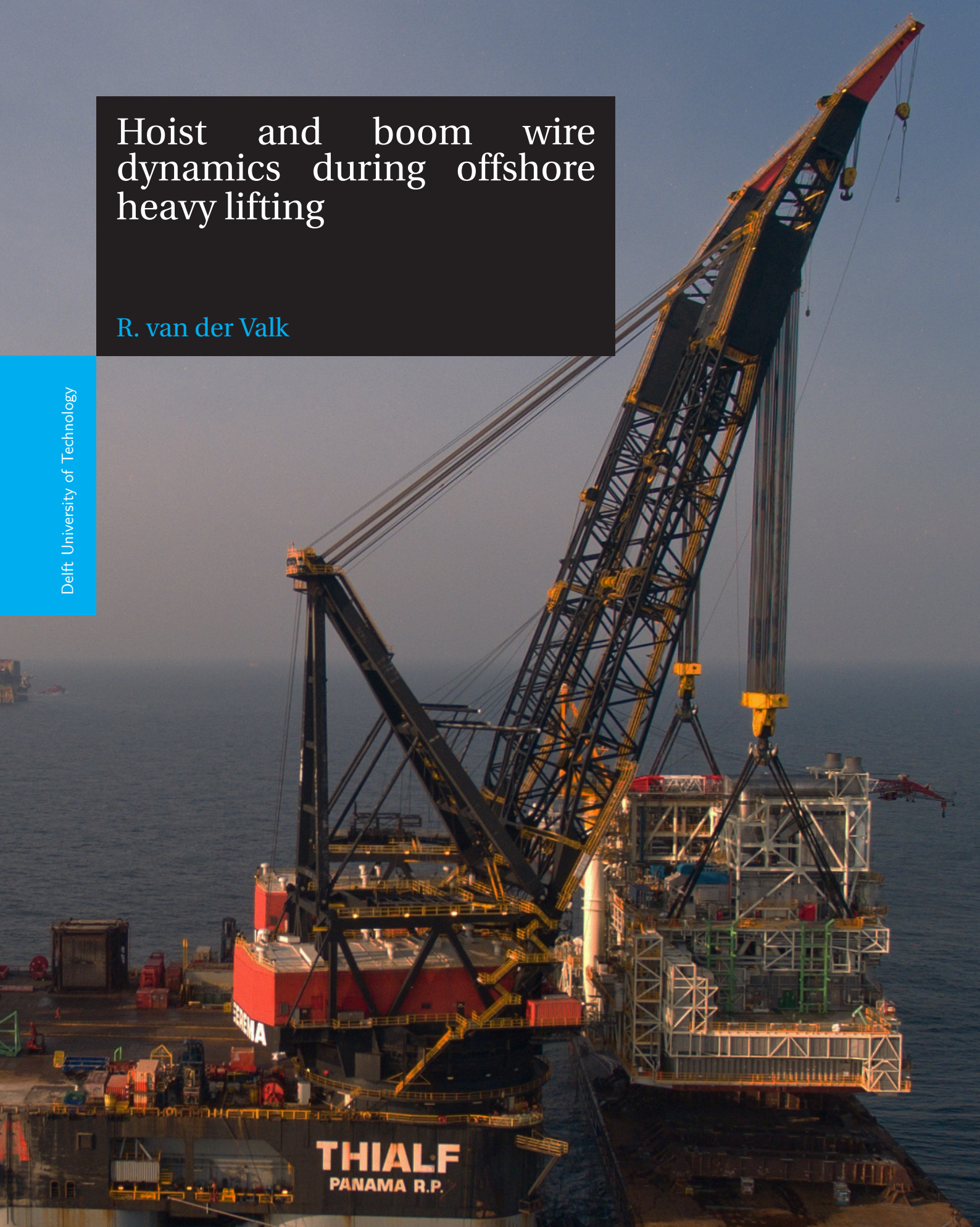
Hoist and boom wire dynamics during offshore heavy lifting

By:

Ramon van der Valk

A thesis presented for the degree of

Master of Science in Offshore and Dredging Engineering
at Delft University of Technology

Supervisors:
prof. dr. A.V. Metrikine,   TUDelft
ir. P. Meijers,   TUDelft
V. Schaap MSc,   HMC
ir. R. van Dijk,   HMC

Offshore and Dredging Engineering
Delft University of Technology
The Netherlands
26-09-2017

An electronic version of this thesis is available at *http://repository.tudelft.nl*.

Preface

This thesis report is the end product of my master study at the Delft University of Technology: Offshore and Dredging Engineering. The thesis study is focused on load fluctuations during an offshore installation of a topside by a semi-submersible crane vessel. The aim of this report is to outline the outcome of my work of the past months.

First of all I am very grateful to Heerema Marine Contractors (HMC) for giving me the chance to perform my research on a very interesting and challenging subject in an environment with highly qualified employees. The thesis study period has been a pleasant period experiencing the excellent working atmosphere at the HMC office in Leiden. In order to complete this graduation study successfully, I received support and advice from many people within the company. I would like to take this opportunity to thank everyone that I have met along the way and that have contributed to the end result of my research.

The end result was only possible thanks to the guidance of the complete graduation committee. Every member has had a specific influence on the end result based on their own expertise. Moreover, I would like to thank the chairman of my graduation committee, Andrei Metrikine. He let me face the challenges of this research and helped me profoundly understand the underlying physics by his recommendations and to-the-point questions. At this point I would also like to dedicate some words to my daily supervisor at the TUDelft, Peter Meijers. His input and fresh sights were of great importance during my meetings with him. He always had important notes that I required in order to make progress. A special thanks goes to Verena Schaap and Radboud van Dijk from the side of HMC for their feedback on daily basis that guided me through the project. Verena has always been very supportive and I would like to thank her for her enthusiasm and expertise, which set the example of a good engineer for me. Further on my gratitude goes to Radboud for introducing me to the topic, giving his admirable suggestions and sharing of his experience with me.

Finally, I want to thank my friends and family for supporting me during my thesis project. They have always been there for me when I needed some necessary distractions to relax my mind. I wish you much fun reading this report and I hope you enjoy it a lot.

R. van der Valk
Delft, September 2017

Abstract

Heerema Marine Contractors (HMC) owns and operates several semi-submersible crane vessels (SSCV) used for offshore heavy lift operations. Throughout the engineering phase of a (dual crane) heavy lift, dynamic lift models are generated by combining bodies with their hydrodynamic properties, inertia and spring-dashpot elements. The models represent the mass-spring system of a heavy lift over the different lift stages during a topside installation. These stages characterize the free floating, load transfer, free hanging and set down phases.

Hook load fluctuations are governed by the relative vertical motion of the load and the crane boom tip. At the load transfer phase this motion is governed by both the motion of the vessel and the barge, whereas for the free hanging phase it is mostly effected by the motion of the vessel. To achieve safe and successful projects, an accurate prediction of the load and motion responses is essential while advising offshore personnel about the lift to perform. At the moment an inconsistency exists between predicted load fluctuations and offshore crane measurements. This is the main reason for this research.

Until now a simplified spring-damper system is used to incorporate the hoist wire reeving system of a crane. This simplification is not fully justified and three goals are set up to model this in a more detailed manner. Firstly, the driving parameters of the load-crane-vessel system are assessed. Secondly the dynamic behavior of the wire reeving system is captured in a numerical model in Simulink. Finally, the dynamic load fluctuations of the model are compared with offshore measurements to both validate the model and analyze the results.

The dynamical model of the load-crane-vessel system is solved in the time domain and it consists of two parts. The first part considers the sheave and wire system of the crane. An equation of motion is derived for each sheave where dry friction is taken into account and leads to a stick-slip effect. This friction originates from the sheave bearings and from the bending friction of the steel wire rope that runs over it. When a load is raised, the stress in each rope part increases from the winch to the dead end. With a lowering operation the effect is the opposite. Due to stick-slip this force difference remains in the crane wires after the operation. The friction factors of the sheaves in the numerical model are tuned with steps observed in offshore load measurements during crane operations.

The second part of the model imposes the measured vessel motions to calculate the motion of both crane boom tips and the topside. This is performed by applying their influences as external forces on the free bodies. With the relative motion the response of the hoist wire forces is determined. A coupling of these two parts can be made by removing the element of the hoist wire in the imposed motion model and replacing it by a pair of two nonlinear forces determined from the sheave wire model. These forces have an opposite sign and are equal in absolute magnitude and phase.

The effect of friction on dynamic hook load fluctuations is also considered with inputs of different amplitudes and frequencies. The hook load fluctuations at the measuring sheave are lower than applied fluctuations in the model when friction is taken into account. The simulated force at the measuring sheave is better represented with higher load fluctuations as the stick condition is exceeded earlier.

Contents

List of Tables

List of Figures

Abbreviations

CoG	Center of Gravity
DAF	Dynamic Amplification Factor
DFT	Discrete Fourier Transformation
DoF	Degree of Freedom
FFT	Fast Fourier Transformation
IFT	Inverse Fourier Transformation
HMC	Heerema Marine Contractors
HTV	Heavy Transport Vessel
MWL	Maximum Working Load
PLC	Programmable Logic Computer
SSCV	Semi-Submersible Crane Vessel
RAO	Response Amplitude Operator
K-IMS	Kongsberg Information Management System
CIS	Crane Information System
SB	Starboard
PS	Port side
PoI	Point of interest
LF	Left front drum
RF	Right front drum
RR	Right rear drum
LR	Light rear drum
MRU	Motion Response Unit
MME	Motion Measuring Equipment

Nomenclature

α	Frequency depended factor	[-]
α_{boom}	Boom Angle	[rad]
α_{slew}	Slew Angle	[rad]
β	Angle between wire ropes	[rad]
$\boldsymbol{B}$	Joint damping matrix	[Ns/m]
$\boldsymbol{B}^*$	Damping matrix	[Ns/m]
$\boldsymbol{F}$	Force vector	[N]
$\boldsymbol{K}$	Joint stiffness matrix	[N/m]
$\boldsymbol{K}^*$	Stiffness matrix	[N/m]
$\boldsymbol{K}_{HW}$	Hoist wire contribution to stiffness matrix	[N/m]
$\boldsymbol{M}$	Joint mass matrix	[kg]
$\boldsymbol{M}^*$	Mass matrix	[kg]
$\boldsymbol{T}$	Joint matrix	[-]
$\boldsymbol{x}$	Joint displacement vector	[m]
$\boldsymbol{x}^*$	Displacement vector	[m]
$\ddot{x}$	Acceleration	[m/s^2]
ΔL	Elongation	[m]
ΔL_{eq}	Equivalent elongation	[m]
Δt	Time step	[s]
δ	Logarithmic decrement	[-]
$\dot{\phi}$	Rotational velocity	[rad/s]
$\dot{x}$	Velocity	[m/s]
γ	Peakedness factor wave spectrum	[-]
$\hat{\theta}$	Pitch amplitude	[rad]
$\hat{\varphi}$	Roll amplitude	[rad]
$\hat{x}$	Amplitude of displacement	[m]
$\hat{z}$	Heave amplitude	[m]
λ	Decay factor	[-]
μ	Friction factor	[-]
μ_{kin}	Kinetic friction factor	[-]
μ_{stat}	Static friction factor	[-]
ω	Frequency	[rad/s]

1

Introduction

1.1. COMPANY INFORMATION

Heerema Marine Contractors (HMC) is a marine contractor specialized in transportation, installing and re-moving of offshore facilities. These include fixed and floating structures, subsea pipelines and infrastructures in shallow waters, deep and ultra deep waters. HMC manages the entire supply chain of offshore construction, from design through to completion. The services include engineering, planning, logistics, project management and execution of projects all over the world. HMC owns and operates several semi-submersible crane vessels (SSCV), used for offshore (dual crane) heavy lift operations for mainly focusing on the oil and gas industry.

1.2. HEAVY LIFT OPERATIONS

In order to facilitate a certain process in an offshore environment several production units need to be installed before operation begins. These production units normally consists of sophisticated equipment made out of steel and require a structural integrity to last a lifetime. For this reason these large and heavy modules can be installed with a semi-submersible crane vessel, which lift this load to its final position. The crane vessels operated by HMC consists of dual cranes, which can be used separately or in tandem, depending on the load to be lifted. The cranes are made up of steel members, mainly consisting of rectangular hollow sections. Both cranes have three hoist blocks (whip, auxiliary and main hoist), with each of them having a certain capacity. For this research it is chosen to focus on one crane vessel in particular, the SSCV Thialf, as most offshore measurements are available. The main block of a crane on this vessel has a maximum capacity of 7100 mT resulting in the total capacity of 14200 mT for a dual lift operation. Throughout the engineering phase of a (dual) heavy lift, dynamic lift models are generated by combining bodies with their hydrodynamic properties, inertia and spring-dashpot elements. The models represent the mass-spring system of a heavy lift over the different lift stages during a topside installation. These stages characterize the free floating, load transfer, free hanging and set down phases. These are described below.

Free floating
The first stage for a typical lift operation is the free floating stage (Figure 1.1). The load that has to be lifted is transported to the offshore location with an Heavy Transport Vessel (HTV) or barge, which is moored against the SSCV. The SSCV is moored with anchors or dynamically positioned along the barge, but the slings are not tensioned yet. Both the crane vessel and the transportation vessel are moving due to influences of wind, waves and current.
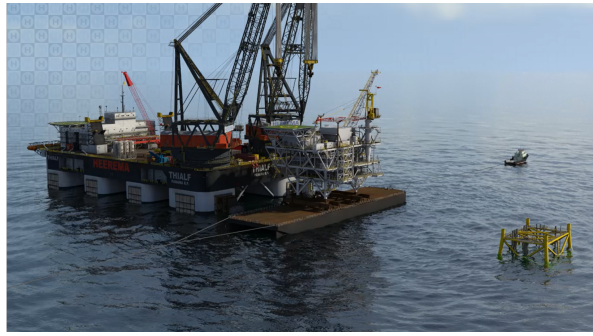
Figure 1.1: Free floating phase

Load transfer

After the free floating stage the actual lift operation starts with the load transfer (or pretension) phase (Figure 1.2) where the barge is positioned along the SSCV and the slings are connected. The SSCV is ballasted to a draft that is close to the operational draft and is trimmed towards the bow. A portion of the total load is transferred by hoisting of the lifting equipment and partly by ballasting. Due to the tension by means of hoisting the vessel starts to pitch towards the stern. Water is pumped from the tanks positioned under the cranes to the opposite site of the vessel to further increase the tension. The remaining load is picked up by de-ballasting the SSCV, until the full load of the module is carried by the cranes and the load lifts off.

Figure 1.2: Load transfer phase

Free hanging

Just before the module comes free of the barge, hoisting is applied to rapidly increase the clearance between the module and the barge to avoid kick back of the barge. When the load is fully transferred from the barge to the crane vessel the load has entered the free hanging phase (Figure 1.3). In this third stage the SSCV is repositioning to the exclusion zone to install the topside on its offshore foundation.

Figure 1.3: Free hanging phase

Set down

After relocation the load is positioned above the substructure and by paying out of the hoist wire it is lowered until contact is made. This last stage is the set down phase (Figure 1.4). Initial load transfer prevents the topside to come loose again which could result in high impact loads on the structure. In order to have slow decrease of the load forces and slow varying motions the load transfer is done by ballasting of the SSCV.

Figure 1.4: Set down phase

The motion and load responses found from dynamic lift models made for each stage are held against the limits of the particular lift to assess the operability criteria of the installation. During the load transfer phase the load of the object to be lifted is transferred from a transport barge to the SSCV. In this phase, the crane vessel and barge have both a different motion behavior and are moving in the waves as one coupled system. When these two bodies move in multiple directions often relatively high hook loads fluctuations occur. Also in the free hanging phase the hook load is influenced by the influence of the environment. Hook load is the term used to describe the load suspended from each crane hook. All lifts are exposed to dynamic effects due to variation in hoisting speed, crane movements, vessel motion, barge motion, lift object motion and numerous other factors. To inform offshore personnel about the load fluctuations due to these variations, the tension in the wires is measured at certain positions. These fluctuations are one of the governing operability criteria while analyzing the feasibility of a certain heavy lift operation.

1.3. PROBLEM DEFINITION

To achieve safe and successful projects, an accurate prediction of the load and motion responses is essential while advising offshore personnel about the lift to perform. Currently, an inconsistency exists between the predicted load fluctuations and the offshore measurements and it is questioned whether safety margins for dynamic effects are correct. The dynamic consequences are at least influenced by the following parameters: environmental conditions, rigging configuration, properties of crane vessel, characteristics of lifting equipment, properties of cargo barge and the weight (distribution) of the object to lift. Until now a simplified spring-dashpot element is used to incorporate the hoist wire reeving system of a crane in modeling practices. Initial researches within HMC [Hartmans, 2016] showed that this simplification is not fully justified and that the hoist wire reeving system behaves in a more complex manner. The goal of this thesis project is to further investigate the sources of the dynamic load fluctuations and how to improve the existing engineering models.

1.4. SCOPE OF WORK

In order to approach the problem three objectives are set up. The methods that are used in order to achieve these goals and the results are threated in this document. The objectives are described below.

1. *Assess the driving parameters of the load-crane-vessel system.*
First the main engineering parameters controlling the dynamic process of a (dual crane) offshore lift are investigated. Such variables allow to create a satisfactorily simulation of operations and tests carried out under a constant- or changing- situation.

2. *Capture the dynamic behavior of the wire reeving system in a numerical model.*
The driving parameters obtained from the first goal are used as input parameters for a numerical model. In order to model the crane dynamics a numerical model of the crane wire reeving and the vessel interaction is made in Simulink. Simulink is a program integrated in Matlab and provides a graphical editor, customizable block libraries and solvers for modeling and simulating dynamical systems. Therefore this is a suitable software tool to model motions and forces for such a lift operation. An environment is created to make a starting point of a numerical model, where the model is extended according to correct outcomes and points of interest.

3. *Analyze the dynamic load fluctuations and improve existing engineering models.*
Together with the offshore measurements from heavy lifts the results from the model are studied. The outcome of this analysis is discussed in this report and is the basis for the conclusions drawn.

1.5. REPORT STRUCTURE

This report starts with an explanation of the theoretical background in chapter 2 where the axis definition, properties of steel wires and background on the friction model are given. In chapter 3 offshore measurements and its characteristics during a topside installation are discussed. Chapter 4 describes how the numerical model for the crane wire reeving is created. Followed by chapter 5 where the composed model for an imposed vessel motion is described. In chapter 6 a comparison study is performed. The discussion of the results and conclusions can be found in chapter 7. In this last chapter the recommendations and future actions for this research are written down as well.

2

Theoretical framework

This chapter describes the theoretical basis for this research. It is divided into five parts which provide a background to avoid further explanation later in this report. The first section explains how the axes of the vessel are defined. Followed by the usage of stiffness and damping in steel wires in sections 2.2 and 2.3. Subsequently a friction model is described for a sliding block and a rotating sheave in section 2.4. In the last part it is explained how a spectral analysis is performed to characterize the frequency content of a signal.

2.1. AXIS AND SIGN DEFINITION

A ship can be considered to have six degree of freedom motions, it can translate and rotate along or about the axes given in Figures 2.1 until 2.3. Three of these involve translation (surge x, sway y, heave z) and the other three rotation (roll ϕ, pitch θ, yaw ψ). The crane boom attached to the vessel has two degree of freedom, the slew angle α_{slew} and the boom angle α_{boom}. Normally during operations the slew angle is not influenced by load variations and is considered as infinitely stiff or fixed. However the boom angle is under the presence of a fluctuating load able to rotate around its hinge point since the boom is suspended by multiple stretchable steel wires.
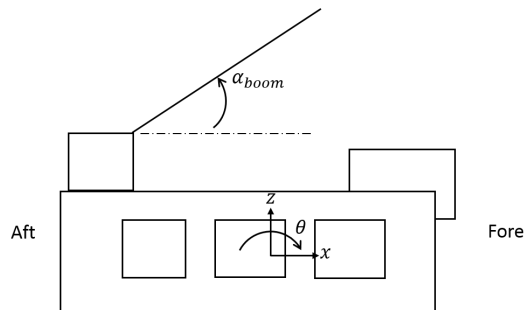
Figure 2.1: Side view axis definition
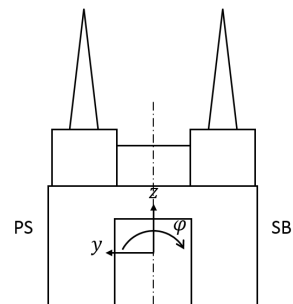
Figure 2.2: Aft view axis definition
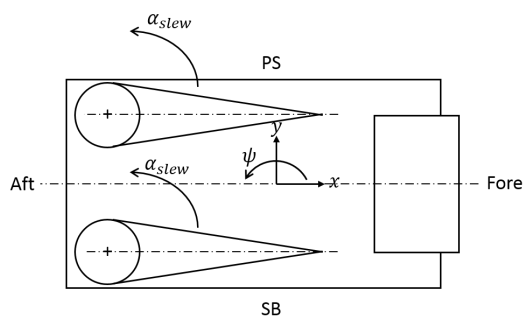
Figure 2.3: Top view axis definition

5

2.2. STIFFNESS OF STEEL WIRES

Considerable interest has been shown in the mechanical characteristics of helically wound steel cables (spiral strands and/or wire ropes) for the usage in both onshore (bridges, elevators and reinforcement structures), and offshore (taut mooring lines, drilling lines and towing ropes) applications [Raoof and Davies, 2003]. Another important utilization is the handling of steel wires in (offshore) cranes to suspend the crane boom and/or to be able to hoist or lower a certain object by using winches. The difference between a spiral strand wire and a wire rope is the way the single wires are laid in successive layers to provide integrity and flexibility. A spiral strand consists of a group of wires laid in helically layers around a central straight core wire. On the other hand, a wire rope has generally six strands laid helically over a central king wire which is consisting of minor separate wire rope or twisted threads. Wire ropes are a lot more flexible in bending, which is why wire ropes are used as elements over pulleys and winch drums in cranes. Figure 2.4 shows the difference between a spiral strand and a wire rope. Also the configuration used at HMC SSCV Thialf, the wire type 6xK36WS IWRC is pictured. The wire ropes used for the main hoist and for the boom suspension are of the same type although their installed length differs. An additional property for these wire ropes is that they are compacted, meaning that the individual wires are as close as possible to each other. This results in a higher effective area. While the wire elongates it starts automatically to twist and to keep this twist as low as possible the cores are oppositely spiraled. To further oppose this effect a combination of left lay and right lay wires are used in a symmetrical reeving configuration in cranes. More wire characteristics of the installed Thialf wires can be found in Table 2.1 from [Bridon, 2016].
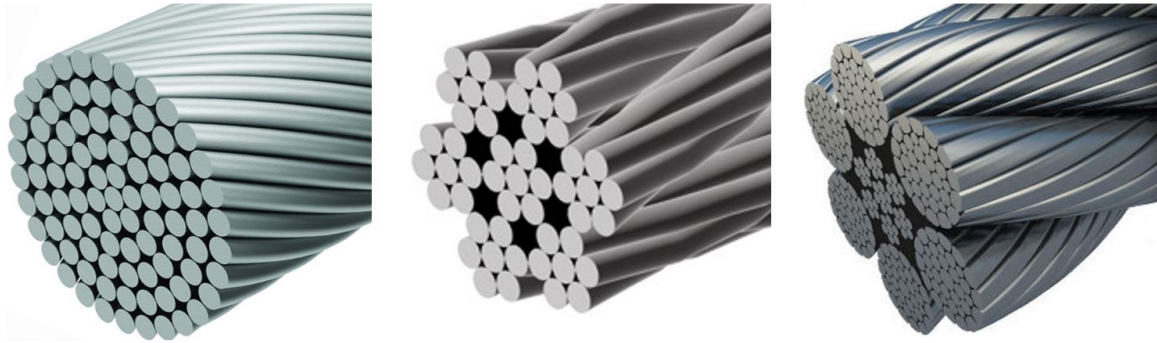
Figure 2.4: Spiral strand, wire rope, 6xK36WS IWRC

Table 2.1: Thialf wire properties

Diameter	D	[mm]	61.7
Effective steel area	A_{eff}	[mm^2]	1939
Area	A	[mm^2]	2990
Weight in air	W_{air}	[kg/m]	16.9
Installed hoist wire length	L_{Hoist}	[m]	4x 2955
Installed boom wire length	L_{Boom}	[m]	2x 3650

In order to model the steel wires as a simplified spring-damper connected between translating and/or rotating bodies, their properties have to be determined. Generally the spring force of a wire is assumed to be linear with the elongation, resulting in a constant spring coefficient, see equation 2.1.

$$F_{linear} = \frac{EA_{eff}}{L} \Delta L = k \Delta L \tag{2.1}$$

The force that is present due to the elongation ΔL is linear with the stiffness $\frac{EA_{eff}}{L}$ or k, where L is the initial length of the wire, E the Young's Modulus of the material and A_{eff} the effective area of a wire rope. The effective area is the net steel area of the cross-section of a wire rope. When comparing two different wire ropes with the same material properties where rope A is twice as long as rope B, the stiffness of rope A is twice as low as rope B. The stiffness EA_{eff} can be obtained from a certificate of a manufacturer, which is determined

from carrying out load cycle tests.

Recently within HMC [Schaap, 2017] destruction tests were analyzed to determine the axial force at which a wire rope, used in the cranes on the SSCV Thialf, breaks. The applied force and elongation of the wire were measured by sensors. From these two parameters the stiffness can be determined. In the executed tests, sections of 5.6 m long were clamped and elongated. The test results are shown in Figure 2.5, where the measured strain is plotted against the applied force. The blue lines are the tests carried out and the red line represents the mean value. The graphs of the test results does not start in (0,0), which is because all clamped segments had a pretension of 20 kN prior to measuring the elongation.
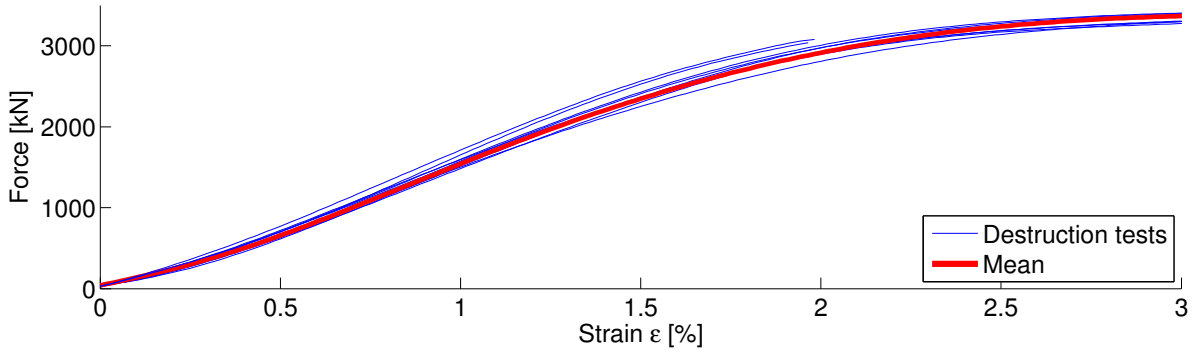
Figure 2.5: Strain vs. axial force from [Schaap, 2017]

With these two obtained parameters, the stiffness for a unit length of 1 m can be determined with equation 2.2. Here L is the length of the test section. This creates Figure 2.6. Obviously the obtained stiffness is not a constant when the applied load is increased and is clearly non-linear. At a low force the wire rope experience a large extension and all individual wires settle a bit. In order to eliminate this non-linear effect the tests were started with a certain pretension to stress the ropes in advance. The central core encounters greatest strain because the helix wires are at an angle with the centroid. Also due to friction between the individual wires in a wire rope, since there is more contact at a higher stress level, the resistance to extend is increased.

$$EA_{eff} = \frac{F}{\Delta L}L \tag{2.2}$$

The maximum working load (MWL) of the wire can be calculated by adding up all the forces that are present during maximum capacity. The maximum hoist capacity for the SSCV Thialf is 7100 mT with a reeving of 20x4 single hoist wires. This capacity is excluding the weight of the main block, the weight of the wires and differences due to friction. The mass of the main block is approximately 236 mT. With equation 2.3 the mass of the hoist wires can be determined. Here W_{air} and L_{Hoist} are the weight in air and the installed length per winch. The total hoist wire mass has to be divided by four as the total mass is supported by four winches.

$$m_{wires} = \frac{4W_{air}L_{Hoist}}{4} = 4*16.9*2955 = 50mT \tag{2.3}$$

The total weight of the wires is partly supported by the boom and partly by the wires itself, 80 % is good approximation for the support by the wires itself. A rough estimation of the friction factor C_f is 1.05. The maximum force in the hoist wire can then be determined with equation 2.4. This makes the MWL then approximately 1000 kN. The corresponding stiffness for the force in the wire rope can be determined from Figure 2.6.

$$MWL = \frac{m_{load} + m_{main\ block} + m_{wires}*0.8}{80}*C_f*g = \frac{7100+236+50*0.8}{80}*1.05*9.81 \approx 1000kN \tag{2.4}$$
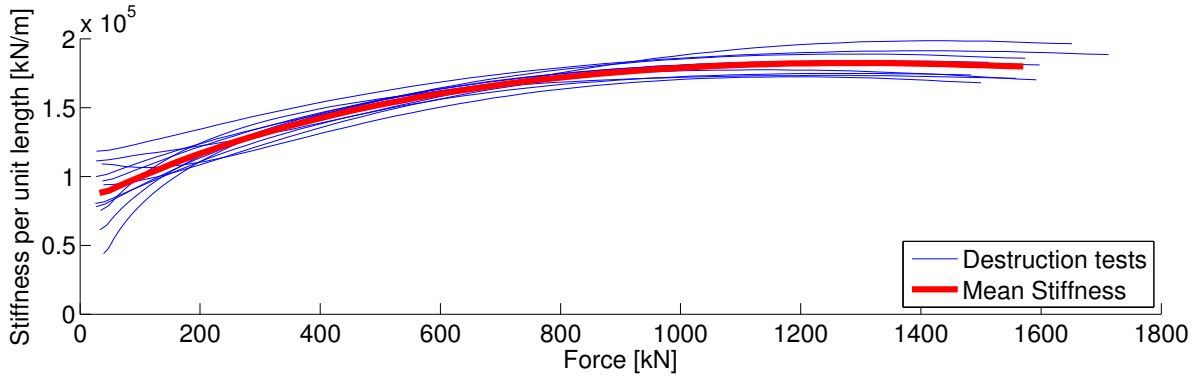
Figure 2.6: Axial force vs. Stiffness

As can be seen in Figure 2.7 the stiffness is depending on the strain as it was also depending on the applied force. The stiffness that is used in this research for wire ropes with the same properties (cross-sectional area, material, etc.) are the ones that were also used in the destruction tests. In order to take the non-linear effect of the stiffness into account, EA_{eff} is written as a function of the strain with a 3rd order polynomial fit of the mean (equation 2.5). The 3rd order polynomial gives three constants c_1, c_2, c_3, where c_1 is the intercept of the line. By taking the stiffness into account the resulting desired nonlinear stiffness force can be calculated, see equation 2.6. For the later described numerical model the stiffness for a single wire is determined by the mean load. Continuously adapting the stiffness value during a simulation would result in a high calculation time.

$$E(\varepsilon) A_{eff} = c_1 + c_2 \varepsilon + c_3 \varepsilon^2 \tag{2.5}$$

$$F_{nonlinear} = \frac{E(\varepsilon) A_{eff}}{L} \Delta L = E(\varepsilon) A_{eff} \varepsilon \tag{2.6}$$
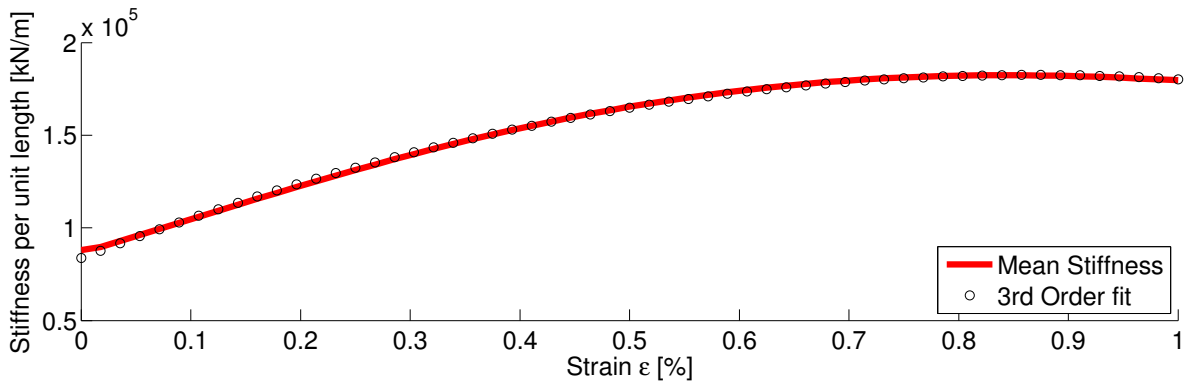
Figure 2.7: Strain vs. Stiffness

For completeness, the stiffness is also divided by the effective cross-sectional area of wires to get the Young's modulus, see equation 2.7 and Figure 2.8. The effective area (or net steel area) is two third of total area ($\frac{\pi}{4} D^2$) stated by [Raoof and Davies, 2003]. Here D is the diameter of the wire. This corresponds well to the value for the effective area given in Table 2.1. Note that the cross-sectional area of the wire during the tests is assumed to be constant, but in fact the diameter slightly decreases due to its elongation. It is remarkable that there is clearly a difference between the theoretical value for the Young's modulus of steel (210 GPa) and the determined value, even when a effective area is taken into account. This is in line with the results found in the referred research, where the Young's modulus of steel wire ropes had more or less the same fraction of the theoretical value. Also in the specification sheet of the wire ropes of the manufacturer an apparent modulus

of 103 GPa can be found [Bridon, 2016], a value in the same order as was determined from the tests.

$$E = \frac{(EA)_{measured}}{A_{eff}} = \frac{(EA)_{measured}}{0.67 \frac{\pi}{4} D^2} \tag{2.7}$$
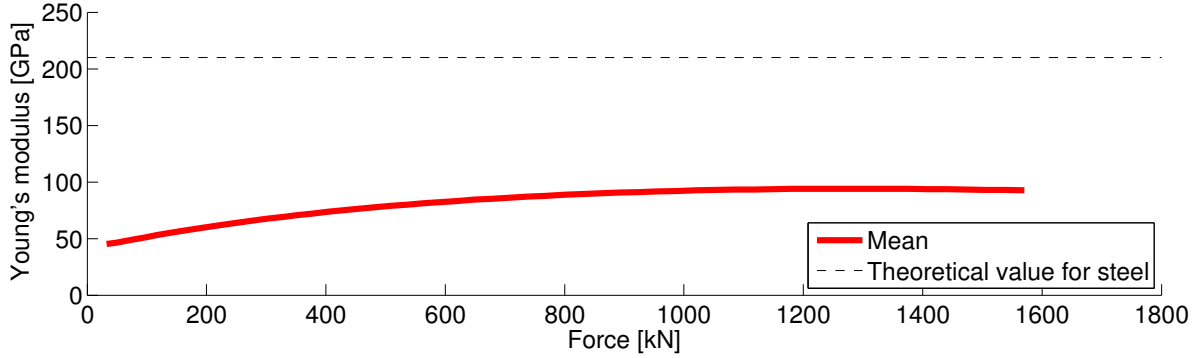
Figure 2.8: Force vs. Young's modulus

2.3. DAMPING OF STEEL WIRES

Damping is the conversion of mechanical energy of a vibrating structure into thermal energy. To quantify the level of damping in a structure the absorbed energy per oscillation can be determined. Primary, there are two basis components that have a contribution to damping in wire ropes, material damping and frictional damping due to the relative motions between single wires. These quantities can be different depending on the material used or how an external load is applied, but the frictional damping between adjacent wires seems to be governing for spiral strands or wire ropes [Chaplin, 1991]. With an axial load the individual wires in the rope elastically deforms, which has an effect on the lay angles, because the wires (and strands) of a rope are twisted into a helical form. This axial tension results in a radial loading and thus radial deformation within the rope. These changes causes frictional shears that reflect the degree of friction and the magnitude of the lateral loads. In the case when a wire rope is bended, for example while moving around a circular sheave, these movements are much greater. The wires try to move to equalize the difference in strains between the inside and outside of a bend. More frictional shears results in more damping. To find a value for the damping, friction is included and thereby the damping effects in the wire. The motion of an unforced damped harmonic oscillator is governed by:

$$m\ddot{x} + b\dot{x} + kx = 0 \tag{2.8}$$

With displacement x, time derivative $\dot{x}$ and 2nd time derivative $\ddot{x}$ and where m is the mass, b the damping and k the stiffness with $m > 0, b \geq 0$ and $k > 0$. It has the characteristic equation:

$$ms^2 + bs + k = 0. \tag{2.9}$$

with characteristic roots

$$s_{1,2} = -b \pm \frac{\sqrt{b^2 - 4mk}}{(2m)} \tag{2.10}$$

Depending on the sign of the expression under the square root, three situations can be distinguished. These are explained now.

- Case 1: $b^2 < 4mk$ (Underdamping)

- Case 2: $b^2 > 4mk$ (Overdamping)

- Case 3: $b^2 = 4mk$ (Critical damping)

Case 1
If $b^2 < 4mk$ then the term under the square root is negative and the characteristic roots are not real. The damping constant b must be relatively small, in order for $b^2 < 4mk$. The system vibrates around the equilibrium with a decreasing amplitude. The damping force enforces this behavior.

Case 2
If $b^2 > 4mk$ then the term under the square root is positive and the characteristic roots are real and distinct. The damping constant b must be relatively large, in order for $b^2 > 4mk$.

Case 3
The last case is where the square root is equal to zero and the characteristic polynomial has two repeated roots, $-b/2m, +b/2m$. With a fixed mass m and stiffness k, choosing b to be the critical damping value. The critical damping is the minimum amount of viscous damping that results in a displaced system returning to its original position without oscillation. The damping value b_{crit} can easily be determined:

$$b_{crit} = 2\sqrt{km} \tag{2.11}$$

Figure 2.9 shows the response for the three cases with initial conditions x=1 m and $\dot{x}$=0 m/s.
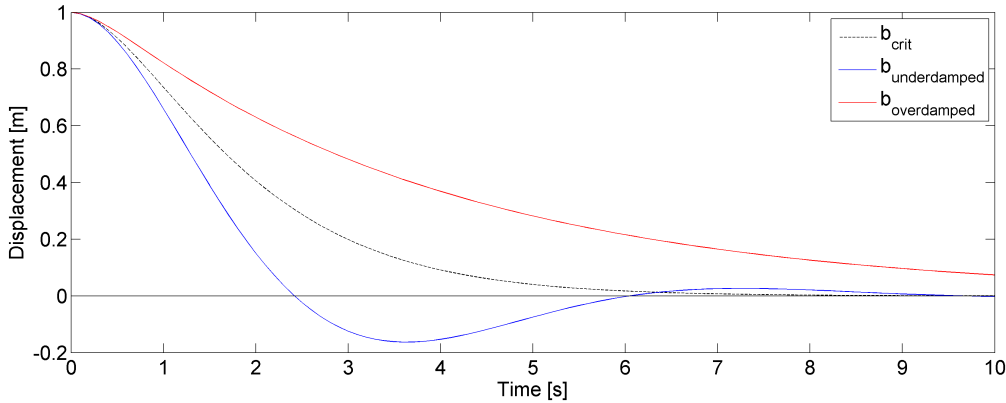
Figure 2.9: Response for three possible damping cases

Generally there are three ways to implement damping while modeling steel wires [Spijkers et al., 2005], namely:

CONSTANT VISCOUS DAMPING
For this type of damping the damping force is proportional to the velocity and is the most common used in the engineering applications when the exact damping mechanism is unknown and the qualitative effects are desired. The energy dissipation E_{diss} per oscillation can be calculated with equation 2.12.

$$E_{diss} = \int_0^T F dx = \int_0^T F\dot{x} dt = b\pi\omega\hat{x}^2 \tag{2.12}$$

Where T is the period of the oscillation, F the damping force, ω the frequency and $\hat{x}$ the amplitude of vibration. Even when the damping is not completely viscous it still has some advantages to approximate it as a constant viscous dashpot by determining an equivalent coefficient. In that case the equivalent viscous damping coefficient b_{eq} is chosen with the same energy that is dissipated per oscillation:

$$b_{eq} = \frac{E_{diss}}{\pi\omega\hat{x}^2} = \frac{b\pi\omega\hat{x}^2}{\pi\omega\hat{x}^2} = b \tag{2.13}$$

FREQUENCY DEPENDENT VISCOUS DAMPING

When the excitation frequency stays the same the energy dissipation normally grows with the square of the amplitude. The equivalent damping coefficient can then be calculated by assuming that the dissipated energy equals to $E_{diss} = \alpha \hat{x}^2$ and can be filled in equation 2.13, which results in equation 2.14. As can be seen the damping depends on the frequency ω of the system, which was not the case in equation 2.13, because the dissipated energy is also depending on the frequency ω.

$$b_{eq} = \frac{\alpha \hat{x}^2}{\pi \omega \hat{x}^2} = \frac{\alpha}{\pi \omega} \tag{2.14}$$

Often the frequency depended factor α is taken constant for the natural frequency ω_n where it should give the same result. For the other frequencies there is an error, however this is a small error, since the amplitude of vibration is small there [Spijkers et al., 2005].

COULOMB DAMPING

The effect of damping of Coulomb damping comes from the fact that energy is absorbed due to sliding friction, where the friction is generated by the relative motion of the two surfaces that press against each other. The equation of motion looks a bit different, see equation 2.15, where F_c stands for the Coulomb friction, normally depending on a dimensionless factor multiplied by the normal force.

$$m\ddot{x} + F_c \frac{\dot{x}}{|\dot{x}|} + kx = 0 \tag{2.15}$$

Again the equivalent damping coefficient follows from the energy dissipated, which equals to $E_{diss} = 4F_c \hat{u}$ for a harmonic motion. Filling this absorbed energy again in equation 2.13, results in:

$$b_{eq} = \frac{4F_c}{\pi \hat{x} \omega} \tag{2.16}$$

DAMPING

The logarithmic decrement δ can be determined by looking at the amplitude of two or more successive peaks (equation 2.17). Since the logarithmic decrement between any two successive peaks is constant, the decrement can be determined from the first peak and the peak n oscillations later. In equation 2.17 this is pictured for the maximums x_i and $x_i + 2$, which can be found in Figure 2.10.

$$\delta = \frac{1}{n} \ln \left(\frac{x_i}{x_{i+2}} \right) \tag{2.17}$$
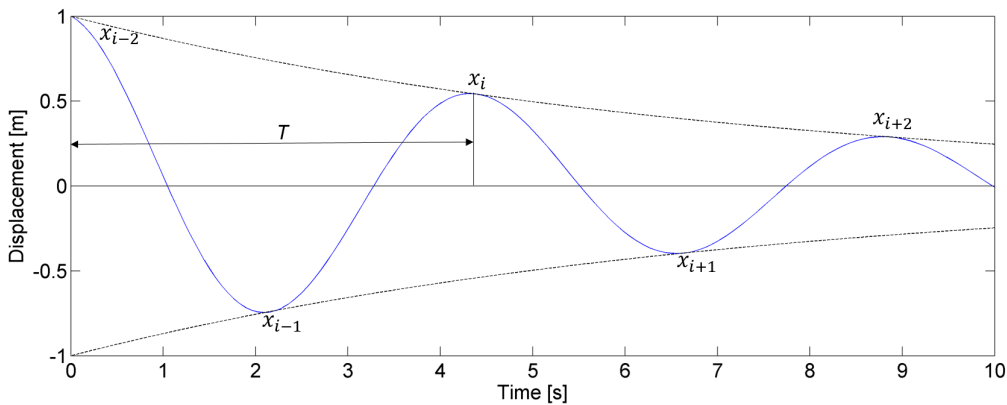
Figure 2.10: Typical decay of an oscillation

The dimensionless damping ζ (damping coefficient divided by the critical damping) can also be calculated by

determining the logarithmic decrement based on measurements or signals created in models for an under-damped system (equation 2.18).

$$\zeta = \frac{b}{b_{crit}} = \frac{1}{\sqrt{1 + \left(\frac{2\pi}{\delta}\right)^2}} \tag{2.18}$$

2.4. STICK-SLIP

Friction is generally described as the resistance to motion when two surfaces slide against each other. In some cases friction is a useful phenomena making many ordinary things possible like walking and braking a car. On the other hand friction can also cause undesirable effects. For mechanical motion systems for example, friction can deteriorate the performance of the system. A possible way to minimize the influences of friction is to compensate for it. In order to be able to compensate the effect of friction, it is necessary to describe the frictional behavior. Since no exact formula for the friction force is available, friction is normally described in an empiric model. In 2.4.1 the stick-slip phenomena is explained for a sliding block and in 2.4.2 friction model for a rotating sheave.

2.4.1. STICK-SLIP OF TRANSLATION

Consider a rigid block with a certain mass lying on a flat surface as shown in Figure 2.11 with the properties as in Table 2.2. Attached to this mass are a linear spring with stiffness k and a dashpot with damping b. Stick-slip is associated with the difference between kinetic and static friction coefficients for two objects with a relative velocity. The reason for two different friction factors is due to difference in two physical processes. When two different surfaces are in rest the possibility exists that they grasp each other at microscopic level. On the other hand when a object is eventually moving over a surface only macroscopic irregularities have an effect on the resistance to move. The force that is required to overcome the friction is larger when the block is in rest than as if it was moving. This friction force in rest is also mentioned as the static friction force and the friction force when the block has a certain velocity is than the kinetic friction. Sometimes the subscript critical is used for the static friction, because when this force is overthrown this kinetic friction force becomes active.
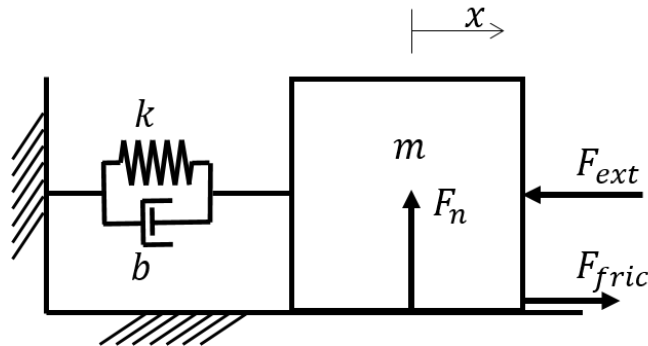
Figure 2.11: Stick-slip of a block on a flat surface

Table 2.2: Properties stick-slip example

Mass	m	[kg]	1.0
Stiffness	k	[N/m]	1.0
Damping	b	[Ns/m]	0.0
Static friction coefficient	μ_{stat}	-	1.0
Kinetic friction coefficient	μ_{kin}	-	0.5

The amplitude of the friction force is depending on the normal force F_n and properties of the surface. The direction is opposite to the velocity and acting perpendicular to the normal force. The normal force is the force that pushes the two objects together. When they are pressed harder, the normal force is higher resulting in a higher friction force. There is no dependency of the friction for the contact area, because when the normal

force is kept constant, the same force is distributed over a larger area and thereby a lower local normal force. Often all influences are simplified to a relation of μ, (equation 2.19) and in a stick-slip situation the factors, μ_{stat} and μ_{kin}. V_{rel} is the relative velocity between the block and the floor in contact. Figure 2.12 shows the transition between μ_{stat} and μ_{kin} when the relative velocity V_{rel} is increasing. It is described with a exponential function to avoid a discrete change, see equation 2.20. This is both undesired for numerical models to evade instability and is a better representative for reality [Martins et al., 1990]. The factor λ has to be chosen such that the interval to make the transition as desired. A higher value of λ decreases the transition time and a lower value makes it longer. The factor λ that is used in the simulations is 1000 resulting a short transition.

$$F_{fric} = -\mu F_n \frac{V_{rel}}{|V_{rel}|} = -\mu mg \frac{V_{rel}}{|V_{rel}|} \tag{2.19}$$
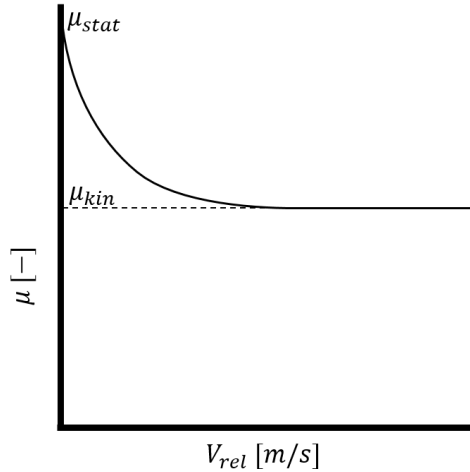
Figure 2.12: Friction coefficients

$$\mu = \mu_{kin} + (\mu_{stat} - \mu_{kin})e^{-\lambda|v_{rel}|} \tag{2.20}$$

With these equations a simple simulation can be performed to analyze the behavior and the influence of a stick-slip in an oscillation. Figures 2.13 until 2.16 shows the response of the forces (external force F_{ext}, spring force F_{spring}, friction force F_{fric} and the resulting force F_{res}). The resultant force is calculated with equation 2.21. As can be seen in the time interval 10-20 s an external force of 5 N is applied and due to the static friction the block does not move (since $F_{ext} < F_{fric_{stat}}$). However when a force of 100 N is applied (interval 20-30 s) the block starts to oscillate (since $F_{ext} > F_{fric_{stat}}$). The block is released at $t = 30$ s and oscillates in its natural frequency. Because of the friction force that is acting in the opposite direction of the velocity the oscillation is damped. Every time the block has a zero velocity and thus the spring force has a local maximum amplitude it is checked whether this amplitude is still higher then the static friction force. When the situation occurs that this local maximum drops below the critical static friction force the block stops oscillating and is at rest. There is still an offset visible in the spring force because the block did not come back in its neutral position. The remaining spring force was lower than the critical static friction force.

$$F_{res} = -F_{ext} + F_{spring} - F_{fric} \tag{2.21}$$
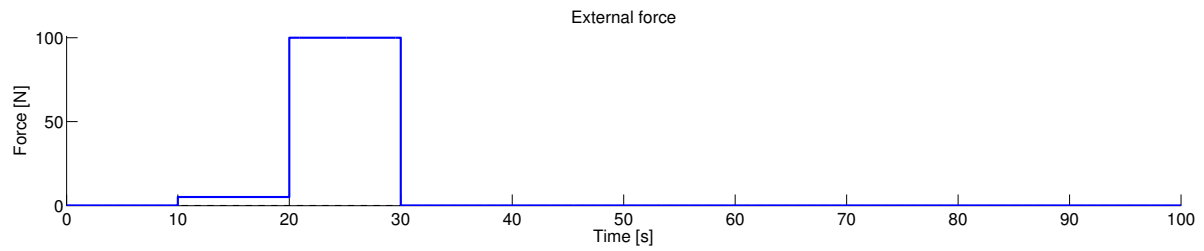
Figure 2.13: External force
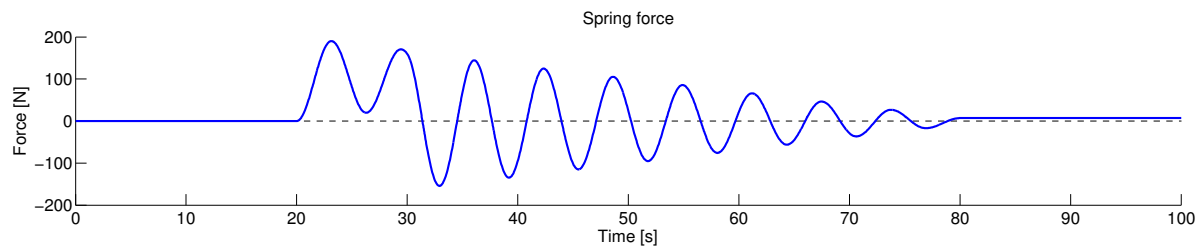
Figure 2.14: Spring force
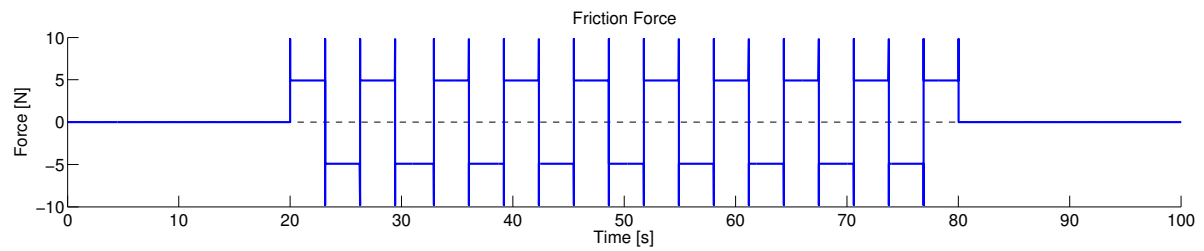
Figure 2.15: Friction force
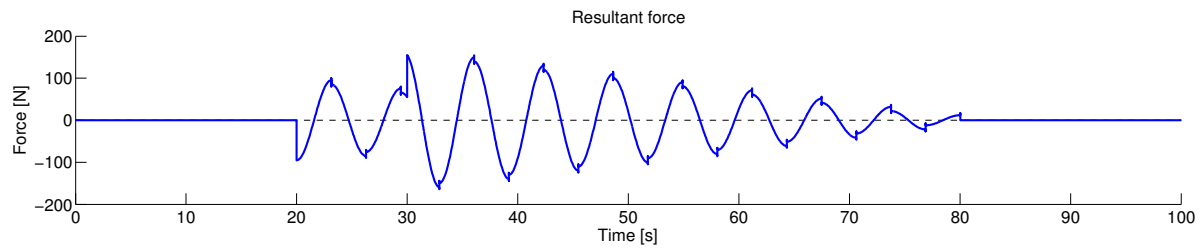
Figure 2.16: Resulting force

The corresponding displacement and velocity of the mass is show in Figure 2.17. These two quantities are precisely out of phase of each other and the offset in displacement is also visible at approximately 80 s where the mass is in rest.
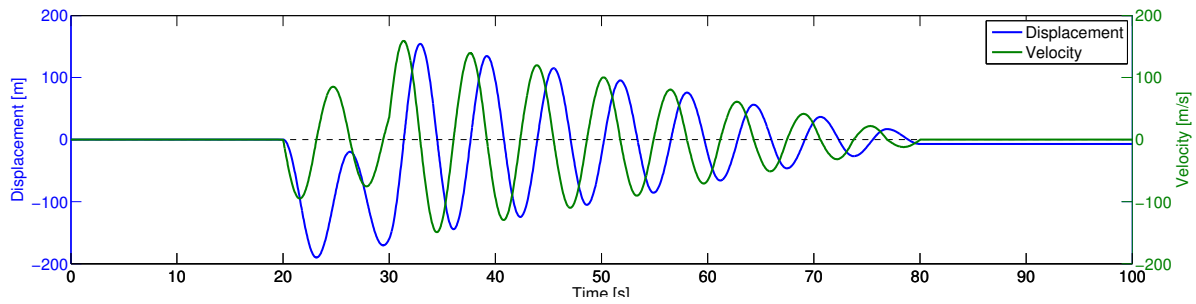
Figure 2.17: Motion of block

2.4.2. STICK-SLIP OF ROTATION

Section 2.4.1 described the stick-slip effects for a mass that is translating on a flat surface. However, the same effect could happen for a sheave that is rotating, see Figure 2.18. The same characteristic figures as produced in 2.4.1 result from the simulation for a rotating sheave friction model. The only difference comes from the quantity force that is turned into a moment and the unit displacement changed to radians instead of meter. See Figures 2.19 until 2.23. The friction, expressed as a moment now, comes from the friction of the shaft and its bearing and due to the bending friction of the steel wire rope that run over the sheave. When a wire rope is bended the outer wire of the rope is more extended than the inner wires. The wires try to move to equalize the difference in strains between the inside and outside of a bend. This causes frictional shears between the single wires. The contact between the individual wire can again be seen as a block sliding over a surface. They only have a relative velocity when the external force is higher than the static friction force, resulting in a stick-slip reaction of the sheave. This effect has earlier been found by [Poe, 2000] where the effects of sheave friction was researched by measuring the tension in steel wires. In this research a series of sheaves were supporting a certain load and an increase in wire tension was found due to the cumulative effect of friction in the sheave bearings and the force required to bend the rope around sheaves. Due to friction in the sheaves, more force was required to lift the weight.
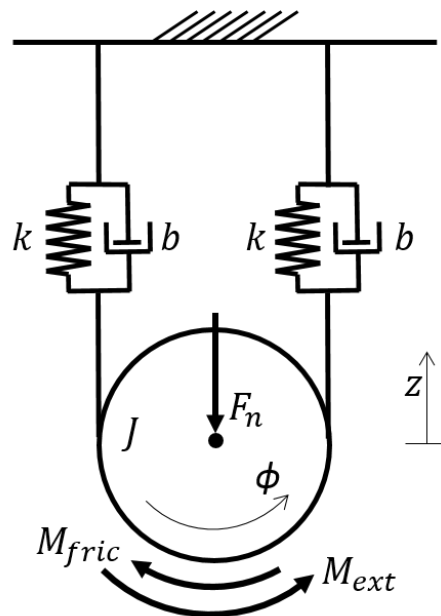
Figure 2.18: Stick-slip of a sheave

If considered that besides the own weight of the sheave an external mass is hanging on the pin of the sheave the total normal force can be calculated with equation 2.22. The total force on the pin comes now due to gravity of the sheave, gravity of the external mass and the dynamic term $m\ddot{z}$. A good example for this external mass could be a crane that picks up a load that is supported by a shaft through the sheave. The friction moment in equation 2.23 differs from equation 2.20 as it is multiplied by a certain radius R to get to a moment.

This arm R is the distance between the center of the sheave and the point where the friction force acts. The resulting moment is calculated with equation 2.24

$$F_n = mg + m_{ext}\ddot{z} \tag{2.22}$$

$$M_{fric} = -\mu F_n r \tag{2.23}$$

$$F_{res} = -F_{ext} + F_{spring} - F_{fric} \tag{2.24}$$
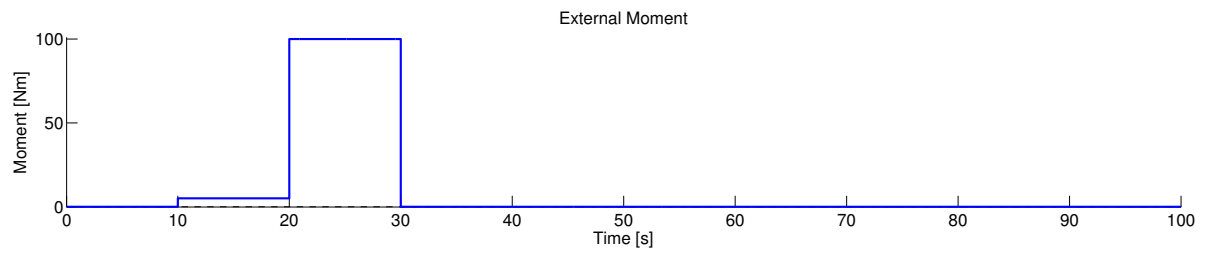
Figure 2.19: External moment
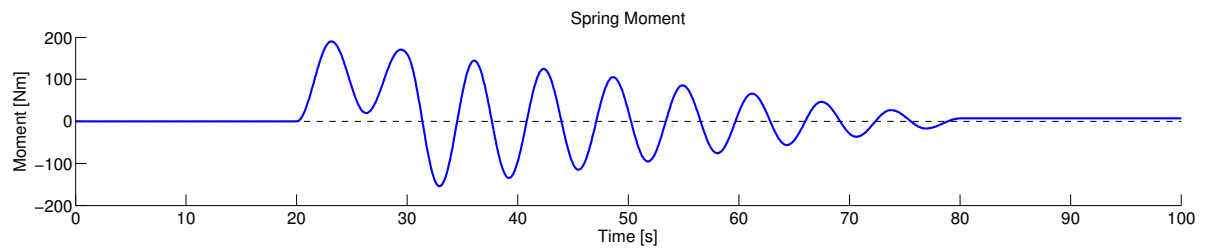
Figure 2.20: Spring moment
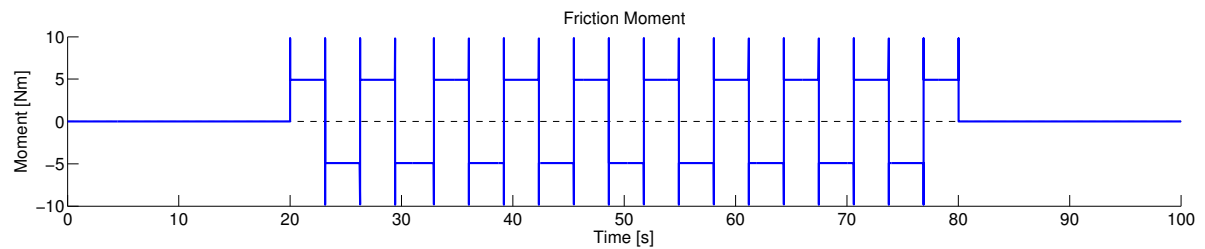
Figure 2.21: Friction moment
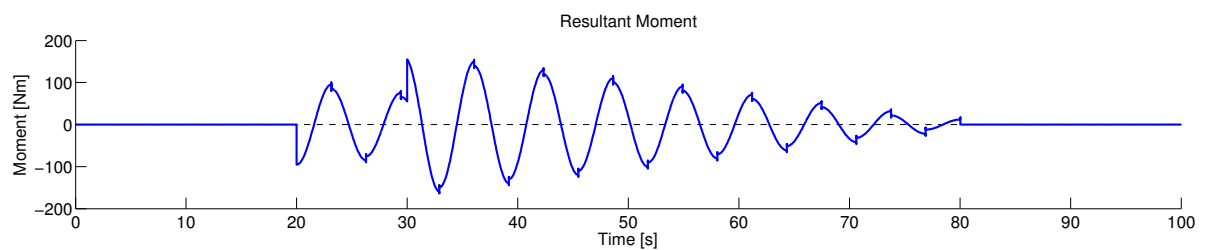
Figure 2.22: Resulting moment
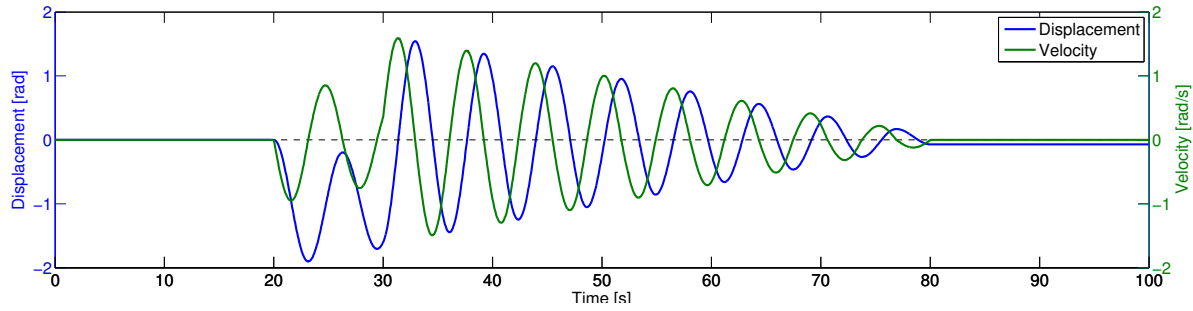
Figure 2.23: Motion of sheave

2.5. SPECTRAL ANALYSIS

Periodic wave forms can be described as the summation of harmonic waves. Fourier transforms (FT) take a signal and express it in terms of the frequencies of the waves that make up that signal. It gives the frequencies that are present in the signal and in what proportions. A wave form can be approximated by a large number of regular waves, each with a different amplitude and phasing with respect to each other. An irregular wave is a linear superposition of regular waves. Many physical interactions depend on the frequency of vibration, and many physically measured signals involve complex wave forms. To understand how a physical system responds to a complex stimulation, you can break that down into a superposition of simple impulses and when considered in isolation the results can be combined.

The Fourier Transform aims to decompose a cycle of an arbitrary wave form into its sine and cosine components; the Inverse Fourier Transform (IFT) goes the other way as it converts a series of sine and cosine components into the resulting wave form. These are referred as the 'forward' (time domain to frequency domain) and 'inverse' (frequency domain to time domain) transforms. The discrete Fourier transformation (DFT) is a Fourier transformation that is commonly applied during digital signal analysis and other relevant disciplines to analyze the frequencies that are present in a sampled time trace. The DFT can efficiently be calculated by the Fast Fourier Transformation (FFT) algorithm [Cooley and Tukey, 1964]. The results of the FFT are the same as with the DFT; the only difference is that the algorithm is optimized to remove redundant calculations and to improve calculation time. More information about discrete Fourier transformations can be found in [Sundararajan D, 2001].

As mentioned before a signal can be thought of as a collection of frequency components. In order to extract these components the situation has to be stationary for the duration of the observation and can then integrated over the time of observation. Measured signals are discretized as they are sampled with a certain sampling frequency f_s. For a signal sampled at discrete times t_n, with a total number of samples N and over the finite duration $N\Delta t$, the so called discrete Fourier transform is used, see equation 2.25. k is the number of frequency components that is considered and $\Delta\omega$ the bin size calculated by $\Delta\omega = \frac{2*\pi}{N\Delta t}$

$$G_k(\omega) = \sum_{n=0}^{N-1} g(n)e^{-i\Delta\omega nk} \tag{2.25}$$

Note that $G(\omega)$ is a complex number. The original signal can be reconstructed with equation 2.26, which is in fact the IFT.

$$g(n) = \frac{1}{N}\sum_{k=0}^{N-1} G_k e^{i\Delta\omega nk} \tag{2.26}$$

By taking the square root of the quadratic terms of the real and imaginary part of the DFT G the amplitude of each separate harmonic wave k can be determined as is done in equation 2.27.

$$\hat{x}_k = \frac{\sqrt{\text{Re}(G_k(\omega))^2 + \text{Im}(G_k(\omega))^2}}{N} \tag{2.27}$$

The phase φ of the harmonic component can be calculate by the angle between the real and imaginary part of the DFT $G(\omega)$ (equation 2.28).

$$\varphi_k = \text{atan}\left(\frac{\text{Im}(G_k(\omega))}{\text{Re}(G_k(\omega))}\right) \tag{2.28}$$

The DFT shows the spectral content of the signal in terms of amplitude and phases of the harmonic elements of the sampled time trace. The power spectral density visualizes how the power of the signal is distributed over the frequencies. The spectral density is scaled such that both the first moment area of m_0 (or area under the spectral density curve) based on frequency and the variance (σ^2) based on the time trace is equal.

For a signal sampled with the sampling frequency $\omega_s = 2\pi f_s$ components of the spectrum can only be extracted for frequencies below $\omega \leq \frac{\omega_s}{2}$. In order to recover all Fourier components of a periodic waveform, it is necessary to have a sampling rate at least twice the highest waveform frequency. This is called the Nyquist frequency (equation 2.29), or the Nyquist limit and is the highest frequency that can be coded at a given sampling rate in order to be able to fully reconstruct the signal. There is also an effect of changing the frequency bin step in creating spectral plots. Choosing a too large steps size results in a smoothed plot where some response around natural periods is under predicted. On the other hand choosing a too fine step size results in a peaked spectrum.

$$\omega_{Nyquist} = \frac{\omega_s}{2} \tag{2.29}$$

Sometimes the period T is used as unit in a spectral density plot in stead of ω in rad/s. This makes it easier to relate peak periods to periods of the incoming waves. For such a case the spectral density $S(\omega)$ becomes $S(T)$. The equation for $S(T)$ is presented in equation 2.30.

$$S(T) = \frac{S(\omega)2\pi}{T^2} \tag{2.30}$$

3

Offshore data processing

The first part (section 3.1) of this chapter explains how the load on the SSCV Thialf is measured and what the characteristics of a typical load curve is for an offshore topside installation. Clarification of the influence of friction and determination of the load correction factor is done in section 3.2. Section 3.3 shows the results of a spectral analysis performed on individual load sensors and their influence to the total load measurement. Lastly offshore measurements by motion sensors are considered in section 3.4.

3.1. LOAD MEASUREMENT

3.1.1. REEVING ARRANGEMENT

As explained earlier, the SSCV Thialf consists of two cranes to perform dual lifts. A typical reeving arrangement for this vessel can be found in Figure B for the 20x4 reeving arrangement. The crane reeving arrangement of a SSCV consists of many sheaves connected with wire ropes in between. For this research the SSCV Thialf has been investigated as a reference case since for this vessel a range of offshore measurements is available. Note that this vessel has two similar cranes with both having the same reeving options.

Depending on the circumstances of the lift the reeving arrangement can be adapted by increasing or decreasing the number of wires between the main block and the boom tip. The possibilities are multiples of four and can be found in Table 3.1. The choice lies here between having the load distributed over more parallel wires or having the ability to reach a high water depth with the main hook. This choice is mainly based on two different basic scenarios. One scenario might be that the SSCV has to lift something from its deck or from a barge to the sea floor at a large water depth (wet operation). Another possible scenario is the case where a load has to be installed on or removed from a substructure above sea level (dry operation). For the understanding of the dynamics of the crane-load-vessel system the highest interest lies within the installation above sea level. The reason for this has an origin in the influence of waves on installations. For dry installations the crane capacity is also higher and therefore more dynamic actions are visible in the measurements. Higher amplitudes and at the same time less accuracy problems are expected. For wet installations the shape and water conditions (for example current direction and velocity) induce extra forces which are hard to predict or measure and therefore hard to implement in a numerical model. This lies not in the interest of this research. The configuration that is shown in appendix B is the situation with the highest amount of single wire ropes (4x20 falls) possible since this configuration is commonly used for dry installations.

Table 3.1: Reeving configurations SSCV Thialf

Reeving	[-]	4x3	4x6	4x8	4x10	4x12	4x14	4x16	4x18	4x20
Maximum static hook load	[mT]	1065	2130	2840	3550	4260	4970	5680	6390	7100
Maximum water depth	[m]	807	340	224	154	107	73	48	29	13

3.1.2. LOAD SENSORS

The depicted configuration in appendix B shows that for each crane a set of two load sensors is installed. The sensors are installed as shafts for two separate sheaves which measure the load that is carried by the wires

that run over this sheave. They are positioned at the opposite end of the winches, where two dead ends are connected. This connection results that two wires ropes become one wire. An uneven elevation of the main block can be compensated by controlling two winches separately and this enables to level it. In total there are four winches installed per crane. The so called load measuring pins are sensors which measures the shear in the shaft of the sheave. With strain gauges the shear is transformed into a current signal which is transported to a programmable logic controller (PLC). A strain gauge is a small device which is able to measure the strain on an object, for example due to a force, moment, pressure, tension, weight or temperature. Typically it consists of a long, thin conductive strip in a zig-zag pattern. As the object is deformed, the foil is deformed, causing its electrical resistance to change. The purpose of the foil is that a small amount of stress in the direction of the orientation of the parallel lines results in a larger strain measurement over the effective length of the conductor surfaces. A larger change in resistance is observed than would be with a single straight-line wire, making the measurement more accurate. The term strain consists of tensile and compressive strain, distinguished by a positive or negative sign. Strain gauges can therefore be used to pick up expansion as well as compression. However in this case the sensor only measures in one direction as wire ropes slacks when the force in the wire becomes below zero.

The applied force on the load pin is measured via the installed strain gauges inside a small bore through the center of the pin (see Figure 3.1). To specify the shear planes in the shaft two grooves are lathed on the outside, positioned at the location of the force being measured. When a load is picked up by the crane the tension in the wire rope that runs over the measuring sheave is increasing, resulting in a higher deflection of the shaft. This deflection is constantly measured by the strain gauge and reported to the PLC [Huisman Special Lifting Equipment BV, 2007]. Depending on the angle β (see Figure 3.2) between the two wires of the sheave and the load pin the force in the wire rope can be calculated with equation 3.1.
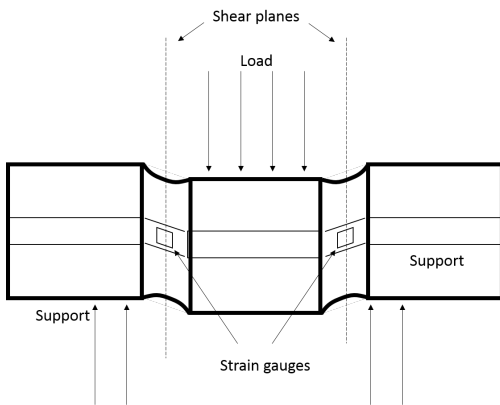
Figure 3.1: Strain gauges on load pin
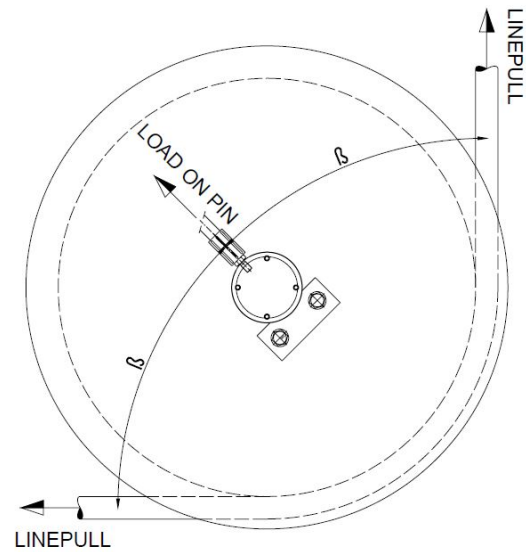
Figure 3.2: Load pin in sheave

$$F_{wire} = \frac{0.5 F_{pin}}{\cos(\beta)} \tag{3.1}$$

Prior to operation the load measuring gauges are calibrate in order to give accurate values for the load that is picked up by the crane. There are some external factors that may cause a difference between the real load and the load on the pin. During the calibration procedure it is already taken into account that the own weight of the sheave, wire rope and main block creates an initial deformation of the load pin and thereby an initial load measurement. The PLC takes this initial situation as the zero load situation. A drawback in the calibration procedure is that the crane is calibrated with the maximum capacity (7100 mT) only. The load measurements at the measuring sheave are done to determine the force of a single wire. For example with a 4x20 reeving arrangement the load for each sensor (out of 2 per crane) should be multiply by 40. The assumption is made

that the load is equally supported. The total load is then the sum of sensor 1 and 2 multiplied by a correction factor. This correction factor is described later in section 3.2.

3.1.3. LOAD CURVE

The various phases (free floating, load transfer, free hanging and set down) for a typical offshore installation of a topside are already explained in section 1.2. Figure 3.3 shows a typical load curve during the installation for the port side crane and Figure 3.4 does this for the starboard crane. The measurements originate from a topside installation project performed by HMC stored in the Crane Information System (CIS). The figure is divided into five parts in time distinguished by four colors. As stated earlier is that the total load measurement (pink line) is carried out by two sensors which are added up (red and blue line). Clearly it is visible that at the first part of the curve the load is almost zero (except own weight of equipment) representing the free floating stage, as there is no tension in the crane wires yet (green interval). However in the second part the tension is increasing from zero to the total load that is carried by the crane (yellow interval). During this phase the load is not increasing completely in a linear line as there is a relative motion between the load and the crane tip due to the dynamic actions. Subsequently the load is more or less a constant value during the free hanging phase where the load is transported from the barge location to the substructure (blue interval). In this phase load fluctuations are present as the vessel is moving by environmental influences of the waves. Additionally at some spots the load curve is lifted to a higher level or brought to a lower level due to crane operations which is explained in more detail in section 3.2. In the fourth phase, or the set down phase, the load is reducing again as the lifted structure is transfered from the crane to the earlier installed foundation(pink interval). When it is fully settled on its offshore support structure and the installation is successfully completed the load reaches zero again. The vessel is back in the free floating phase.
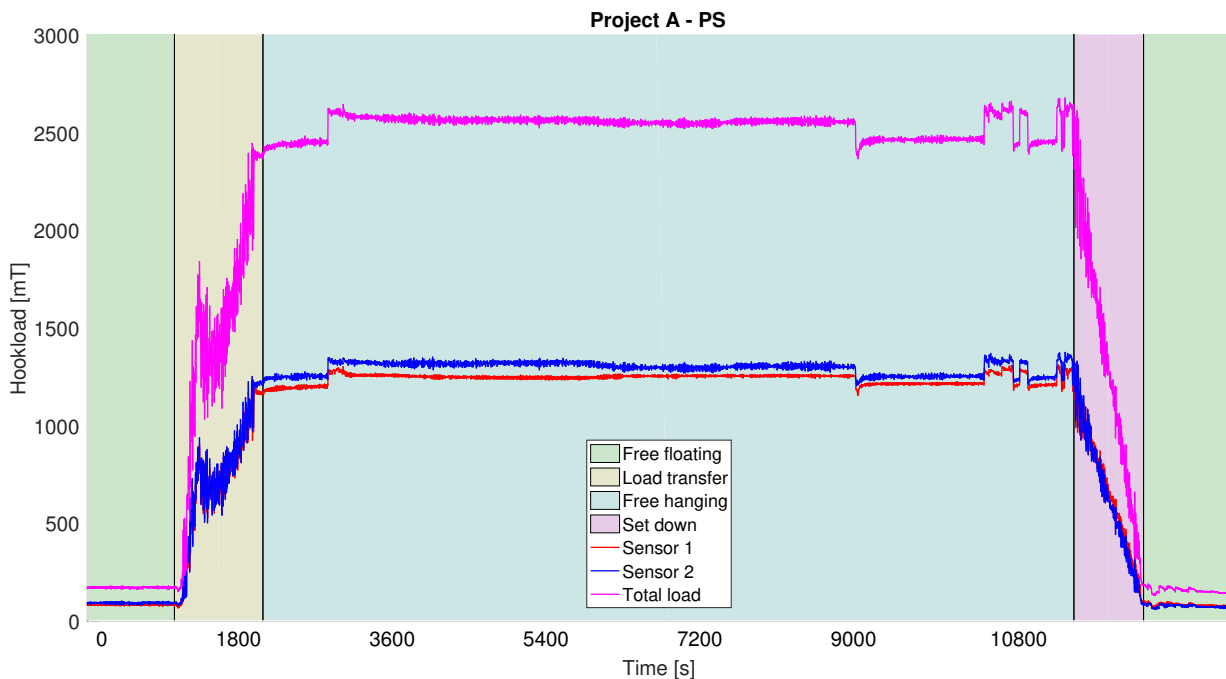
Figure 3.3: Load port side crane
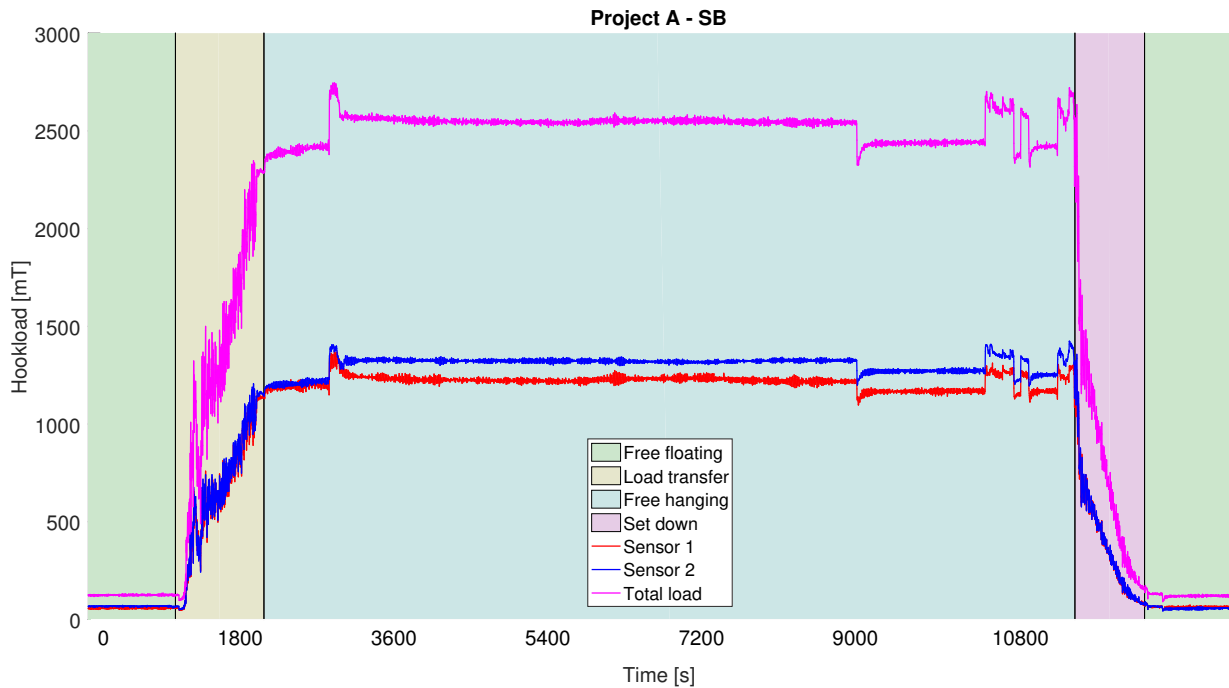
Figure 3.4: Load starboard crane

When comparing the total load supported by the port side and starboard crane there is only a small difference in the total load that is carried by the cranes. This does not always have to be the case as it depends on the weight distribution of the load. When there is an eccentricity in the position of the CoG one crane has to pick up more load than the other crane to compensate the moment created by this offset. An unequal elevation of the lift points or unequal sling angles could also give this same consequence.

3.2. LOAD CORRECTION FACTOR

As explained in section 3.1 at the free hanging phase where the load curve is expected to be constant (excluding dynamical influences) several steps appeared in the load signal. These jumps originate from crane operations performed in this stage. Figure 3.5 shows in detail the time trace of the load signal during the free hanging phase of the port side crane. This figure also shows the sign of the velocity of the crane winches. A positive winch velocity (paying in) corresponds to a hoist operation and a negative winch velocity (paying out) to a lowering operation. When comparing the free hanging part of the load with the crane operation a relation between those two is found. When the crane operator is hoisting the load, there is a step down in the signal and when lowering there is a step up. After the operation is completed the load is still on a different level as it was before, showing a stick-slip effect. In order to correct for this the PLC applies a correction factor C_f after the load of sensor 1 is added up with sensor 2. The corrected load is determined with equation 3.2. The correction factor can be determined with equation 3.3.
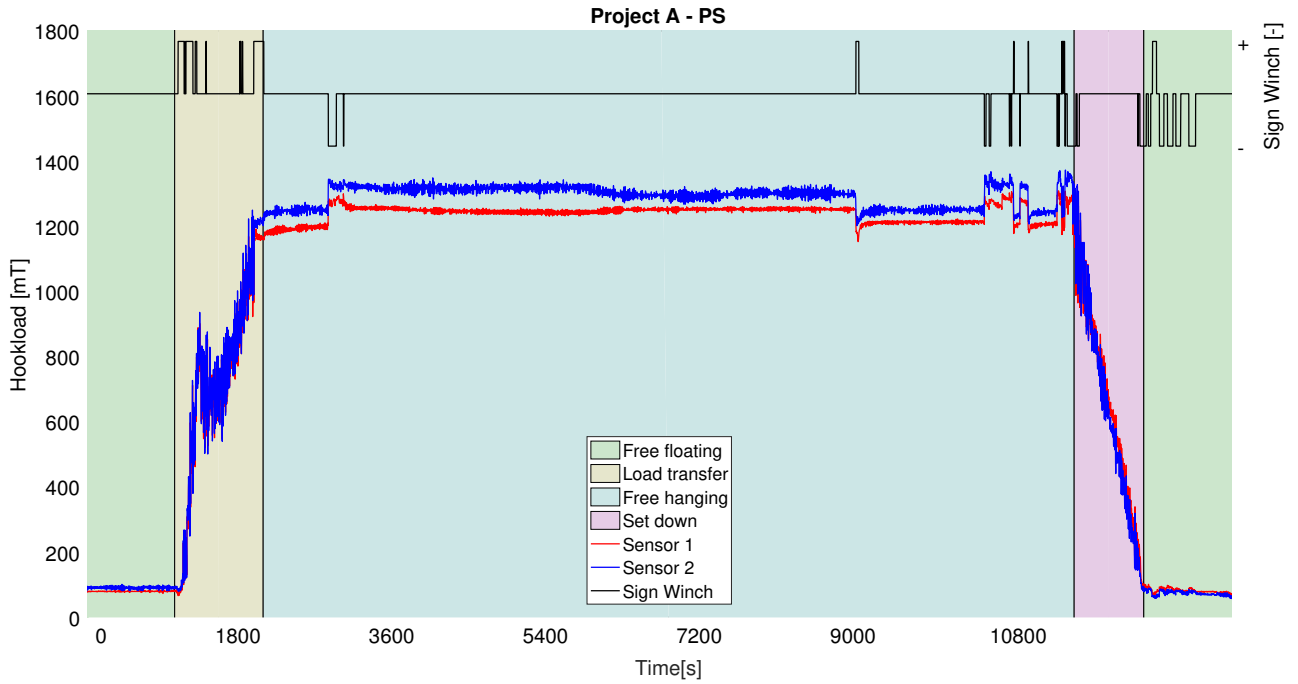
Figure 3.5: Load individual sensors port side

$$Load_{corrected} = C_f(Load_{sensor1} + Load_{sensor2}) \tag{3.2}$$

$$C_f = \frac{Load}{Load + \Delta Load} \tag{3.3}$$

The required load correction factors are determined for several installation projects performed by the SSCV Thialf in the past to get a sense for the amplitude of the friction. This is done by averaging all steps in the signal during the free hanging phase for each sensor and for each operation (hoisting and lowering). Table 3.2 summarizes these correction factors for the port side crane and Table 3.3 for the starboard crane. In Figure 3.6 and Figure 3.7 these values are visualized for the port side crane. Figure 3.8 and 3.9 does the same for the starboard crane. In these figures the correction factor from the actual calibration procedure is added as well represented in red, see Table 3.4.

Table 3.2: Observed load correction factors C_f for the port side crane

	Load [mT]	Lowering		Hoisting		Reeving
		Sensor 1	Sensor 2	Sensor 1	Sensor 2	
Project A	5000	0.94	0.94	1.02	1.03	4x14
Project B	4300	0.91	0.90	1.06	1.06	4x20
Project C	3476	0.96	0.96	1.06	1.04	4x20
Project D	4418	0.92	0.90	1.02	1.03	4x20
Project E	9092	0.90	0.92	1.05	1.05	4x20
Project F	8630	0.91	0.92	1.05	1.04	4x20
Project G	8400	0.86	0.87	1.03	1.04	4x20
Project H	9400	0.89	0.91	1.03	1.03	4x20
Project I	10200	0.90	0.91	1.03	1.04	4x20
Project J (single lift)	3100	0.81	0.85	1.02	1.03	4x20
Average		0.90	0.91	1.04	1.04	
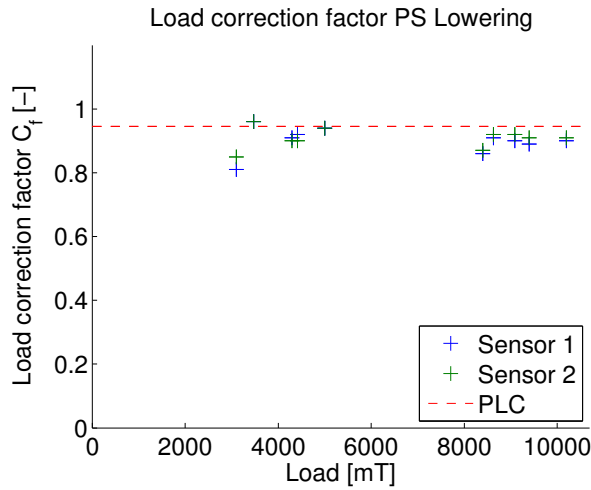
Figure 3.6: Load correction factor PS lowering
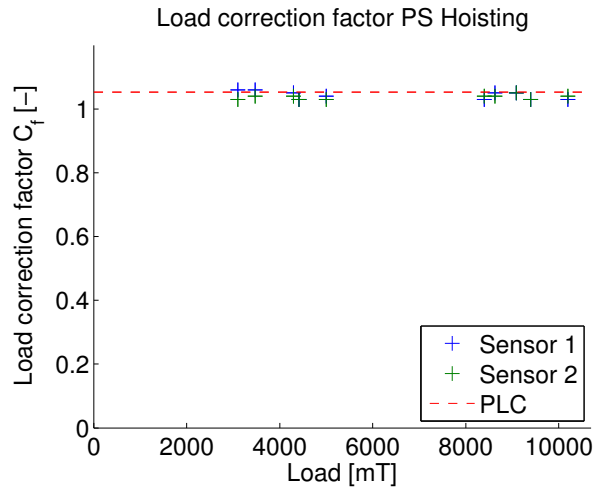
Figure 3.7: Load correction factor PS hoisting

Table 3.3: Observed load correction factors C_f for the starboard crane

	Load [mT]	Lowering		Hoisting		Reeving
		Sensor 1	Sensor 2	Sensor 1	Sensor 2	
Project A	5000	0.91	0.89	1.03	1.04	4x20
Project B	4300	0.91	0.93	1.06	1.09	4x20
Project C	3476	0.93	0.95	1.07	1.06	4x20
Project D	4418	0.92	0.94	1.06	1.05	4x20
Project E	9092	0.93	0.91	1.05	1.05	4x20
Project F	8630	0.92	0.93	1.07	1.06	4x20
Project G	8400	0.91	0.93	1.04	1.05	4x20
Project H	9400	0.90	0.89	1.02	1.03	4x20
Project I	10200	0.91	0.91	1.03	1.04	4x20
Average		0.92	0.92	1.05	1.05	
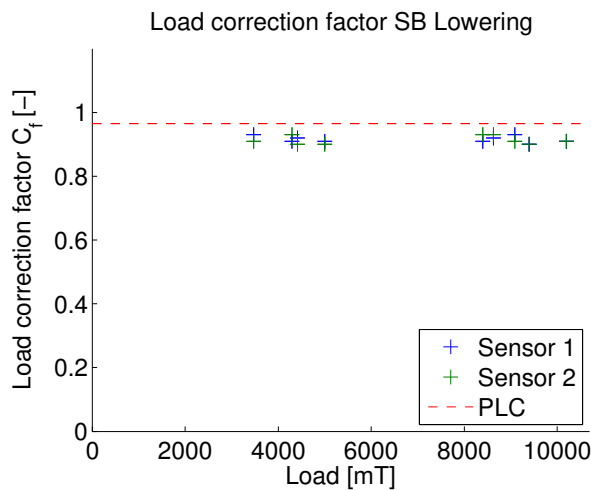
Figure 3.8: Load correction factor SB lowering
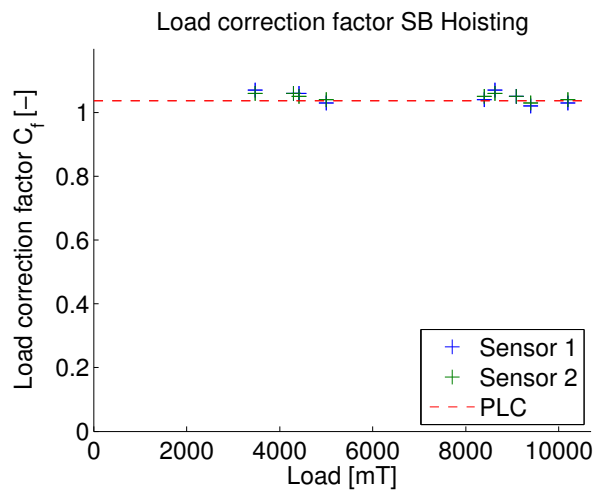
Figure 3.9: Load correction factor SB hoisting

The correction factor C_f is kept constant in the PLC for the load that is supported by the crane. It seems that this is a good approximation as the relative steps that come from the read-out of the sensor are independent

of the load. For the lowering phase the difference is the largest between the calibration value and the actual value. However the load is corrected in a way that the displayed value for the crane driver is higher than the actual topside load, being therefore on the conservative side. It can be concluded that the required load correction factors for the hoisting operation comes closer to the value in the crane PLC than for the lowering operation. It might appear that some projects differ a lot from the PLC value, but this comes from the fact that the sensors are not calibrated again after the reeving arrangement is adapted for another project.

Table 3.4: Load correction factors C_f SSCV Thialf

	Port side	Starboard
Hoisting	1.0524	1.0366
Stop after hoisting	1.0000	1.0000
Lowering	0.9550	0.9276
Stop after lowering	0.9650	0.9452

The load curves are corrected with the correction factors from Table 3.4 which are determined by calibration tests performed. The load characteristics are now corrected as shown in Figure 3.10 for the port side crane.
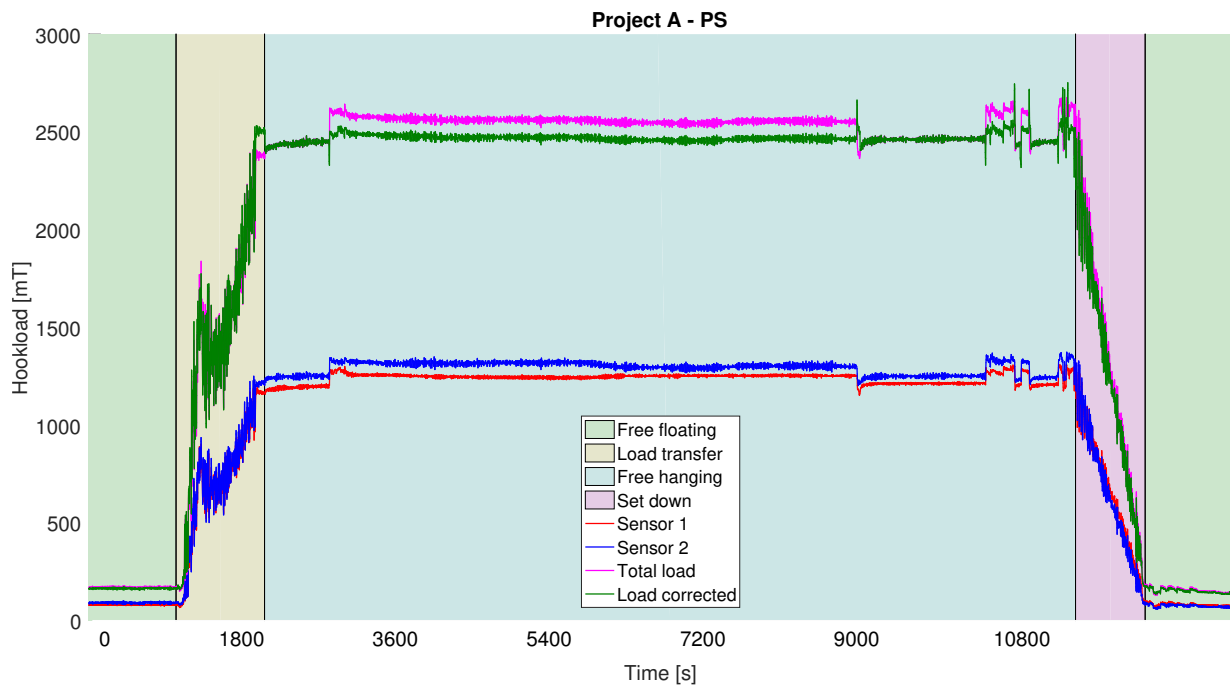
Figure 3.10: Crane load port side with correcting

3.3. SPECTRAL ANALYSIS

For a stationary part of a signal it is possible to perform a spectral analysis. This signal can be thought of as a collection of frequency components. In order to extract these components the situation has to be stationary for the duration of the observation and the duration should be long enough. Creating spectra from signals that cover a short period should be done with care. As a rule of thumb hundred cycles should be present in the time signal to be able to create a proper spectrum. The effect of frequency bin size is explained before in section 2.5. This section goes into depth in the frequency components of individual load sensors and their relation with the total load measurement for both the starboard and port side crane.

3.3.1. LOAD TRANSFER STAGE

Firstly this is performed for the load transfer stage and later for the free hanging stage for the same topside installation that was considered in the previous section. The load response of this stage is relatively short and therefore the frequency analysis can only be made of short load measurement. It was found that the load in this stage is in phase. The square root of the zeroth order moment m_0 of the total signal correspond more

or less to the sum of the individual square roots zeroth order moments. See Figures 3.11 and 3.12 for the response of the load transfer stage respectively for the port side and starboard cranes. The $\sqrt{m_0}$ based on the area is plotted in the legend. A detailed time trace of the load measurement in Figure 3.13 shows clearly that the total signal is made up out of the two individual sensors measuring in phase.
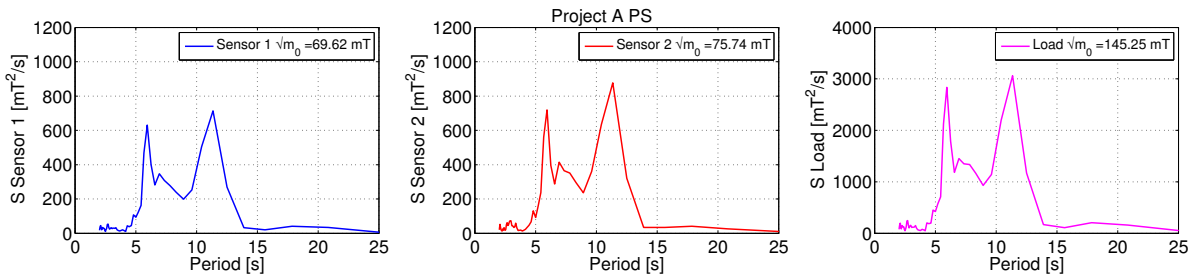
Figure 3.11: Spectrum load PS - load Transfer
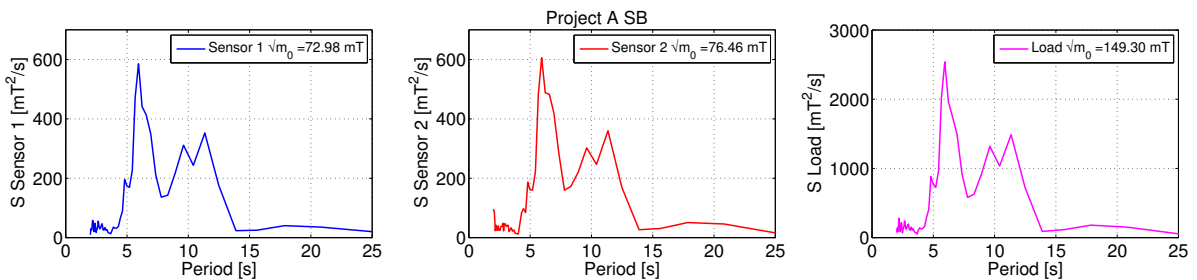
Figure 3.12: Spectrum load SB - load Transfer
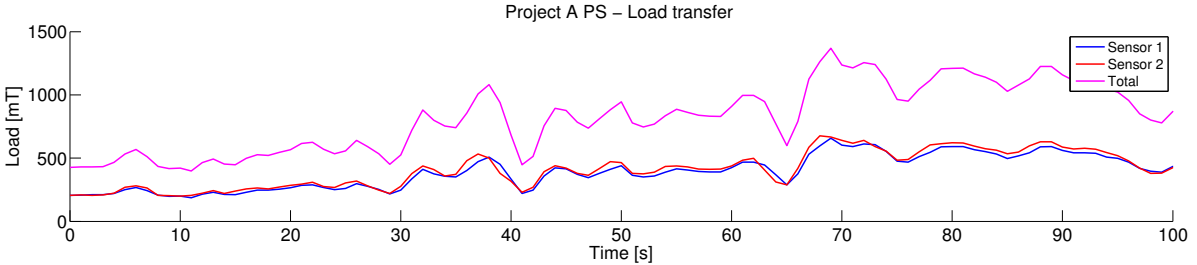
Figure 3.13: Time trace PS - load transfer

3.3.2. FREE HANGING STAGE

Figure 3.15 shows the PS crane response for the free hanging stage. Figure 3.16 does the same for the SB crane. The corresponding time traces were given earlier in Figure 3.3 for the PS crane and Figure 3.4 for the SB crane. In Figure 3.14 the time trace of the port side crane during the first 500 s is given in detail.
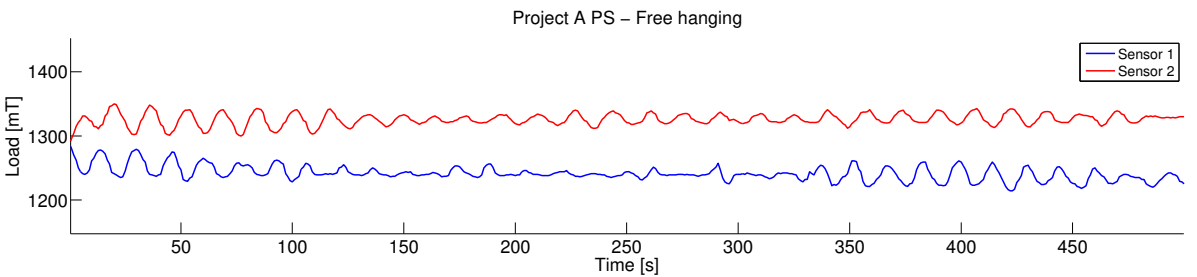
Figure 3.14: Time trace PS - free hanging
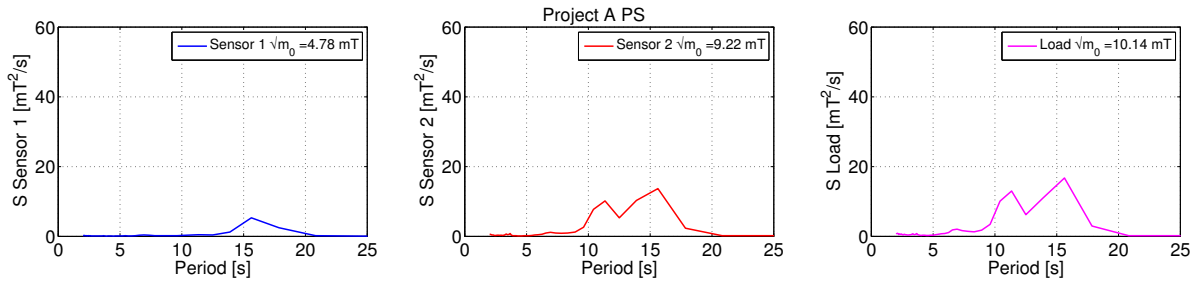
Figure 3.15: Load Spectrum PS- free hanging
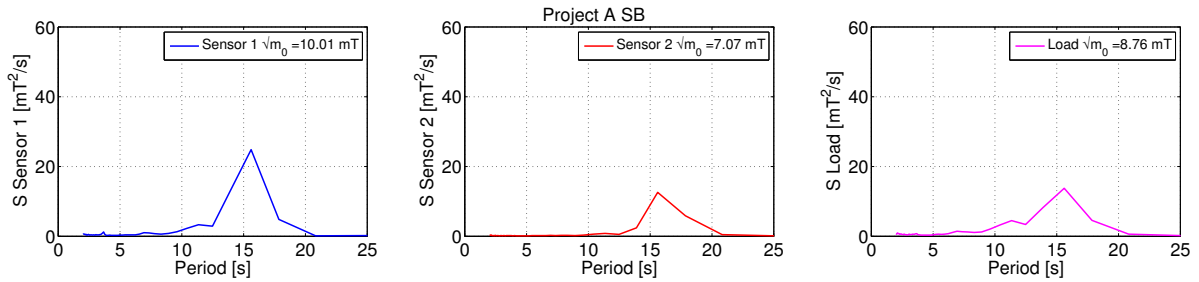
Figure 3.16: Load spectrum SB - free hanging

Remarkable is that the individual sensors do not measure the same amount of energy and not the same peak periods can be distinguished. Clearly in the time trace it is visible that the measurements by the individual sensors cancel each other out at some points. Also are the sensors measuring a difference of around 75 mT whereas they were equal in the load transfer phase. A spectral analysis was performed for all projects performed by the SSCV Thialf with available data sets. The graphs are made up in the same manner and are displayed in appendix D. An attempt was made to model the rotation of the main block in LiftDyn and thus the out of phase elongation of the hoist wires that are measured. However this did not lead to a difference in the phase plot (Figure E.3) at the corresponding mode, being the sway-roll mode (topside-Thialf). More elaboration on this topic can be found in appendix E. Further research is required to investigate what is happening in every certain project and how to model this rotation.

3.4. MOTION MEASUREMENT

This section describes how the motions of a particular vessel are measured. On board of the SSCV Thialf a Motion Response Unit (MRU) is installed. The MRU measures translational change in velocity by means of accelerations and rotational change in position by means of angular velocity. These changes are used to determine the position and orientation of the vessel in six degrees of freedom (DoF). Inertial motion measurement can similarly be divided into two tasks: inertial orientation measurements and inertial linear translation measurements. Inertial orientation measurement requires a gyro-like device which physically measures angular acceleration, angular velocity or angular displacements. Some sensors physically measure angular rate, and integrate the rate over time to compute the angular displacement in the sensor interface. This allows an angular rate sensor to perform like an angular displacement sensor. The inertial linear translation measurement requires acceleration measurement. There exists no inertial sensor that directly measures the physical linear velocity. Consequently, the linear motion is integrated over time twice to obtain the translation and this puts high requirements on the accelerometers.

Using a rate of change measurement system to measure position and orientation is known to introduce drift. Over time this drift influence grows and the position and orientation of the vessel with respect to the target platform becomes inaccurate. In order to correct for the drift other sensors like a GPS is used to correct the signal over time. Also, the orientation measurement must be very accurate to take the unavoidable gravitational component of the acceleration into account. The motion data of the SSCV Thialf is stored both in IRIS and K-IMS (Kongsberg Information Management System). However research performed earlier [Ottens, 2016] concluded that the measurements by the IRIS system are filtered. Therefore only the motion measurements

of K-IMS are used in the latter imposed motion model described in chapter 5.

Normally the motion of the load is also measured during its lift operation by a MME (Motion Measuring Equipment). This equipment consists of a 6DOF sensors, a GPS, a transmitter, a receiver, batteries, and a solar panel. These devices are standalone and placed on the topside in the free floating stage. Via remote monitoring an analysis can be performed during critical events of the installation. The data is saved locally and can be used for later studies. Synchronizing two different measurement systems, one for the motion of the vessel and one for the motion of the load could not be done accurately enough to impose them simultaneously in the imposed motion model in chapter 5.

4

Numerical model

In this chapter it is described how the equations of motion are derived to set up the numerical model of the crane assembly. Firstly, an overview is given of various rigging equipment which are part of the total lifting equipment in section 4.1. In 4.2 section of this chapter an explanation is given to acquire the motions of the various sheaves in the crane reeving. Hereafter section 4.4 is about damping of steel wires and section 4.5 describes the equivalent stiffness due to the serial and parallel parts of the hoist wire reeving. Finally the resulting motions of the sheaves and the individual wire rope forces are explained in section 4.6 and 4.7.

4.1. RIGGING EQUIPMENT

During lift operations the connections between the crane hook and the load are called rigging materials. This generally consists of slings or grommets and spreader bars. A sling (Figure 4.1) is a steel wire rope with eyes and/or sockets at both ends and where applicable, connected by means of shackles. This steel wire consists of strands twisted around a core wire. Use of a synthetic material is also possible, but left out of this research, since steel wires are commonly used. On the other hand a grommet (Figure 4.2) is a sling with an endless steel wire and is produced from one single length of steel wire rope.

Figure 4.1: Sling

Figure 4.2: Grommet

Spreader bars (see Figure 4.3) are designed to spread the connection points of a sling. Basic spreader lifting bars have two connection points or lugs distributed evenly on the top side of the bar, usually at each end. These lugs evenly divide the weight of the load and are eliminating the stress on a single lifting point. The underside of a spreader bar usually has two (or more) attachment points from which the load is suspended. The attachment points on a spreader bar allow for a direct upward hoist, and stop the load being damaged by angled slings wearing against it.

Figure 4.3: Spreader bar

Figure 4.4: Main block

All attachments from the load to be lifted and the crane are made at the block. The crane vessels that HMC owns have three lifting capacities being the whip hoist, the auxiliary hoist and the main hoist. The focus of this thesis is on the main block (see Figure 4.4). It consists of four prongs made out of steel where the eyes of the rigging equipment are laid over. Appendix A derives the equations of motion for a topside that is attached to the main block. The lower part of the main block is able to hinge along two axes build up on one side of the structure. In order to avoid that it is pushed away due to the wind while having no load tug wires are attached. Connected on top of the main block are the hoist wires which run to the boom tip and go through the crane structure to end up in one of the four crane winches.

4.2. SHEAVE FRICTION MODEL

This section describes the model created which relates an applied force at the main block and operation of the crane to the forces of the individual wire ropes. Earlier in section 3.1 it was clarified how the measurement sheaves are making a signal presented to the crane driver from the forces in some individual wires. As can be seen in the reeving arrangement of the crane in Figure 4.5 some parts of the wires are in parallel and some parts are in series. As there are eighty wires (4x20) in parallel to support the main hook a number of eighty sheaves are present for only the parallel part. The reeving diagram is subdivided by four colors which correspond to the letters A until D to make a clear distinction (see Table 4.1).

Table 4.1: SSCV Thialf reeving distinction

Color	Letter	Position	Winch
Purple	Left	A	Left Front Drum
Green	Center Left	B	Right Front Drum
Blue	Center Right	C	Left Rear Drum
Orange	Right	D	Right Rear Drum

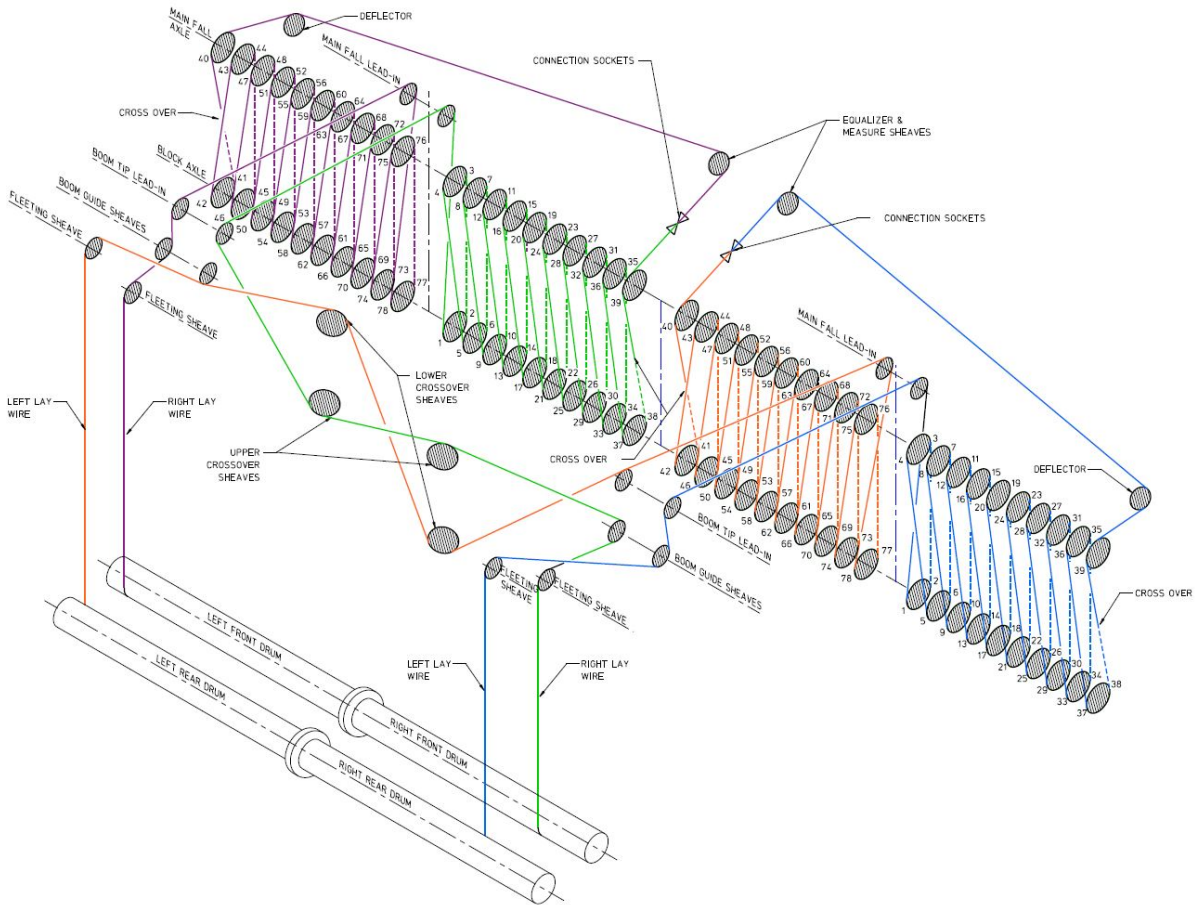Figure 4.5: Load port side crane

A more detailed overview of the reeving in 2D with the position of the sheave axles can be found in Figure 4.6. In Figure 4.7 the part is shown where the parallel wires come together in the main block. The sheaves of the main fall axle are associated with the sheaves shown in Figure 4.8 positioned at boom tip.
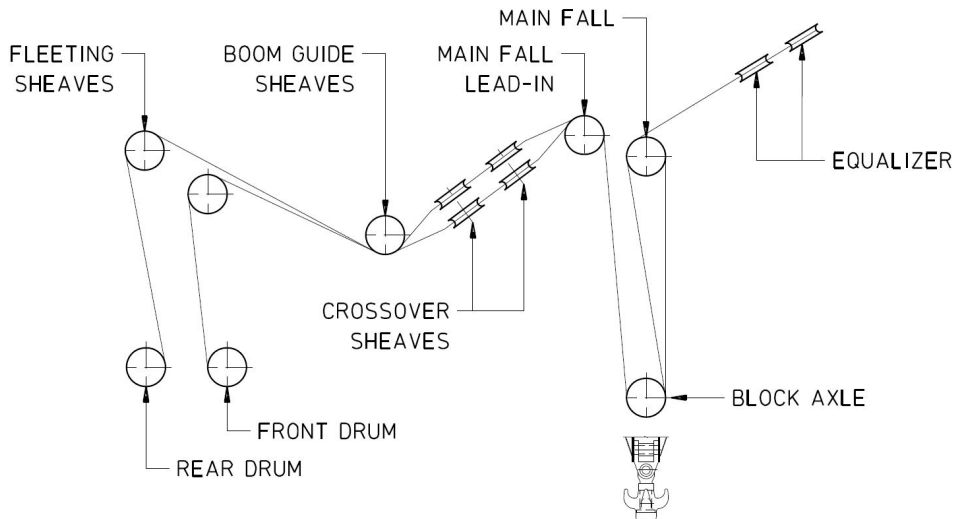

Figure 4.6: 2D view of crane reeving arrangement

31

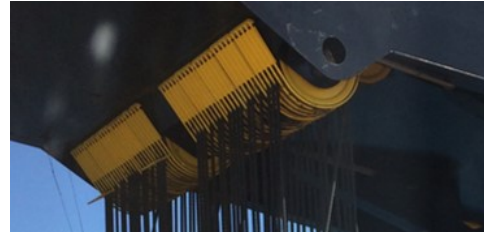Figure 4.7: Top view of block axle at main block

Figure 4.8: Main fall axle

Additionally two times eleven sheaves are configured in the crane structure to direct the wire from the crane winches to the parallel parts of the reeving and also to direct the wire to the equalizer sheaves. At the equalizer sheaves two separate wire parts are connected with connection sockets to combine it to one. Note that these two equalizer sheaves measure the load of the wire that runs over it by determining the stress in the sheave pin with strain gauges. Further explanation on this topic was earlier described in section 3.1. For each sheave that is present in the reeving configuration an equation of motion is derived. A visualization of a typical sheave is found in Figure 4.9 and the sheave properties as they used in the model can be found in Table 4.2. The mass moment of inertia is determined by making a 3D drawing in Solidworks where it is automatically determined.
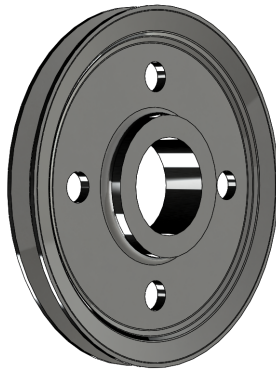
Figure 4.9: Sheave in the crane reeving

Table 4.2: Sheave properties

Radius	R	[m]	0.7
Mass moment of Inertia	J	[kgm^2]	150
Mass	m	[kg]	650

4.3. EQUATIONS OF MOTION SHEAVE

Consider the same dynamical system from section 2.4.2 depicted in Figure 4.10. It consists of an extensible wire that is pulled over a sheave as shown in the figure. Both ends are fixed to the earth and assumed to be immovable. Such a configuration describes systematically the rotation ϕ_i of a sheave. The parameters of the system are indicated in the figure. The sheave is assumed to have radius R, mass moment of inertia J and rotate about its axis with dry friction. It is assumed that no slip occurs between the sheave and the wire, which also implies that the wire can be assumed not to extend (to keep the initial length) over the contact area with the sheave. This results in the same wire displacement as the angular displacement multiplied by the radius. It is justified to use this assumption because the normal force of the wire is high resulting in a high contact friction between the wire and the groove of the sheave. The segments of the wire are extensible and their motion is governed by the equation for longitudinal motion of a rod.

Figure 4.10: Extensible wire attached to fixed points over a sheave

The dynamic interface condition is the dynamic balance of moments applied to the sheave. This balance can be found in equation 4.1.
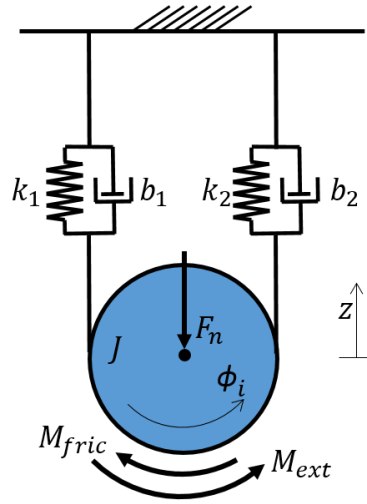
$$J\ddot{\phi}_i = k_1 R^2(-\phi_i) + k_2 R^2(-\phi_i) + b_1 R^2(-\dot{\phi}_i) + b_2 R^2(-\dot{\phi}_i) - M_{fric} + M_{ext} \qquad (4.1)$$

where $\phi(t)$ is the angle of rotation of the sheave that is assumed to be positive in the counterclockwise direction and $\dot{\phi}(t)$ its time derivative. k and b are the stiffness and damping coefficients of the steel wire. M_{fric} (equation 4.2) and M_{ext} are the friction moment and external moment respectively. This friction moment is derived earlier in section 2.4.2.

$$M_{fric} = -\mu F_n r \qquad (4.2)$$

The dynamic balance of vertical forces is written in equation 4.3.

$$m\ddot{z} = k_1 R^2(-\phi_i) + k_2 R^2(\phi_i) + b_1 R^2(-\dot{\phi}_i) + b_2 R^2(\dot{\phi}_i) - F_{pin} \qquad (4.3)$$

where z is the translation of the sheave in vertical direction, $\dot{z}$ its time derivative and m the mass of the load to be lifted. Due to the dynamic effect of the translation in z-direction the value of the force on the pin of the sheave F_{pin} is not a constant value. This leads to a change in the friction moment in equation 4.2. The friction moment results in a difference between the force in wire 1 and in wire 2. Later in section 4.7 the determination and the validation of the friction factors is explained in order to correspond to the friction forces which are determined during calibration tests. The forces in the individual wires are calculated by taking the sum of the restoring and damping force, see equation 4.4.

$$F_{wire} = kR\phi_i + bR\dot{\phi}_i \qquad (4.4)$$

Three different cases are possible whether the sheaves can beside rotate also translate as they are not fixed in the crane structure:

- Fixed position between sheaves

- Fixed position top sheave, free translation bottom sheaves

- Free translation of two sheaves connected to sheave i

These cases are explained separately:

Case 1: Fixed position between sheaves
In the first case (Figure 4.11) a situation is considered where sheave i is connected by wire 1 at sheave $i-1$ and wire 2 at sheave $i+1$. The two later sheaves are fixed in the crane structure and have a fixed distance related to sheave i. The dashed lines represent continuities of the wires after the sheave. The force in wire

1, positioned between sheave $i-1$ and i, is calculated with the angular displacement and angular velocity of those sheaves, see equation 4.5. The same holds for the force in wire 2, see equation 4.6. By determining the elongation on both sides of the sheave the resulting moment can be determined with equation 4.7.
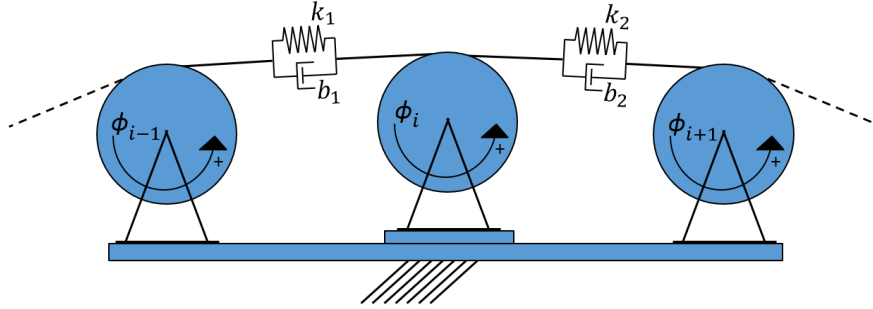

Figure 4.11: Case 1: Sheave i connected with two fixed sheaves

$$F_1 = k_1(\phi_{i-1}R - \phi_i R) + b_1(\dot{\phi}_{i-1}R - \dot{\phi}_i R) \tag{4.5}$$

$$F_2 = k_2(\phi_i R - \phi_{i+1}R) + b_2(\dot{\phi}_i R - \dot{\phi}_{i+1}R) \tag{4.6}$$

$$\sum M_{\phi_i} = k_1 R^2(\phi_{i-1} - \phi_i) + k_2 R^2(-\phi_i + \phi_{i+1}) + ... \\ b_1 R^2(\dot{\phi}_{i-1} - \dot{\phi}_i) + b_2 R^2(-\dot{\phi}_i + \dot{\phi}_{i+1}) - M_{fric} \tag{4.7}$$

Case 2: Fixed position top sheave, free translation bottom sheaves
The second case (Figure 4.12) describes a situation where one sheave is able to rotate and is fixed in all other directions and one sheave is able to rotate and translate. This extra translation results in an additional term z for the elongation of the spring, see equation 4.8 and 4.9 for the forces and equation 4.10 for the total moment. The extra term is underlined.
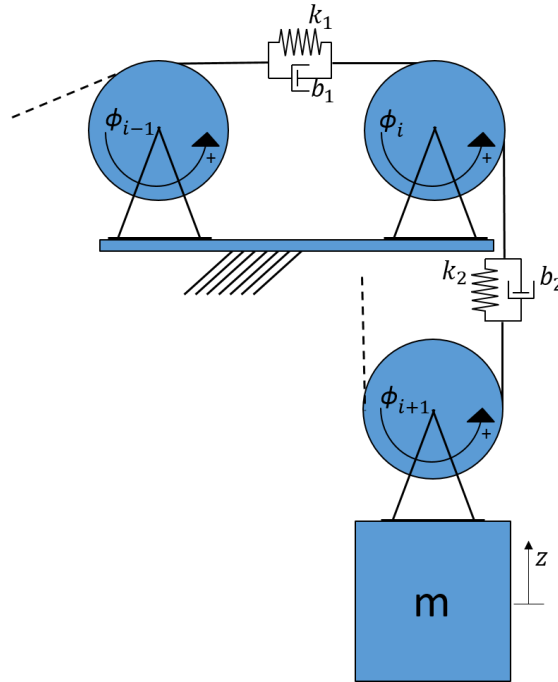

Figure 4.12: Case 2: Sheave i connected with one fixed to the crane and one fixed to the main block

$$F_1 = k_1(\phi_{i-1}R - \phi_i R) + b_1(\dot{\phi}_{i-1}R - \dot{\phi}_i R) \tag{4.8}$$

$$F_2 = k_2(\phi_i R - \phi_{i+1}R - \underline{z}) + b_2(\dot{\phi}_i R - \dot{\phi}_{i+1}R - \underline{\dot{z}}) \tag{4.9}$$

$$\sum M_{\phi_i} = k_1 R^2(\phi_{i-1} - \phi_i) + k_2 R(-\phi_i R + \phi_{i+1}R + \underline{z}) + ...$$
$$b_1 R^2(\dot{\phi}_{i-1} - \dot{\phi}_i) + b_2 R(-\dot{\phi}_i R + \dot{\phi}_{i+1}R + \underline{\dot{z}}) - M_{fric} \tag{4.10}$$

Case 3: Sheave connected with two free translation sheaves

The third and last case (Figure 4.13) illustrates the condition where sheave i is attached to two other sheaves which are able to rotate and translate in one direction. This translation leads to an additional term z in both calculations of the wire forces, see equation 4.11 and 4.12 for the forces. The total moment is determined with equation 4.13. Both additional terms are underlined.
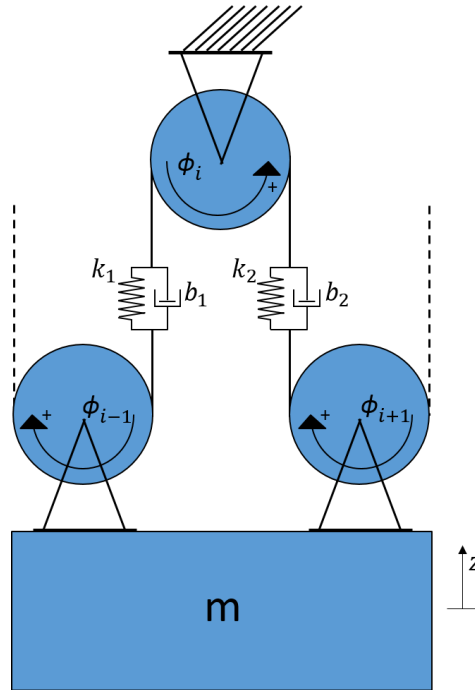

Figure 4.13: Case 3: Sheave i connected with two free sheaves

$$F_1 = k_1(\phi_{i-1}R - \phi_i R - \underline{z}) + b_1(\dot{\phi}_{i-1}R - \dot{\phi}_i R - \underline{\dot{z}}) \tag{4.11}$$

$$F_2 = k_2(\phi_i R - \phi_{i+1}R - \underline{z}) + b_2(\dot{\phi}_i R - \dot{\phi}_{i+1}R - \underline{\dot{z}}) \tag{4.12}$$

$$\sum M_{\phi_i} = k_1 R(\phi_{i-1}R - \phi_i R - \underline{z}) + k_2 R(-\phi_i R + \phi_{i+1}R + \underline{z}) + ...$$
$$b_1 R(\dot{\phi}_{i-1}R - \dot{\phi}_i R - \underline{\dot{z}}) + b_2 R(-\dot{\phi}_i R + \dot{\phi}_{i+1}R + \underline{\dot{z}}) - M_{fric} \tag{4.13}$$

With the three cases a model is created with all the sheaves present in the crane reeving configuration. This creates a 1D model in the direction of the hoist wires with 102 degree of freedom. It solves for each sheave its equation of motion with dry friction which can result in a stick-slip effect. The distance between all sheaves is not equal due to the structure of the crane and construction choices of the crane manufacturer. In some parts the distance is fixed, but in some parts the distance between the sheaves and thus the length of the wire is depending on for example the angle of the boom or the gap between the main fall lead in and the main hook. The spring stiffness k of a wire rope segment is therefore not constant.

4.4. DAMPING OF STEEL WIRE ROPES

In section 2.3 the damping in the axial direction of steel wire ropes is already widely discussed. For the numerical model one of the variables is also the amount of damping that is present in the steel wire ropes. The damping effects the motion of sheaves in the numerical model that is created. However, without a specialized experiment it is hard to predict what the exact value for the damping is as it depends on many variables. It is a fact that for steel wire ropes the damping is a function of the amplitude, frequency and history of the vibration [Vanderveldt et al., 1973].

Viscous damping (due to the internal friction and among other things) of wire ropes is therefore not a constant value. Still a considerable amount of damping should be taken into account. An initial value to verify the model a percentage of the critical damping is used for the axial elongation of the wires. [Chaplin, 1991] states that the logarithmic decrement δ lies within a range of 0.02-0.20 for six strand and multi-strand ropes. With equation 2.18 an estimate for the damping ratio ζ can be made which can be used to find an absolute value for the damping coefficient b with equation 4.14.

$$b = \zeta b_{crit} = \frac{1}{\sqrt{1 + \left(\frac{2\pi}{\delta}\right)^2}} 2\sqrt{km} \qquad (4.14)$$

Where ζ is the dimensionless damping coefficient, m the mass of the load and k the stiffness of the wire. The value for the damping that is used is to δ=0.1 which correspond to a ζ of 1.6%.

4.5. EQUIVALENT STIFFNESS

As was explained earlier in section 3.1.1, it is clear that there is not an equivalent distance between the sheaves in the crane wire reeving configuration from appendix B. Partly of the reeving is in parallel and partly of the total reeving is in series. Because of this the stiffness of the reeving can be written as an equivalent stiffness k_{eq} build up by the individual components of stiffness of wire ropes between two sheaves. In general the stiffness k can be calculated with equation 4.15 when a constant Young's Modulus E and effective cross-sectional area A_{eff} is assumed.

$$k = \frac{EA_{eff}}{L} \qquad (4.15)$$

For springs in parallel or in series the equivalent stiffness, elongation and force can be calculated following Table 4.3:

Table 4.3: Equivalent stiffness, elongation and force

Quantity	Unit	Parallel	Series
Equivalent spring constant	[N/m]	$k_{eq} = k_1 + k_2$	$\frac{1}{k_{eq}} = \frac{1}{k_1} + \frac{1}{k_1}$
Elongation	[m]	$\Delta L_{eq} = \Delta L_1 = \Delta L_2$	$\Delta L_{eq} = \Delta L_1 + \Delta L_2$
Force	[N]	$F_{eq} = F_1 + F_2$	$F_{eq} = F_1 = F_2$

Figure 4.14 and 4.15 shows how the wire rope is going through the system from the drum to the dead end where two wires originate from two different winches are connected. The colors in the figures correspond to the colors of the wire reeving illustrated in appendix B. The purple wire is passing through a number of four sheaves before it is part of the parallel section, whereas the green wire has to pass six sheaves. As the orange and blue part are exactly symmetrical to the blue and purple part respectively they are not depicted. Later a factor 2 is applied to take their contribution to the overall stiffness into account. The corresponding lengths L_1 until L_{10} between each sheave is determined from drawings of the construction of the crane and are summarized in Table 4.4 for the purple part and in Table 4.5 for the green part. Note that L_2 and L_6 are a function of the boom angle α_{boom} as the wire would become larger when the boom is horizontal compared to a nearly vertical situation.
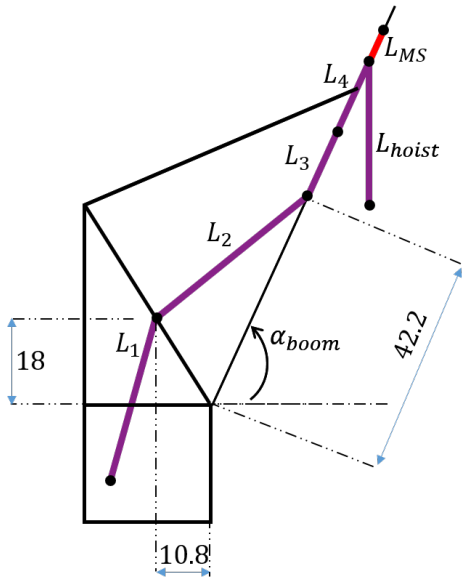
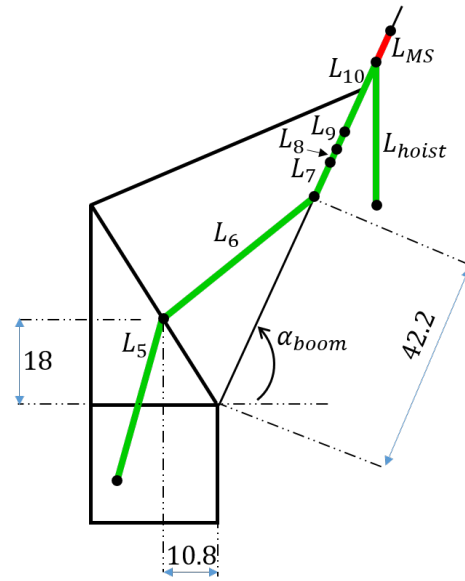Figure 4.14: Position sheaves part A of crane reeving

Figure 4.15: Position sheaves part B of crane reeving

Table 4.4: Length between sheaves purple part

		From	To	Length
L_1	[m]	Left rear drum	Fleeting sheave	27.5
L_2	[m]	Fleeting sheave	Boom guide sheave	$f(\alpha_{boom})$
L_3	[m]	Boom guide sheave	Boom tip lead-in	28.8
L_4	[m]	Boom tip lead-in	Main fall lead-in	20.5

Table 4.5: Length between sheaves green part

		From	To	Length
L_5	[m]	Left rear drum	Fleeting sheave	27.5
L_6	[m]	Fleeting sheave	Boom guide sheave	$f(\alpha_{boom})$
L_7	[m]	Boom guide sheave	Lower crossover sheave 1	12.8
L_8	[m]	Lower crossover sheave 1	Lower crossover sheave 2	3.2
L_9	[m]	Lower crossover sheave 2	Boom tip lead-in	12.8
L_{10}	[m]	Boom tip lead-in	Main fall lead-in	20.5

In general the stiffness of each single hoist wire segment is determined by its stiffness EA_{eff} and the length that is suspended. For the parts in both Figures 4.14 and 4.15 the stiffness can be calculated with equation 4.16. For the stiffness k_2 and k_6 the calculation for the length depending on the boom angle α_{boom} has been incorporated, see equation 4.17. Also the stiffness k_{MS} for the wire part between the load measuring sheave and the main fall lead-in can be determined by its length. This wire rope part has a fixed distance of 12.8 m.

$$k_i = \frac{EA_{eff}}{L_i} \tag{4.16}$$

$$k_2 = k_6 = \frac{EA_{eff}}{L_2} = \frac{EA_{eff}}{\sqrt{(10.8 + 42.2\cos(\alpha_{boom}))^2 + (-18 + 42.2\sin(\alpha_{boom}))^2}} \tag{4.17}$$

After taking the contribution of each segment correctly into account the total equivalent stiffness of the serial part of the hoist wires can be calculated with equation 4.18 for part A (and D) of the reeving and 4.19.

$$k_{1-4} = \left(\frac{1}{\sum_{i=1}^{4} k_i}\right)^{-1} \tag{4.18}$$

$$k_{5-10} = \left(\frac{1}{\sum_{i=5}^{10} k_i} \right)^{-1} \tag{4.19}$$

The quasi-static displacement of the main block in the model can be determined with equation 4.20. Here n_{falls} is the total number of parallel wires that is in the reeving arrangement, being 4x20 for the example in appendix B. Note that the stiffness k_{hoist} depends on the length of the hoist wires (distance from crane tip to main block) that are suspended. The quasi-static displacement is computed by the gravity force F_g that corresponds to the suspended load.

$$\Delta z = \frac{F_g}{k_{hoist}} + \frac{\frac{2F_g}{n_{falls}}}{k_{1-4}} + \frac{\frac{2F_g}{n_{falls}}}{k_{5-10}} + \frac{\frac{4F_g}{n_{falls}}}{k_{MS}} \tag{4.20}$$

However, when taking the corresponding wire lengths and using the definition of a constant stiffness $k = \frac{F}{\Delta z}$ equation 4.20 can be rewritten as 4.21 to get an equivalent stiffness for the hoist wires including the wires in the crane structure and the redistribution over the sheaves. The constant c is fixed due to the length between the sheaves in the crane structure and only depends on the crane boom angle α_{boom} in equation 4.22. It is derived by rewriting equation 4.18, 4.19, 4.17 and 4.20.

$$k_{eq} = \frac{EA_{eff}n_{falls}}{L_{hoist}n_{falls} + c} \tag{4.21}$$

$$c = 358.4 + 4 * \sqrt{(440 + 911 * \cos(\alpha_{boom}) + 1780 * \cos(\alpha_{boom})^2 - 1519 * \sin(\alpha_{boom}) + 1780 * \sin(\alpha_{boom})^2)} \tag{4.22}$$

4.6. SHEAVE MOTIONS

The numerical model is created for the whole reeving arrangement as depicted in appendix B. An overview and explanation of the model in Simulink can be found in appendix F. As was explained in section 3.2 earlier a step in the hook load is found while operating the crane both in lifting and lowering. Therefore there are two base cases studied, one of the cases is a hoisting operation and the other case a lowering operation.

4.6.1. INITIAL CONDITIONS

Both cases start with an initial load of 3000 mT hanging in the crane. Due to the elongation of the wires between the winches and the main fall axle all sheaves have an initial rotation. The elongation needs to be redistributed over the other sheaves in the parallel part. Moreover due to the load all the wires in the parallel part elongates equally as well. Both results in a initial displacement of the load in z-direction simultaneously. The initial condition of the topside can be checked with the equivalent stiffness calculated earlier in section 4.5. The corresponding initial conditions are the values of the displacement at t=0 s (before any crane operations) in Figure 4.17.

4.6.2. LOWERING

Figure 4.16 shows the wire displacement over the winch in meters. As the crane is controlled by a set of four winches each winch pays out a total of 1.0 m simultaneously in this case. The lowering operation starts at t=1 s and ends at t=11 s. Due to the choice of sign for the winch (paying out is positive) the displacement goes from 0 m to 1.0 m. The topside displaces from its initial condition (-0.0672 m) to its final situation at -0.1172 m. A total wire length of 4.0 m was distributed over 80 wires, resulting in an overall topside displacement of $\frac{4}{80} = 0.05$ m negative. This equals a decrease of the topside height of $-0.1172 - -0.0672 = -0.05$ m.
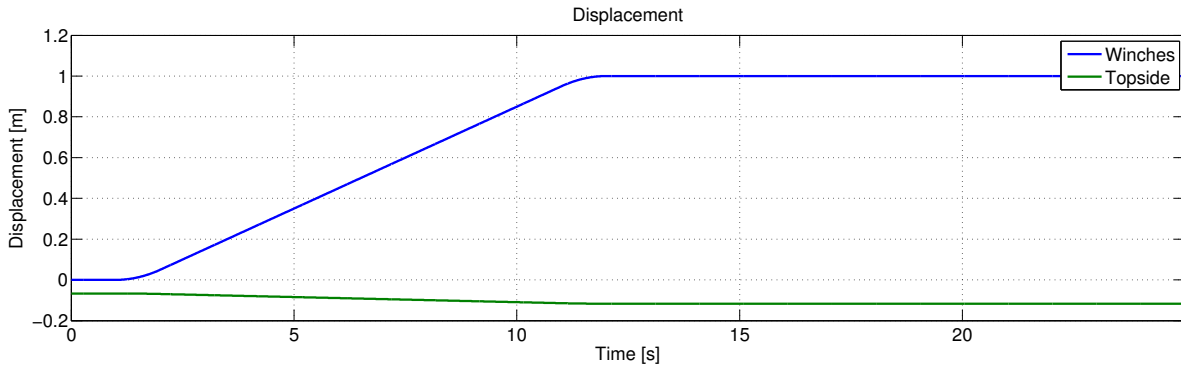
Figure 4.16: Wire displacement of winches and displacement of topside during lowering

In Figure 4.17 the wire displacement of each sheave for part A of the sheave assembly is drawn. This wire displacement x is calculated by the rotation of the sheave multiplying by the radius (equation 4.23). The numbering of the sheave goes from left to right from the crane reeving diagram in appendix B. The top sheaves are the ones at the main fall axle and the bottom sheave are on the block axle. Again the displacement starts at t=0 s on its initial condition due to the initial load that elongated all hoist wires. While paying out wire by the winch the sheaves close to the winch have rotated more than the ones further away. This results in a higher relative wire displacement. As the crane reeving consists of four parts the other wire displacement graphs (for part B, C and D) can be found in Figures G.1 until G.3 of appendix G.

$$x = \phi_i R \qquad (4.23)$$
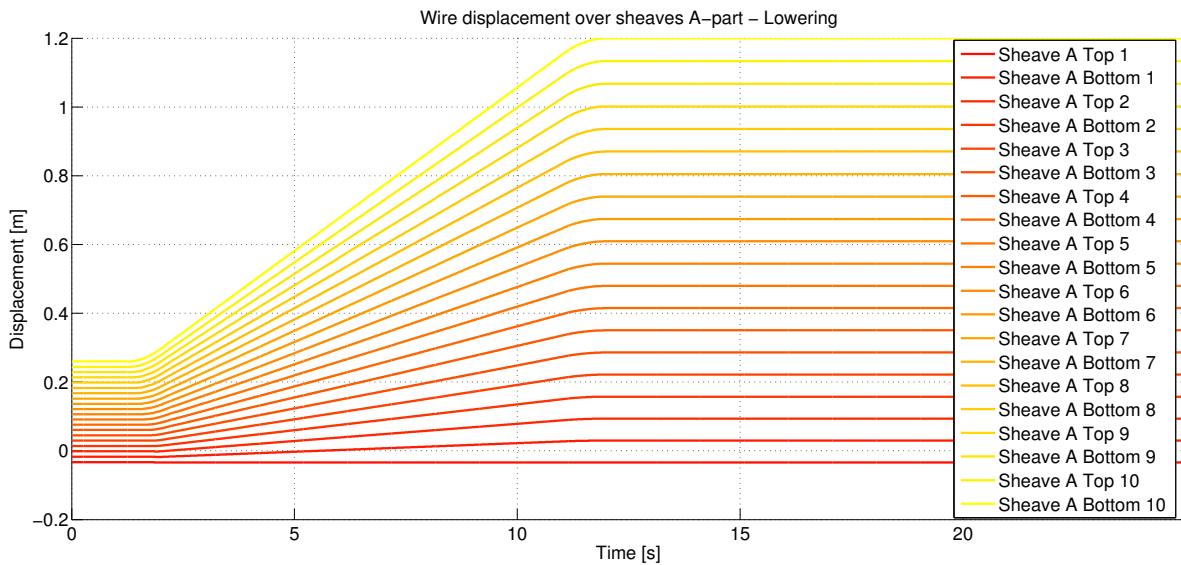
Figure 4.17: Wire displacement over sheaves of part A (purple) during lowering

Besides the sheaves that are in the parallel part of the reeving sections the sheaves in the serial part should also have rotated. As the winches all pay out 1.0 m the same amount has to pass the serial sheaves because they are between the winch and the parallel part. The load of the topside provides constantly a tension on the wires and therefore the serial sheaves rotate as well. Table 4.6 gives the associated abbreviations for these sheaves and Figure 4.18 displays the displacements. An equal increase between t=1 s and t=11 s of 1.0 m is present everywhere.

Table 4.6: Abbreviations of sheave in crane structure

	Left front drum	Right front drum	Left rear drum	Right rear drum
Fleeting sheave	LF1	RF1	LR1	RR1
Boom guide sheave	LF2	RF2	LR2	RR2
Lower crossover sheave 1	n.a.	RF3	LR3	n.a.
Lower crossover sheave 2	n.a.	RF4	LR4	n.a.
Boom tip lead-in	LF3	RF5	LR5	RR3
Main fall lead-in	LF4	RF6	LR6	RR4
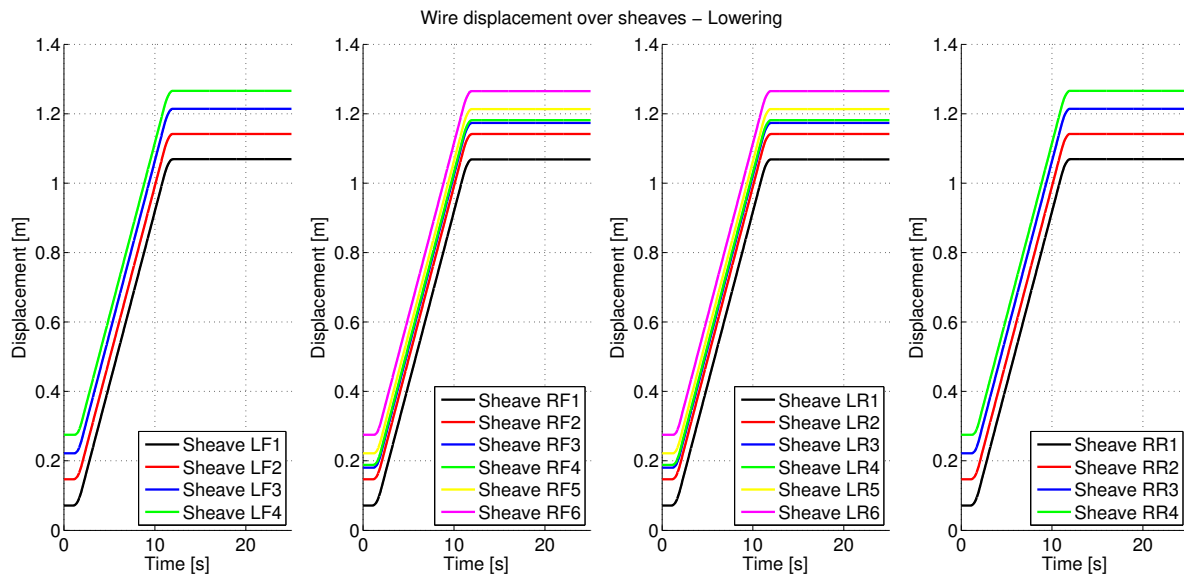
Figure 4.18: Wire displacement over sheaves in crane structure during lowering

4.6.3. HOISTING

The previous section showed the case for lowering where this section does the opposite for the hoisting case (Figure 4.19. Instead of a positive winch displacement a decrease of 1.0 m is now taking place as it is pulling in the wire. The topside is going from its initial condition (-0.0672 m) to a new situation at -0.0172 m. A total wire length of 4.0 m was pulled in from 80 wires, resulting in an overall topside displacement of $\frac{4}{80} = 0.05$ m positive. This equals an increase of the topside height of $-0.0172 - -0.0672 = 0.05$ m.
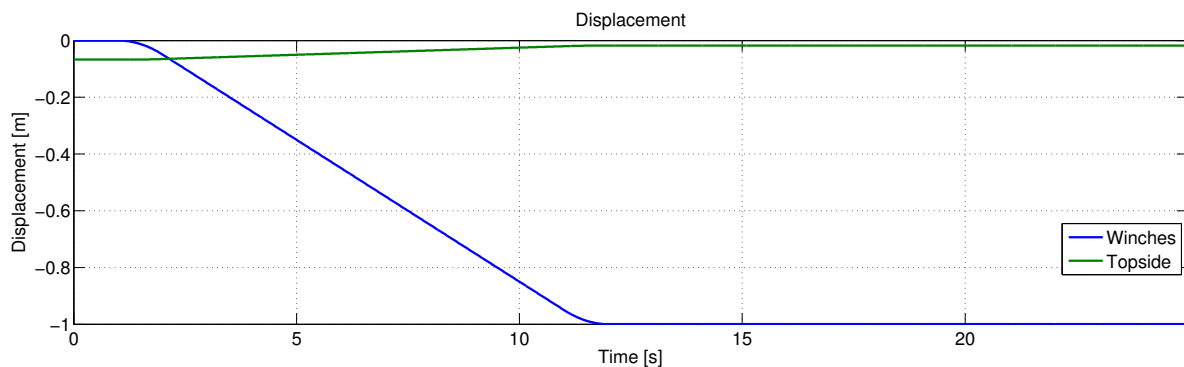
Figure 4.19: Wire displacement of winches and displacement of topside during hoisting

The wire displacement graph of the sheaves of part A are given in Figure 4.20. It begins in the same position as for the other case but the displacement has a negative direction now. Logically a sheave would rotate in the opposite direction whether the crane is lifting or putting something down. The other wire displacement graphs (for part B, C and D) can be found in Figures G.4 until G.6 of appendix G.
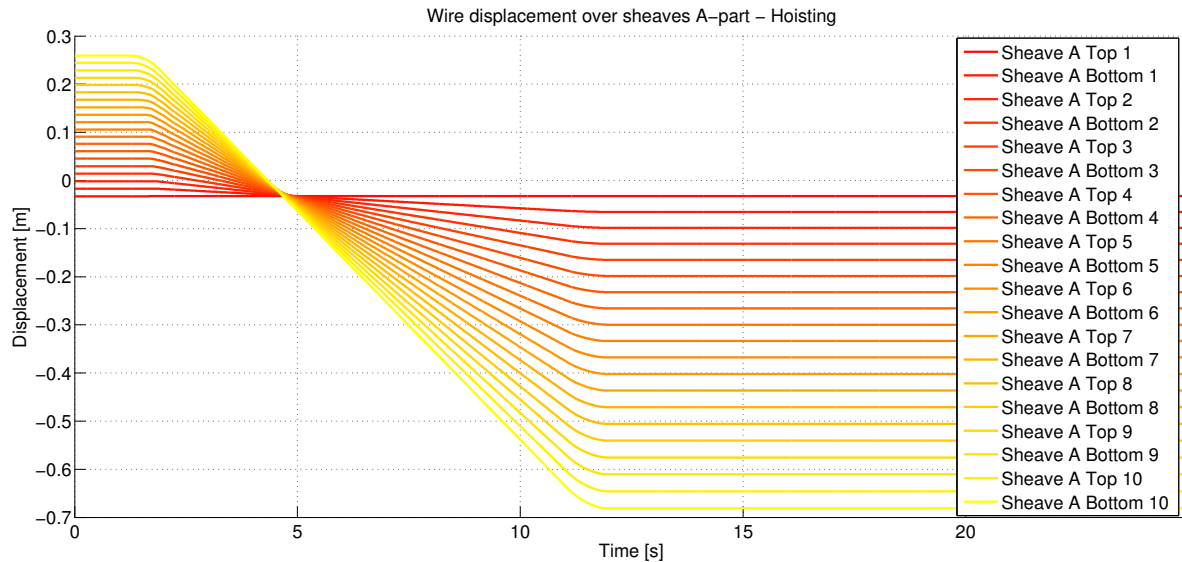
Figure 4.20: Wire displacement over sheaves of part A (purple) during hoisting

Figure 4.21 shows the wire displacement of the sheaves in the crane structure. From their initial condition to their end situation a total of -1.0 m wire has passed each sheave in total.
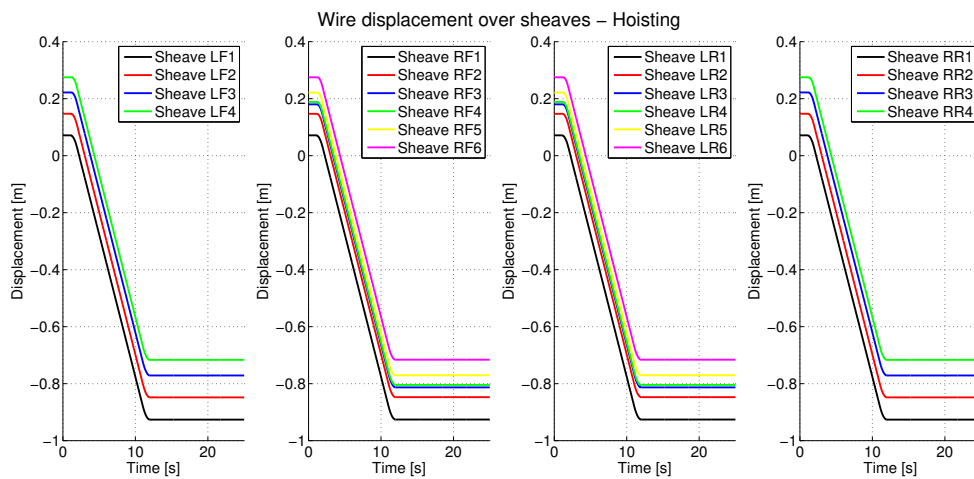

Figure 4.21: Wire displacement over sheaves in crane structure during hoisting

4.7. WIRE FORCES

From the rotational velocity and displacement of each sheave the force of each wire segment can be calculated as was explained earlier in section 4.2. When there is no friction taken into account in the model the coefficients μ_{kin} and μ_{stat} are zero. When a load is statically supported by a multiple part wire rope reeving system, the load on each rope part is equal to the weight of the load supported. The load on each rope part is the total load divided by the number of parts of rope supporting the load (3000 mT in this case):

$$Force = \frac{Load}{n_{falls}} = \frac{3000\text{mT}}{80} = \frac{3000 * 9.81}{80} = 367.9\text{kN}. \tag{4.24}$$

But, when taking friction into account and the same load is raised, the stress in each rope part increases progressively from the dead end to the lead line. This increased stress is due to the cumulative effect of friction in the sheave bearings and the internal friction force between the fibers in a wire rope.

Additionally in order to have equilibrium, those parts of a multiple reeving nearest to the winch have a slightly higher load than their proportionate load. While those farthest away from the drum have a lower load and the sum of all forces all parts supporting the load are equal to the weight of the topside. There are also forces due to accelerating and decelerating of the load, but these are not included in the aforementioned discussion, since the suspended load is normally displaced with a constant velocity.

When the hoisting operation is ended at a certain moment in time, the force difference in the wires is still present. This phenomenon is also happening in reality as was found in offshore measurements, see section 3.1. The same results were found in the outcome of the model, see Figure 4.22. In this figure the force in the twenty hoist wires of part A are plotted. At t=0 s the force in each wire is constant as the load is equally distributed. At t=1 s the hoisting operation started and a force difference between every two neighboring wires is present. When the operation is completed at t=11 s the discrepancy is still present. This effect originates from the stick-slip effect described in section 2.4. Similar figures for part B, C and D of the reeving can be found in appendix H in Figures H.4 until H.6. Around t=2 s one can see a damped oscillation in the forces when the topside is suddenly being brought in motion and at t=12 s where it is suddenly being brought to rest again.
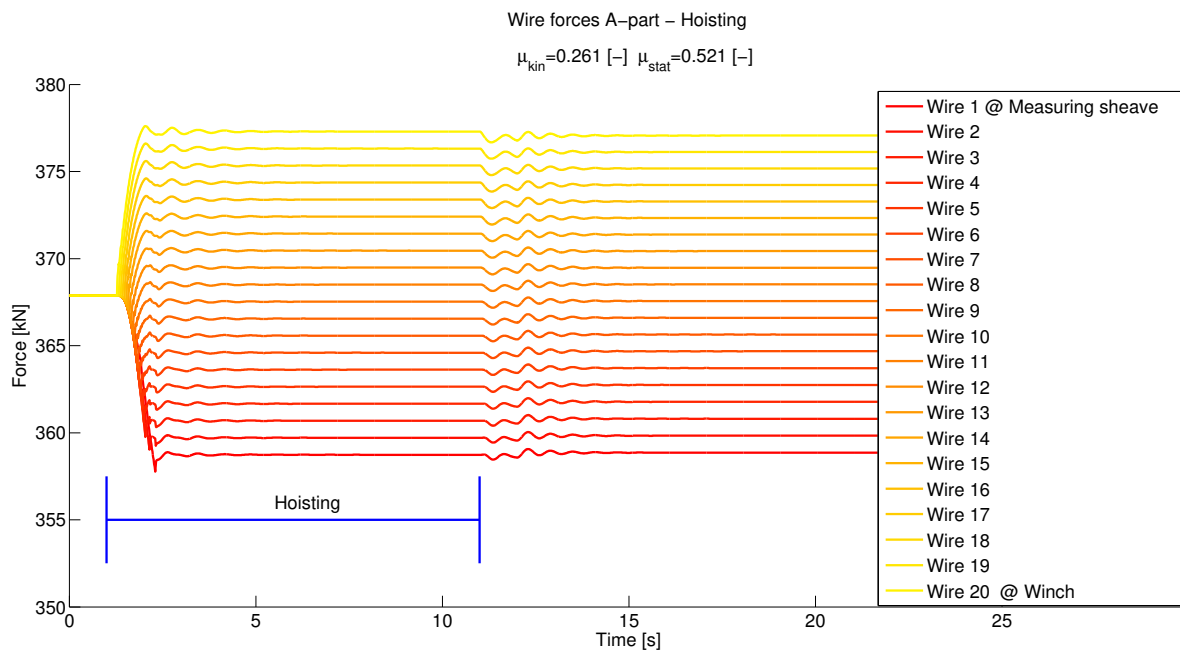
Figure 4.22: Wire forces of part A (purple) of crane reeving during hoisting

In stead of looking at the force difference between individual wires it is also interesting to see how the difference between the suspended load and the forces at the modeled measurement sheaves correlate. In section 3.2 the numerous correction factors used in the crane PLC were mentioned. The sheave friction factors are tuned based on a friction factor of 1.05 for both hoisting and lowering in order to show the effect, thus a decrease or increase of the load by 5%. This resulted in a μ_{kin} of 0.261 and μ_{stat} of 0.524. Constant friction factors are assumed for each sheave, but due to unequally wear this does not have to be the case obviously. From Figure 4.23 can be seen that the load difference corresponds to exactly 5% of the suspended load.
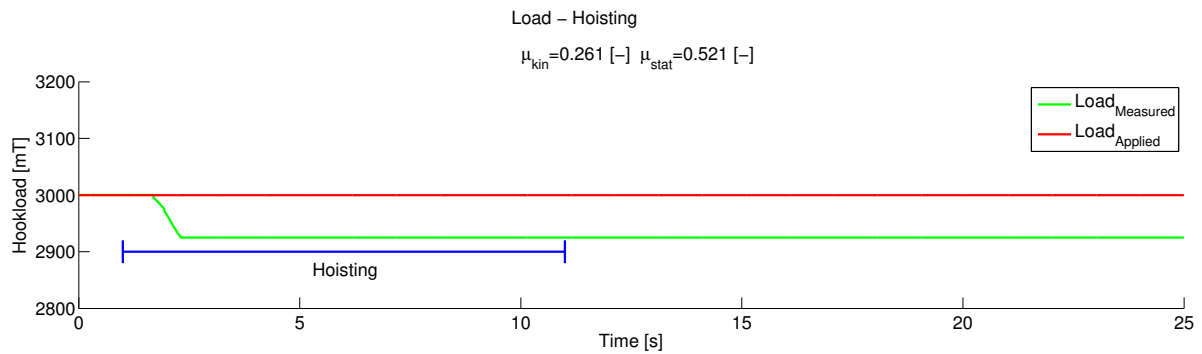
Figure 4.23: Combined wire force on measurement sheaves during hoisting

The opposite case, lowering, is also considered. The force distribution is again plotted in Figure 4.24 while using the same friction factors. The spreading of the individual wire forces is now in the opposite direction as for the hoisting operation. The force at the measuring sheave has increased and at the winch has decreased, which was found in section 3.1 as well. Similar figures for part B, C and D of the reeving can be found in appendix H in Figures H.1 until H.3.
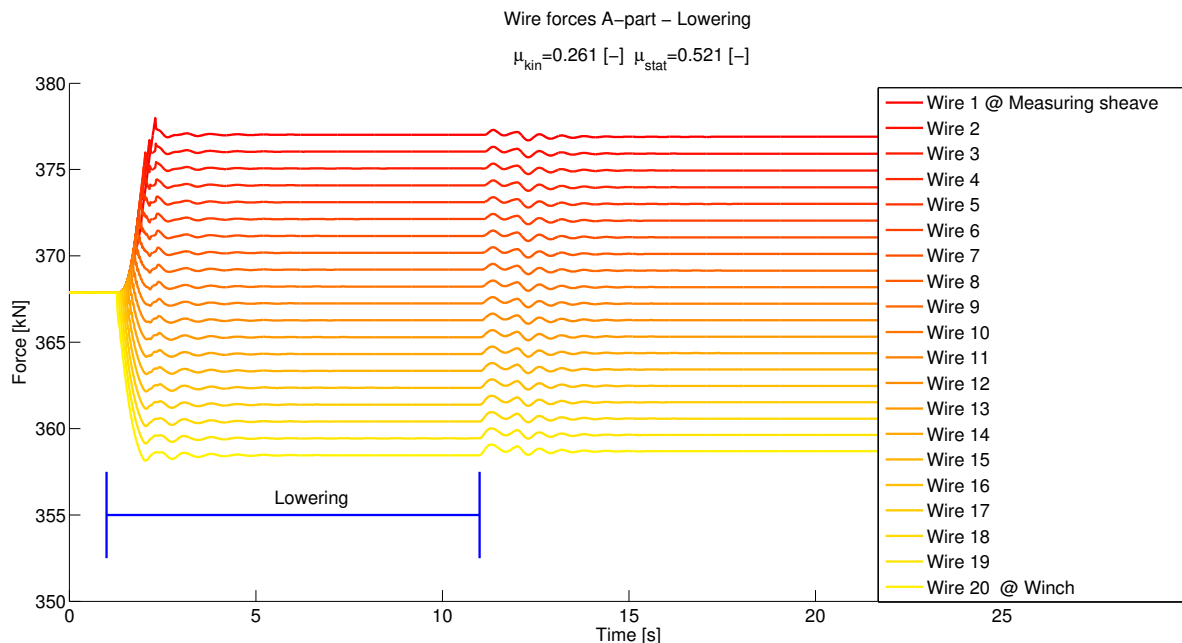
Figure 4.24: Wire forces of part A (purple) of crane reeving during lowering

When zooming in on the model load measurement (see Figure 4.25) a similar step due to cumulative friction is found around t=1 s, but now in the opposite direction as what was found for a hoisting operation. After the operation the force is still present. The same phenomenon, a decrease in measured load during hoisting and an increase in measured load during lowering, as in reality is now modeled with a friction for each sheave. A similar model could be created for one of the other vessels of HMC: the DCV Balder. In the force measurements of this vessel it was observed that the effect is opposite. During hoisting the hook load increases and during lowering measurements show a decrease in hook load. When you look at the crane wire reeving of this vessel in appendix C the measurement sheaves are positioned close to the winches. This is opposite of the location at the SSCV Thialf where they are as far as possible from the winches. While looking at Figures 4.22 and 4.24 the force in the opposite direction as well if you compare wire 1 (at measuring sheave) and 20 (at winch). If a similar model was made for the Balder crane reeving the same effect as in reality would be recognized. However the load sensors are there positioned close to the winch, resulting in the opposite effect in the load measurement. Later in chapter 5 it is described how a coupling is made between this reeving model of

the SSCV Thialf and an imposed model motion model. This is done to incorporate it in the load-crane-vessel system.
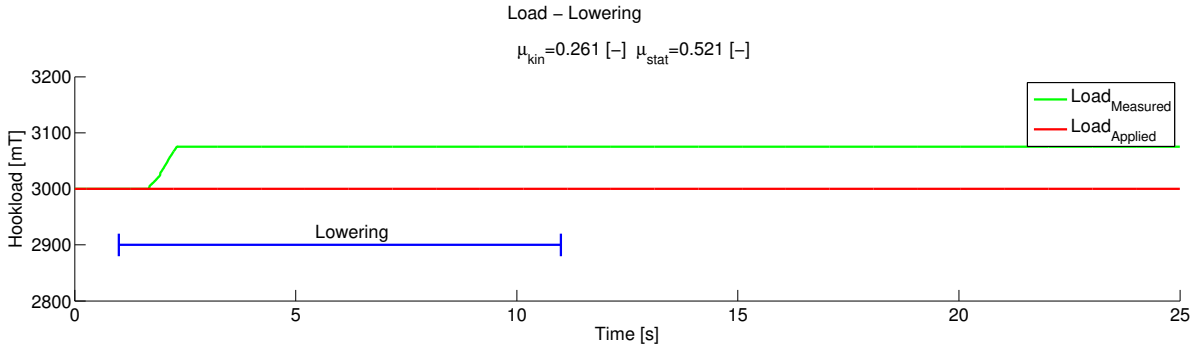
Figure 4.25: Combined wire force on measurement sheaves during lowering

5

Imposed motions model

This chapter outlines the numerical model created to impose the vessel motion. Section 5.1 explains the reason why this model is created and how the hoist wire response is obtained. The derivation of the equations of motion is described in section 5.2. This is firstly performed by solving the Lagrangian's for a 3D spring pendulum for a single lift model and followed by creating the motion matrices for a dual lift model with LiftDyn. To verify the outcome of the model several base cases are made of which the outcome is discussed in section 5.3. In section 5.4 of this chapter it is explained how the model from chapter 4 is integrated with the imposed motion model.

5.1. HOIST WIRE RESPONSE

5.1.1. FREQUENCY DOMAIN

In order to gather the responses of the hook load due to the environment it is possible to solve a model in time domain or frequency domain. When working in frequency domain a wave spectrum describing the sea state is used to get the response of the hoist wire by determining the force Response Amplitude Operator (RAO). This could be done with a prediction of the sea state on the desired location from long term wave statistics or by the actual sea state measured with a wave rider buoy. Using measurements from a buoy is only possible during an installation itself or when the project is finished. For critical lifts the sea is observed by a buoy during the installation to know the conditions of the sea. These can either be described by a 2D wave spectrum or a 3D wave spectrum. In a 3D wave spectrum the direction is incorporated as the wave spectra are discretized and each wave component has a direction. The force RAO of a hoist wire can be obtained by creating a model in which separate bodies are able to move freely and are connected to each other by spring-dashpot elements. These bodies represent the vessel, the rigid parts of the crane assembly and the load each having their own inertia properties. A total mass, damping and stiffness matrix can be composed. As the mass and damping for a vessel is frequency depended (added mass and damping due to water) this is formed for a range of frequencies. With this model the relative motion and velocity RAO between the connection points of this element can be determined. Together with the stiffness and damping properties of the spring-dashpot element the force RAO can now be deducted. The response due to the environment can be computed by multiplying the force RAO squared with the wave spectrum in equation 5.1 (see Figure 5.1).

$$S_{force} = S_\zeta |RAO_{force}|^2 \tag{5.1}$$

As explained in chapter 3 the load in the crane and thus the forces in the hoist wires are measured as well. By doing a spectral analysis on the measured hook load the behavior can be compared with the computed response.
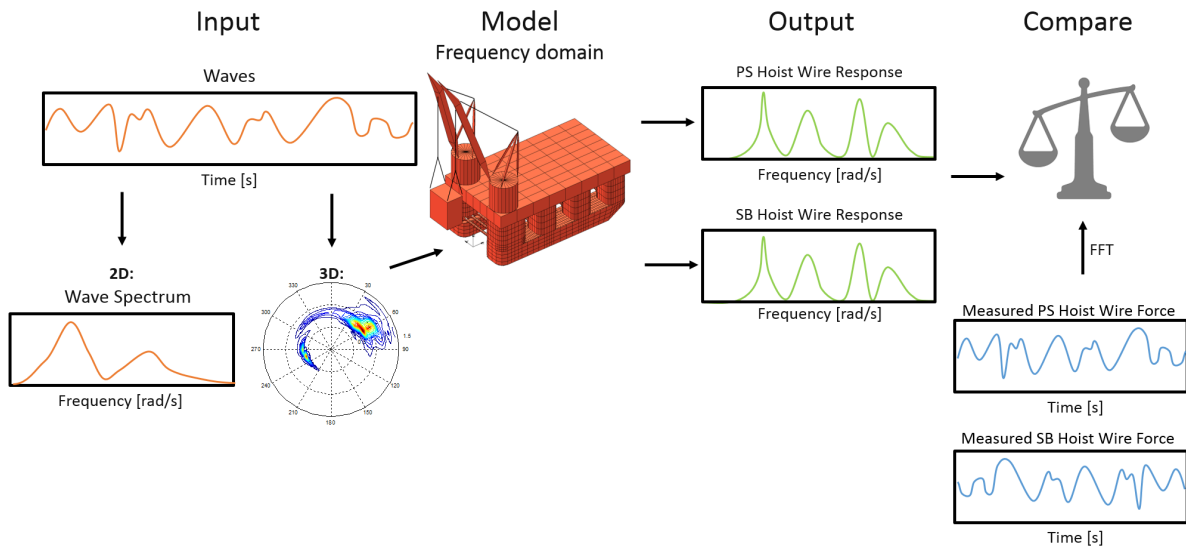
Figure 5.1: Response frequency domain model

5.1.2. Time domain

Another way for determining the response of the hoist wire forces is by kinetically imposing the measured motions of the vessel in a numerical model. Due to the inertia of different components of the load-crane-vessel system a relative motion is present. The vessel motions have an influence on the motions of the boom which is in connection with the main block and the suspended load. The relative motion results in dynamic forces occurring with one or more modes that are amplified. This results in multiple natural periods. For the reason that the vessel motions are measured in time domain it is possible to solve this in time domain as well. See Figure 5.2. By using this procedure the inaccuracies of wave measurements and the change of an incorrect wave diffraction analysis are skipped. The same mass, damping and stiffness matrices created for the frequency model can be used for a fixed frequency. The frequency depended parts for the vessel due to the water are no longer considered as the vessel motions are no longer free variables. Its displacement and velocities (by taking the derivative) are known from the measurements. It could also be possible to impose the motions of the load, however the mass of the vessel is a order of magnitude higher and the motion of the topside is already implicit taken into account. In the imposed motions model only heave, roll and pitch of the vessel are considered. The other three degree of freedom of the vessel (surge, sway, yaw) are not of relevance because they are in the horizontal plane. After applying the motion of the vessel the simulation gives a response of the motion of each free body. In order to minimize an initial transient the simulation is performed twice. In the first run the imposed motions are constant and equal to its first value. With a high damping value the initial conditions are determined. The relative motion between the two connection points of the spring-dashpot element gives an elongation or compression of this element. After multiplying the stiffness with the elongation and the damping with its time derivative the forces of the spring elements and thus the hoist wire force can be computed. The simulation lasts as long as the time trace of the measured vessel motion is stationary. The time trace of the determined hoist wire force has logically exactly the same length. After performing a spectral analysis for both the obtained time trace out of the model and the offshore measured hoist wire force, they can be compared in terms of frequency components. The non-linear effect of the hoist wire forces from the sheave model in chapter 4 can be included as well in time domain.
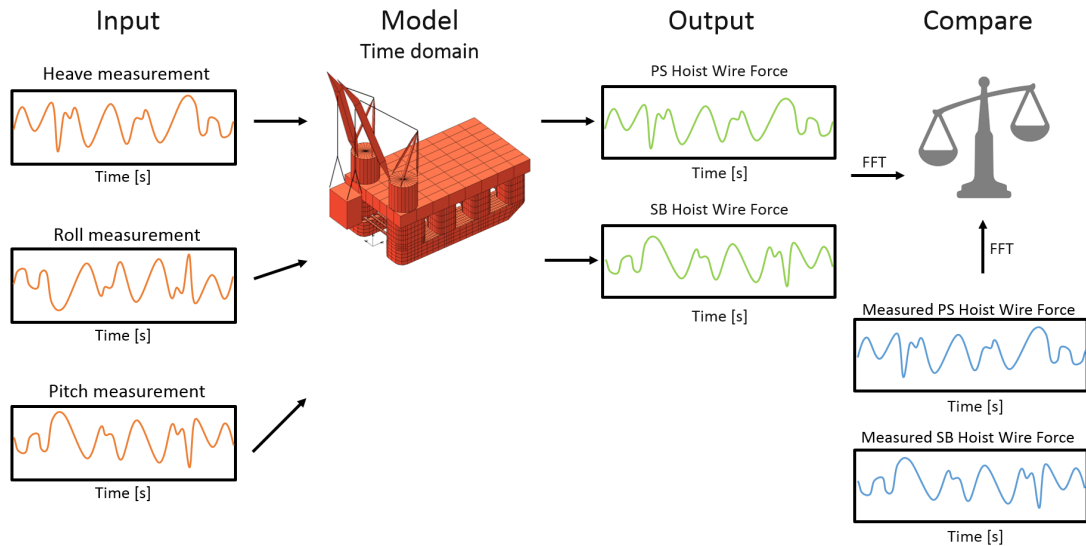
Figure 5.2: Response imposed motion model

5.2. EQUATION OF MOTION

The required input for the model described in section 4.2 is either the applied force on the main hook of a crane resulting in a certain displacement or an applied displacement resulting in a force in the hoist wires represented as a spring element. This section illustrates how this force or displacement is determined by relating the motions of the vessel and the load. The motion measurement was described earlier in section 3.4 in this report. In order to kinetically impose the measured motions of the SSCV in the total system the equations of motions are derived. This is firstly performed by solving the Lagrangian for a single lift and later on by obtaining the motion matrices from LiftDyn, a HMC in-house multi-body dynamics software.

5.2.1. SINGLE CRANE LIFT WITH LAGRANGIAN

One way to obtain the equation of motion is by solving the Lagrangian. The derivation can be found in appendix I for a single lift. Here the kinetic, potential and dissipation energy of the system is set up. The appendix is divided into two parts: the first part consist of a spring pendulum with a fixed suspension point and the second part with a suspension point that is able to translate in three directions. This extra part in terms of a translation corresponds to the motion of the crane tip due to the motion of the vessel which originates from environmental influences. As the Lagrangian is only solved for a single lift it is not further discussed from here, because the highest interest lies in a dual crane lift.

5.2.2. DUAL CRANE LIFT WITH LIFTDYN

In the previous section it is discussed how a motion can be imposed to determine the response of the load for a single crane lift for a free hanging mass. However HMC's vessels are specialized in performing lifts with two cranes (dual lifts). Deriving it with a Lagrangian would be more complicated due to the interaction between the numerous degree of freedom by two crane tips. In order to model and to derive the motion matrices HMC in-house software LiftDyn was used. LiftDyn is a linear frequency domain software. As it is limited in doing frequency domain calculations it is unable to imposed measured motions of the vessel as time traces. On the other hand it is not possible to couple the model from chapter 4 to incorporate non-linear effects due to the stick-slip which have to be solved in time domain. The export function of the model in LiftDyn also consists of the mass matrix M^*, the damping matrix B^* and the stiffness matrix K^* for a range of frequencies. These matrices are used to calculate the response of the motion and of the forces acting between rigid bodies. An overview of a typical modeled dual lift can be found in Figure 5.3. In the next paragraphs fixed properties of the vessel are considered, project related properties that were input of the model can be found in appendix K.
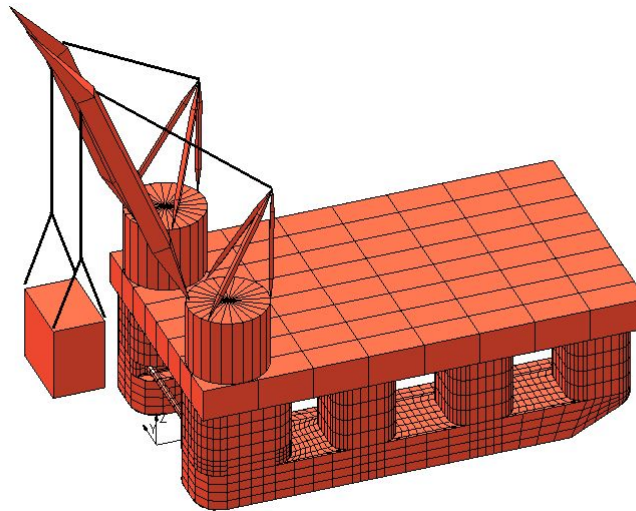
Figure 5.3: Model overview LiftDyn

The system normally consists of six bodies (vessel, load, starboard crane boom, port side crane boom, starboard main block and port side main block) each with six degree of freedom (three translations and three rotations), resulting in a total of 36 degree of freedom system. Some of these degrees of freedom are omitted as they are part of another body. This is explained later on. Figure 5.4 shows the visualization of the body of the vessel without the crane boom and Table 5.1 gives the properties of the body. Note that stiffness and damping due to interaction with the water is not given as it is of no importance while imposing the measured motion in time domain. Also make notice of the fact that the position of the CoG differs for each project and even for each installation phase as additional load is carried by the vessel or a different ballast sequence is used. Now project specific properties are used.
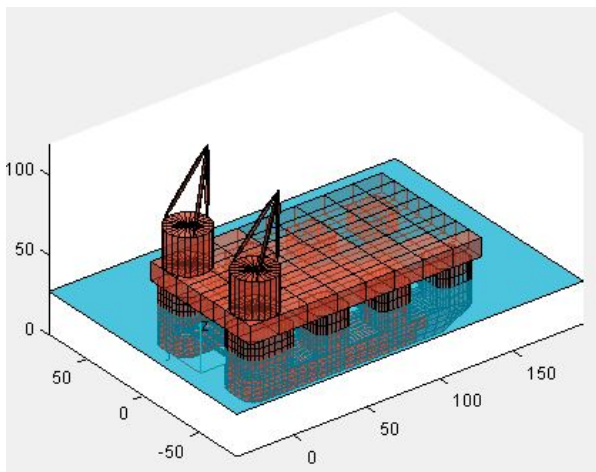
Figure 5.4: SSCV Thialf body

Table 5.1: Properties SSCV Thialf with 26.6m draft

Mass	[mT]	165800
Radius of gyration x-axis	[kgm^2]	38
Radius of gyration y-axis	[kgm^2]	59
Radius of gyration z-axis	[kgm^2]	65

Figure 5.5 shows the visualization of the body of the crane boom and Table 5.2 gives the properties of this body. Only the radius of gyration around the y-axis is given as the crane boom is only able to rotate around this axis while hinging at the vessel body. The properties are similar for the port and starboard crane boom. The position of the CoG is with respect to the local coordinate system of the crane boom where the origin lies at the hinge point and the x-axis is directed along the crane boom to the crane tip.
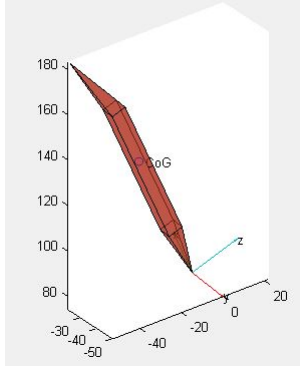
Figure 5.5: Crane boom body

Table 5.2: Properties crane boom

Mass	[mT]	1003.7
Radius of gyration y-axis	[kgm²]	36.05
CoG position	[m]	(61.3, 0, -0.205)

Figure 5.6 shows the visualization of the body of the main block of the crane and Table 5.3 gives the properties of this body. There are no radius of gyration given since the main block is modeled as a point mass which is only allowed to translate and not rotate. This can be read in appendix E where this rotation is added, but gave no difference in the outcome. The properties are similar for the port and starboard crane main block.
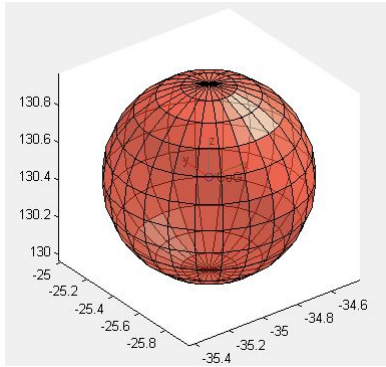
Figure 5.6: Crane main block body

Table 5.3: Properties crane main block

Mass	[mT]	236
CoG position	[m]	(0 0 0)

In reality steel wires are used to support or transfer forces between bodies. This is done to attach the load to the crane's main block, to make a connection to the crane tip and to support the crane boom. In the model these steel wires are represented as in-line springs or connectors. These single springs are included in the total stiffness matrix K^* by defining it between a point on body n and a point on body m. This spring relates the motion of the point of body a relative to body b with a force vector. The forces working on each body are equal but opposite in sign.

Particular bodies have constrains or are connected to other bodies. An example for this is the body for the crane boom which has a hinge point at the aft of the SSCV. This results in less degree of freedom because the crane boom is only able to rotate around the hinge point. The other five translations and rotations can be omitted. This multi body dynamic software is taking care of how these bodies are combined by creating a joint matrix T_{joint}. How this joint matrix is constructed is not be explained in this report, because it is already widely described in the manual of the software [Meskers, 2000]. This joint matrix specifies the relation between the motion of a body around the CoG and the motion due to their connection. With these joint matrices the actual matrices for the system with this relation can be calculated, see equation 5.2.

$$\begin{aligned}
\boldsymbol{M} &= \boldsymbol{T}'_{joint} \boldsymbol{M}^* \boldsymbol{T}_{joint} \\
\boldsymbol{B} &= \boldsymbol{T}'_{joint} \boldsymbol{B}^* \boldsymbol{T}_{joint} \\
\boldsymbol{K} &= \boldsymbol{T}'_{joint} \boldsymbol{K}^* \boldsymbol{T}_{joint}
\end{aligned} \tag{5.2}$$

IMPOSING OF PRESCRIBED MOTION
Consider an example with a general 3DOF system, with mass-matrix $\boldsymbol{M}$, Damping matrix $\boldsymbol{B}$ and stiffness matrix $\boldsymbol{K}$ (all [3x3] for a particular problem, see equation 5.3). All variables are free variables. When the matrices

are written out with [3x3] matrices the equation looks like equation 5.4. Now when one of the three degree of freedom (x_3 in this case) is described by a predetermined time trace its influence to the other variables (x_1 and x_2) are written as forces on the right hand side of the equation, see equation 5.5.

$$M\ddot{x} + B\dot{x} + Kx = F \quad \text{with} \quad \mathbf{x} = \begin{bmatrix} x_1 \\ x_2 \\ x_3 \end{bmatrix} \tag{5.3}$$

$$\begin{bmatrix} m_{11} & m_{12} & m_{13} \\ m_{21} & m_{22} & m_{23} \\ m_{31} & m_{32} & m_{33} \end{bmatrix} \ddot{x} + \begin{bmatrix} b_{11} & b_{12} & b_{13} \\ b_{21} & b_{22} & b_{23} \\ b_{31} & b_{32} & b_{33} \end{bmatrix} \dot{x} + \begin{bmatrix} k_{11} & k_{12} & k_{13} \\ k_{21} & k_{22} & k_{23} \\ k_{31} & k_{32} & k_{33} \end{bmatrix} \mathbf{x} = \begin{bmatrix} F_1 \\ F_2 \\ F_3 \end{bmatrix} \tag{5.4}$$

$$\begin{bmatrix} m_{11} & m_{12} \\ m_{21} & m_{22} \end{bmatrix} \ddot{x} + \begin{bmatrix} b_{11} & b_{12} \\ b_{21} & b_{22} \end{bmatrix} \dot{x} + \begin{bmatrix} k_{11} & k_{12} \\ k_{21} & k_{22} \end{bmatrix} \mathbf{x} = \begin{bmatrix} F_1 - m_{13}\ddot{x}_3 - b_{13}\dot{x}_3 - k_{13}x_3 \\ F_2 - m_{23}\ddot{x}_3 - b_{23}\dot{x}_3 - k_{23}x_3 \end{bmatrix} \tag{5.5}$$

The same that was performed for the 3DOF system also holds for the load-crane-vessel situation. There are three prescribed displacements (heave z, roll ϕ and pitch θ motion of the vessel) on a 36x36 stiffness matrix. When this system is solved the obtained motions have to be transfered back to the motions at the CoG of each body. With other words, the added relation between bodies that are connected have to be removed. This can be performed by multiplying the joint matrix T_{joint} with the displacement vector $\mathbf{x}$ to get $\mathbf{x}^*$ (equation 5.6).

$$\mathbf{x}^* = T_{joint}\mathbf{x} \tag{5.6}$$

When the motions at the CoG of each body are solved from the system it is required to calculate the force in each spring-damper element. Consider a spring-damper that is acting between two bodies and is attached at a certain location of the body. A motion transformation matrix can be created which relates the motion of a body at the CoG to the motion of point located somewhere else at that particular body see equation 5.8. By multiplying this matrix with the motion at the CoG, the motion at the desired point of interest can be found. The vectors a and b are the positions of the CoG and the point of interest (PoI).

$$T_{motion\,a \rightarrow b} = \begin{bmatrix} 1 & 0 & 0 & 0 & (b_z - a_z) & -(b_y - a_y) \\ 0 & 1 & 0 & -(b_z - a_z) & 0 & (b_x - a_x) \\ 0 & 0 & 1 & (b_y - a_y) & -(b_x - a_x) & 0 \\ 0 & 0 & 0 & 1 & 0 & 0 \\ 0 & 0 & 0 & 0 & 1 & 0 \\ 0 & 0 & 0 & 0 & 0 & 1 \end{bmatrix} \tag{5.7}$$

$$\mathbf{x}_b = T_{motion}\mathbf{x}_a \tag{5.8}$$

When this calculation is performed for both positions of the attachment of the spring element on both bodies the length of the spring element can be calculated for each moment in time (equation 5.9). Together with the initial length of the connector which is calculated with the initial conditions of the body (equation 5.10) the elongation can be determined, see equation 5.11. This is performed for each time step to calculate the force in the spring-damper during the whole simulation. Finally the corresponding force in the spring-dashpot element is now computed (equation 5.12) with its stiffness and damping properties.

$$L = \sqrt{(b_x - a_x)^2 + (b_y - a_y)^2 + (b_z - a_z)^2} \tag{5.9}$$

$$L_0 = \sqrt{(b_{x_0} - a_{x_0})^2 + (b_{y_0} - a_{y_0})^2 + (b_{z_0} - a_{z_0})^2} \tag{5.10}$$

$$\Delta L = L - L_0 \tag{5.11}$$

$$F = k\Delta L + b\dot{\Delta L} \tag{5.12}$$

5.3. SIMPLIFIED CASES

Four simplified cases are studied to check whether the imposed motions of the vessel are resulting in expected responses. The first case consists of the vessel being fixed in all degrees of freedom, as if it is standing on the bottom of a canal. A regular sinusoidal force is applied at the center of gravity of the topside. The amplitude of the force was 100 mT. To cover the range of the natural periods of the system the simulation was performed with a frequency range of $[\frac{2\pi}{30}\ \frac{2\pi}{0.1}]$. On certain frequencies of the applied load the force in the hoist wire is amplified. The amplitude of the hoist wire force is determined from the resulting time trace and are plotted against the frequency to create a response graph. The peaks in the graphs should correspond to the natural periods of the system. For the damping a default value of ζ 1.5% of the critical damping is used. An increase of axial hoist wire damping would result in a lower amplitude at the natural periods. Another way of determining the natural frequencies is by using the Matlab function *eig(K,M)*, which returns the generalized eigenvalues based on **K** and **M**, the stiffness and mass matrix. These natural periods and their corresponding mode can be found in section L.4 in the appendix. They are valid particularly for the model of project A that was consider as the properties of the load (like CoG, mass, inertia) and of the vessel (slew angle, boom angle, mass) are different for every offshore installation. Anyway, it is still important to check whether the same responses are found from the *eig*-function and the imposed model. These cases are summarized in Table 5.4. Beside the case where a force is applied also the imposed motions of the vessel are varied. Each degree of freedom that is imposed is considered. Again for a wide range of frequencies the simulation is done with a regular sinusoidal wave to draw the response graph. The heave motion had an amplitude of 0.1 m, the roll and pitch motion with an angle amplitude of 0.1 degrees. The response graph is made for a set of four items. Firstly the response of the hoist wire force is considered four all cases, see Figures 5.7, 5.8, 5.9 and lastly 5.10.

Table 5.4: Figure overview of obtained responses

Case	Response hoist wire force	Response module	Response Main block	Response Crane tip
Force on topside	Figure 5.7	Figure 5.11	Figure 5.12	Figure 5.13
Imposed Heave	Figure 5.8	Figure L.1	Figure L.2	Figure L.3
Imposed Roll	Figure 5.9	Figure L.4	Figure L.5	Figure L.6
Imposed Pitch	Figure 5.10	Figure L.7	Figure L.8	Figure L.9
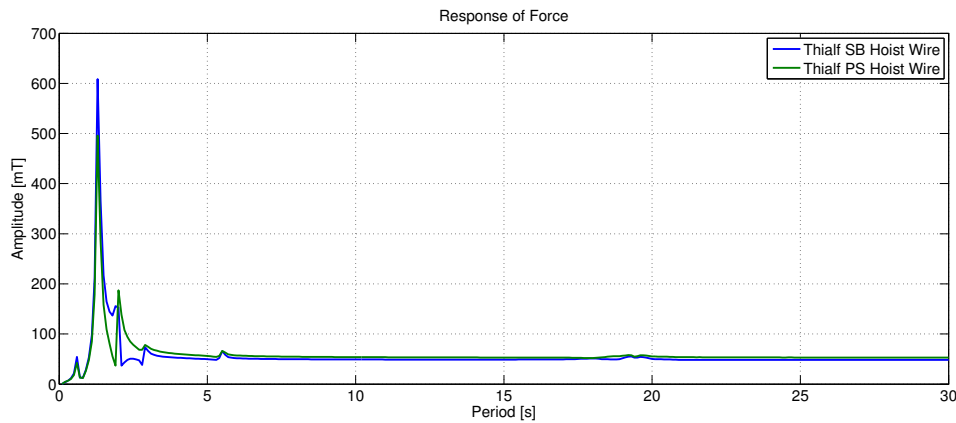
Figure 5.7: Response hoist wire force due to sinusoidal force at topside
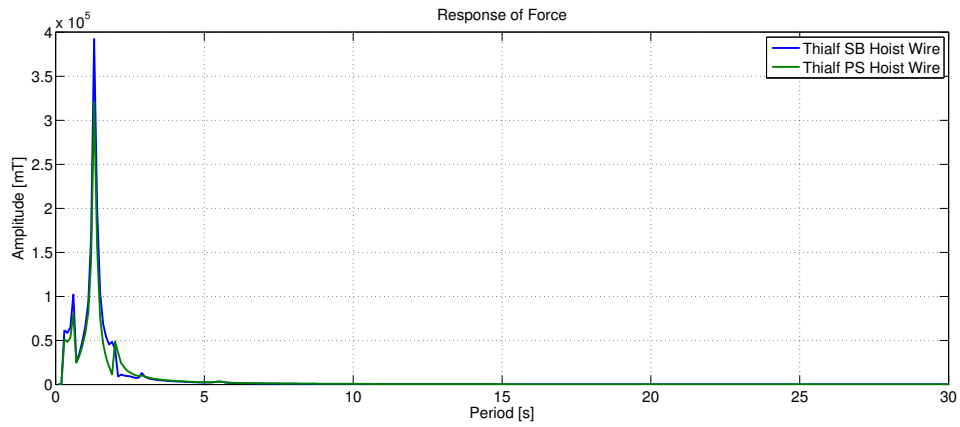
Figure 5.8: Response hoist wire force due to sinusoidal heave motion
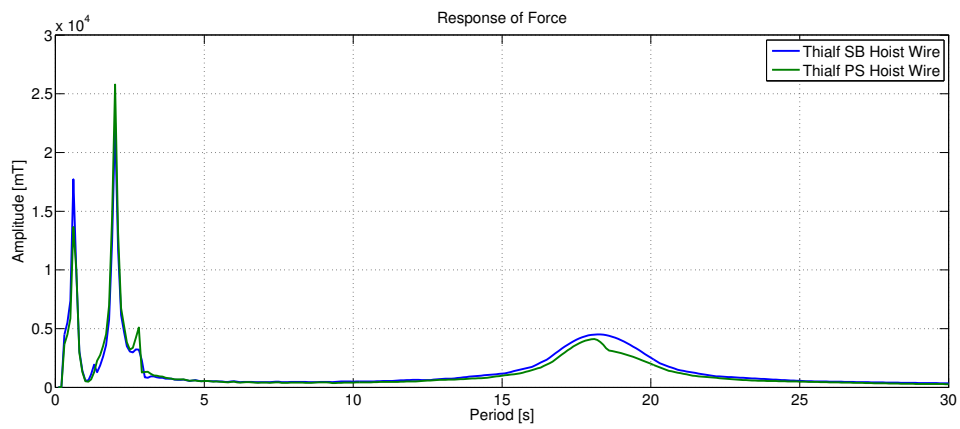
Figure 5.9: Response hoist wire force due to sinusoidal roll motion
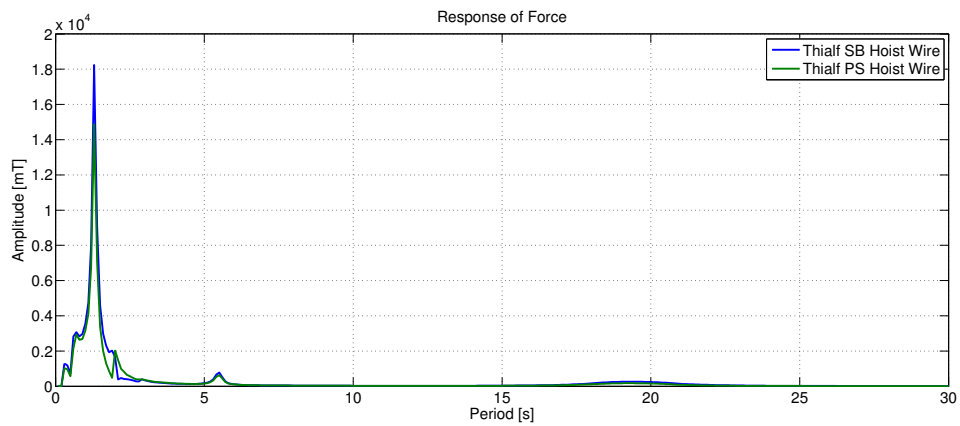
Figure 5.10: Response hoist wire force due to sinusoidal pitch motion

Also the motion response of the topside (or module), main block and crane tip are given. For the first case (applied force) they can be found in 5.11 until 5.13 and for the other cases in appendix L. The peaks in the response spectra match with the found natural periods in the same appendix.
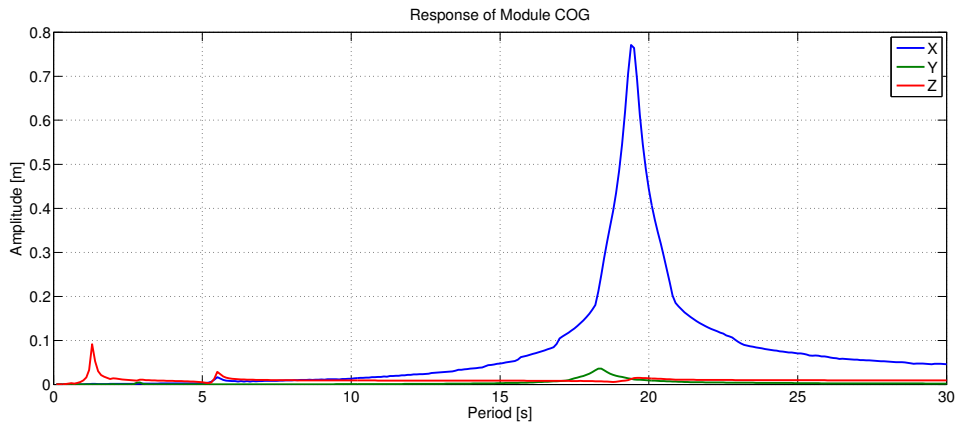
Figure 5.11: Response module due to sinusoidal force at topside
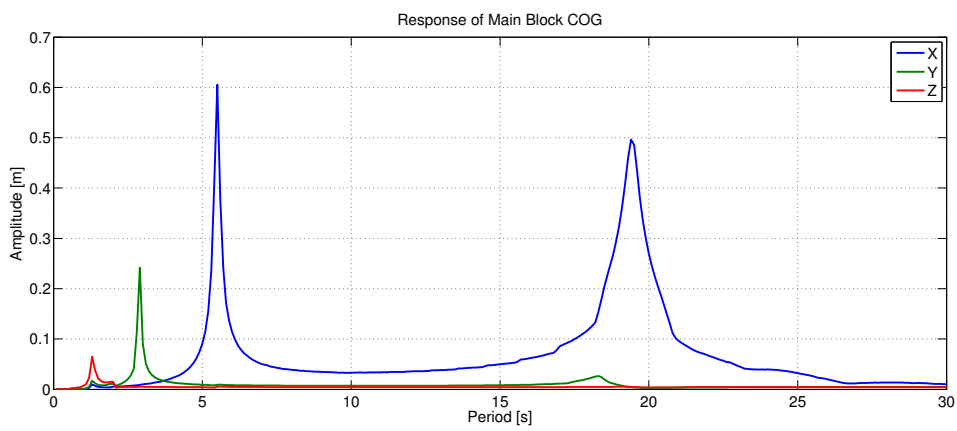
Figure 5.12: Response main block due to sinusoidal force at topside
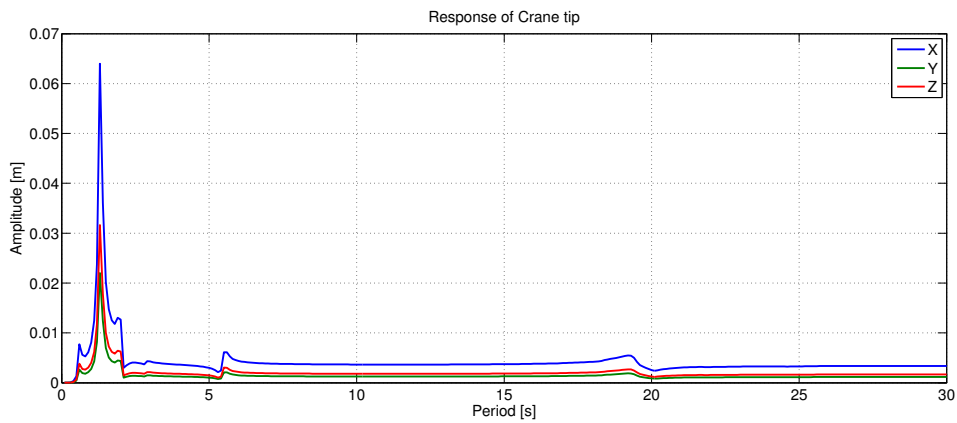
Figure 5.13: Response crane tip due to sinusoidal force at topside

5.4. COUPLING OF TWO MODELS

This section describes how the sheave friction model and the imposed motion model discussed earlier in section 4.2 and in subsection 5.2.2 are coupled to one model. The sheave wire model in in one direction. The required input is either a displacement in the direction of the wires (the 1D direction) or a force that is applied in line. This can for example be represented as a force that is applied on the main block axle whereas other

sheaves are positioned at the crane tip. In the imposed motion model the hoist wires are represented by a single spring element, see Figure 5.14.
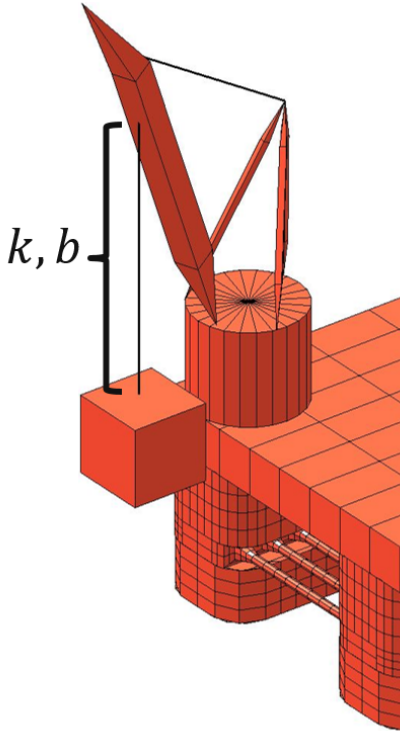
Figure 5.14: Hoist wire represented as a linear spring-dashpot
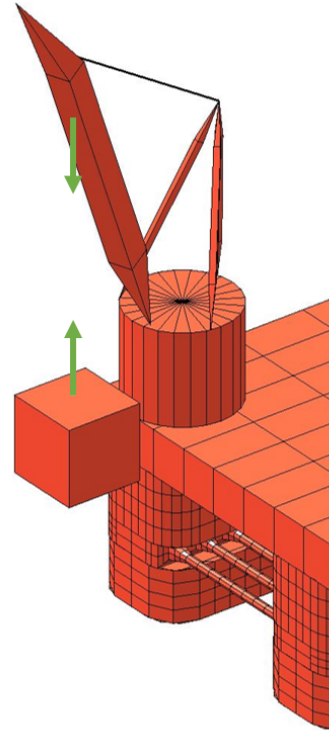
Figure 5.15: Hoist wire represented as a pair of forces

This connector element has a connection between the same two positions as mentioned before for the sheave model. It is modeled as a completely vertical spring. It has a contribution to the total stiffness matrix $\boldsymbol{K}^*$ and damping matrix $\boldsymbol{B}^*$. As this component is vertical it is governed by the motions of five variables. These five variables are the three imposed motions of the vessel (heave z, roll ϕ, pitch θ), the z-motion of the main block z_{mb} and the rotation of the boom α_{boom}. The contributions to the total stiffness matrix $\boldsymbol{K}^*$ of a hoist wire with constant stiffness k are given in equation 5.13. The displacement vector $\mathbf{x}$ consists of the five variables that have influence on the elongation of the hoist wire spring element. The force in the hoist wire element depend on the total elongation due to one or more displacements of these variables. R_ϕ, R_θ are the arms from the CoG of the vessel to the crane tip. R_{boom} represents the crane radius. Note that only the derivation of the restoring force is considered. The same method for the damping contributions has been taken into account. Both element contributions are removed from the stiffness and damping matrices for the hoist wire of the starboard and port side crane. This ends up in a system which cannot be solved as the displacement of the topside goes to minus infinity because it is unsupported. However if an additional force is added to the force vector the load is supported again. This is shown in Figure 5.15. This extra force is now coming from the nonlinear sheave wire model and a coupling is made.

$$\boldsymbol{K}_{HW}\boldsymbol{x} = \begin{bmatrix} k & -kR_\phi & kR_\theta & -kR_{boom} & -k \\ -kR_\phi & kR_\phi^2 & -kR_\phi R_\theta & kR_\phi R_{boom} & kR_\phi \\ kR_\theta & -kR_\theta R_\phi & kR_\theta^2 & -kR_\theta R_{boom} & -kR_\theta \\ -kR_{boom} & kR_{boom}R_\phi & -kR_{boom}R_\theta & kR_{boom}^2 & kR_{boom} \\ -k & kR_\phi & -kR_\theta & kR_{boom} & k \end{bmatrix} \begin{bmatrix} z \\ \phi \\ \theta \\ \alpha_{boom} \\ z_{mb} \end{bmatrix} \tag{5.13}$$

However for the imposed motion model the variables of the vessel do not require an equation of motion as their displacements are known from measurements. The contribution of the hoist wire is only of importance for the equations of the boom rotation α_{boom} and the z-motion of the main block z_{mb}. The stiffness matrix of the hoist wire element from equation 5.13 can therefore be simplified by deleting the first three rows of the

matrix. The restoring force F_{rest} on the main block and the restoring moment $F_{rest} * R_{boom}$ of the boom are left over. This results in equation 5.14.

$$
\begin{bmatrix} F_{rest} \\ F_{rest} * R_{boom} \end{bmatrix} = \begin{bmatrix} -kR_{boom} & kR_{boom}R_\phi & -kR_{boom}R_\theta & kR_{boom}^2 & kR_{boom} \\ -k & kR_\phi & -kR_\theta & kR_{boom} & k \end{bmatrix} \begin{bmatrix} z_{vessel} \\ \phi_{vessel} \\ \theta_{vessel} \\ \alpha_{boom} \\ z_{mass} \end{bmatrix} \tag{5.14}
$$

If equation 5.14 is divided by the stiffness k of the element it ends up in equation 5.15. ΔL represents the elongation of the hoist wire in the direction of the element. As mentioned earlier this was the required input for the sheave wire model. With the obtained elongation a force is calculated in the sheave wire model and applied on the main block and at the crane tip. Now the bodies in the model can get in equilibrium again.

$$
\begin{bmatrix} \Delta L \\ \Delta L * R_{boom} \end{bmatrix} = \begin{bmatrix} -R_{boom} & R_{boom}R_\phi & -R_{boom}R_\theta & R_{boom}^2 & R_{boom} \\ -1 & R_\phi & -R_\theta & R_{boom} & 1 \end{bmatrix} \begin{bmatrix} z_{vessel} \\ \phi_{vessel} \\ \theta_{vessel} \\ z_{mass} \\ \alpha_{boom} \end{bmatrix} \tag{5.15}
$$

In short the element of the spring of the hoist wire is removed from the model. This element is replaced by a pair of two forces. These forces are equal in magnitude and phase. Their value has an opposite sign. When removing the stiffness and damping contributions of the hoist wires correctly from their corresponding matrices and applying the forces on the correct bodies the model is coupled.

6

Comparison study

In this chapter first the influence of friction on the dynamic hook load measurement is discussed in section 6.1. Section 6.2 shows a sensitivity analysis for the friction factors that are used. In section 6.3 the comparison is made between the imposed motion model and offshore measurements. Later in section 6.4 the comparison is made between a spring element and the sheave model for the representation of the crane hoist wires.

6.1. EFFECT OF FRICTION ON DYNAMIC LOAD MEASUREMENT

With the sheave wire model described in chapter 4 the effect of friction on the dynamic load measurement is studied. This is performed for a total of 9 different environmental conditions. Jonswap spectra are created for three different significant wave heights H_s and three different peak periods T_p. The peak-enhancement factor γ is set constant at 1.0. The used combinations are created with the following variables:

- H_s = [1.0m, 2.0m, 3.0m]

- T_p = [8s, 12s, 18s]

From linear frequency domain software LiftDyn a force RAO for a typical dual lift is taken to act as an example of the force acting in a hoist wire. This force is then applied on the hook in the sheave wire model and compared with the force that is measured in the model at the same position where the measuring force is in reality. The simplification of the model and what the forces represent can be found in Figure 6.1. The measured force points to the position of the measuring sheave.
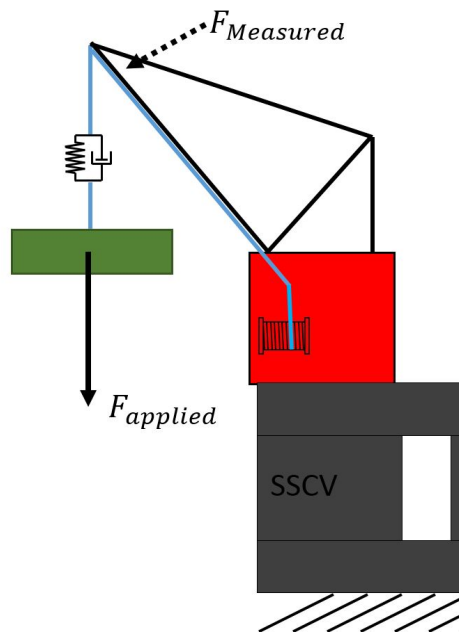
Figure 6.1: Applied and measured force representation

By comparing these two forces the influence of the friction and the resulting stick-slip motion on the load measurement can be investigated. The force RAO can be found in Figure 6.2. In this simplified case the force RAO is taken from a single wave direction as the input wave spectrum is also coming from a single direction (a 2D wave spectrum).
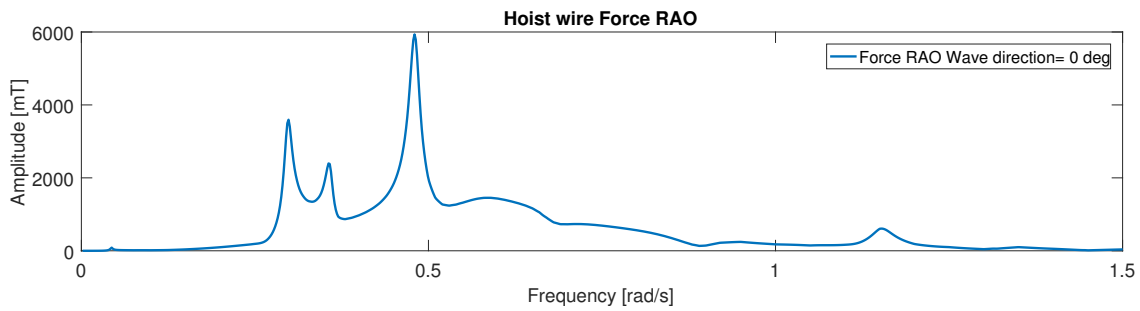
Figure 6.2: Force RAO

In Figure 6.3 the input wave spectrum and the resulting force response from the force RAO is given. The force response is calculated with equation 6.1. In this example it is done for a single case being the lowest significant wave height of $H_s = 1.0$m and lowest peak period of $T_p = 8$s. It is however done for all cases and summarized later. Figure 6.4 shows the corresponding wave height and Figure 6.5 corresponding load fluctuation for this sea state. The wave train is created by doing a IFFT with a random phase. The zeroth order moment m_0 of the spectrum should correspond to variance σ^2 of the time trace. The load fluctuation is also created with a IFFT where the phase angle is a combination of the random wave phase and the RAO force related phase.

$$S_{force} = S_\zeta |RAO_{force}|^2 \tag{6.1}$$
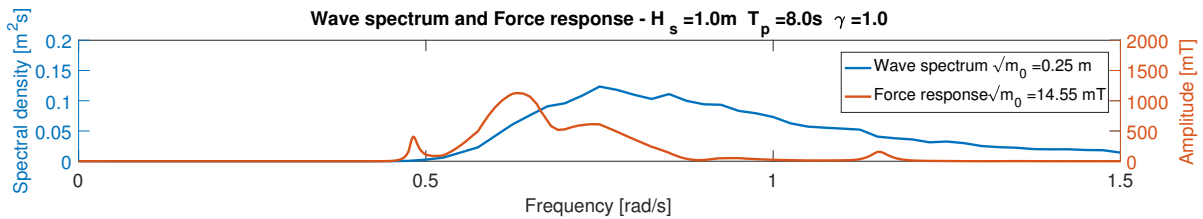
Figure 6.3: Input wave spectrum and corresponding force spectrum
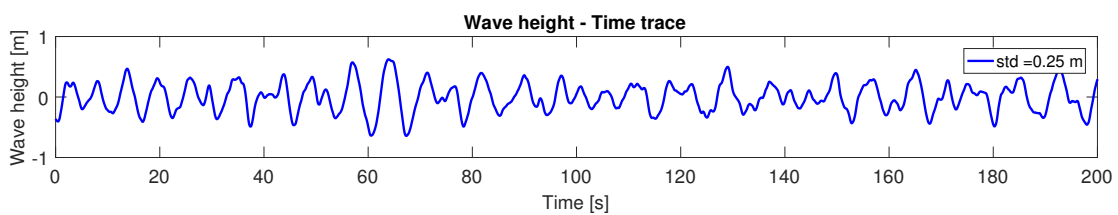
Figure 6.4: Time trace wave height
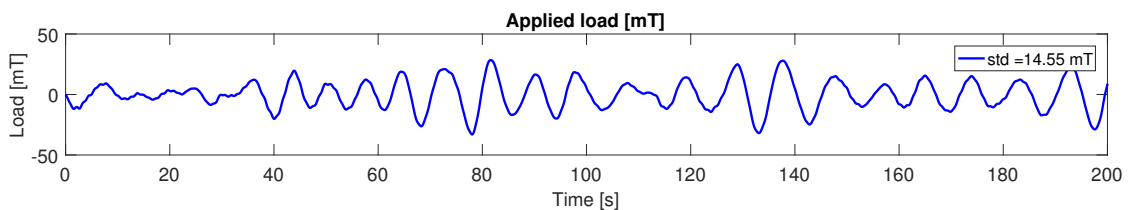
Figure 6.5: Time trace hoist wire force

With the applied loads as input for the model the simulation is performed twice for each sea state that is considered. The first simulation run is done with the static and kinetic friction factors being zero and the second run with the friction factors that were tuned by offshore measurements. The derivation of the factors is done by creating the same increase of the hook load due to crane operations in a quasi-static situation. A lower response in the measured hook load is now found as due to the stick-slip effect the applied load cannot be fully reconstructed at the measuring sheave in the model. See Figure 6.6 where both time traces of the load measurement are given. At two points the simulated measured load is different. Firstly the peaks are lower and secondly the load is constant at certain points when the sheave is in stick condition.
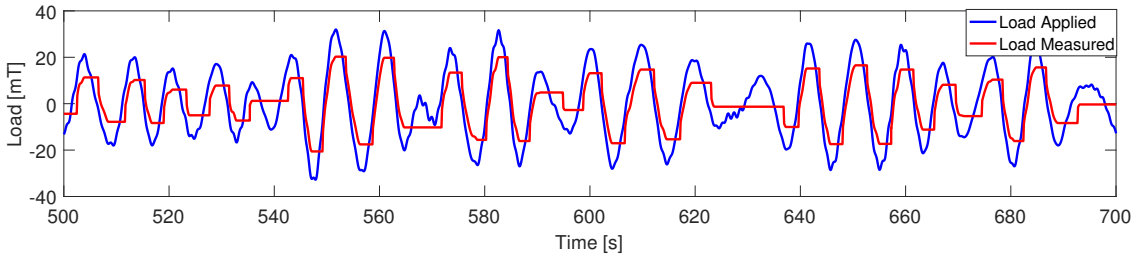
Figure 6.6: Time trace applied vs. measured

Figure 6.7 shows the response of the load that is applied in the model and the simulated measured load for the no friction case. Expected was that both spectra lie on top of each other as the friction has no influence and this is also the outcome of the model. Figure 6.8 shows the response where the friction is taken into account. Now the response of the simulated load measurement is lower.
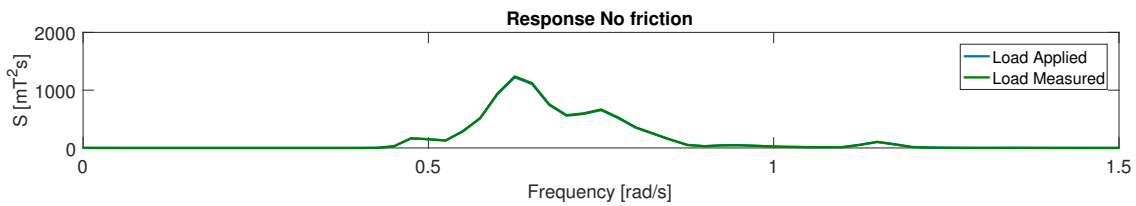
Figure 6.7: Output force spectrum: no friction
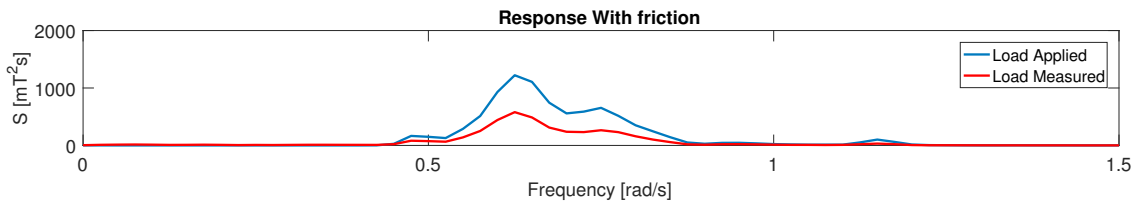
Figure 6.8: Output force spectrum: with friction

From the two time traces in Figure 6.6 a RAO can be computed to relate the applied force to the measured force for a range of frequencies. This shows how load fluctuations applied at the main block relate to measured hook load fluctuations for a certain sea state, see Figure 6.9. The RAO for the no friction case is equal to 1 as there is no difference between those two. However for the case with friction the RAO is lower than one as due to friction to observed load fluctuations at the modeled measuring sheave in 6.6 are smaller.
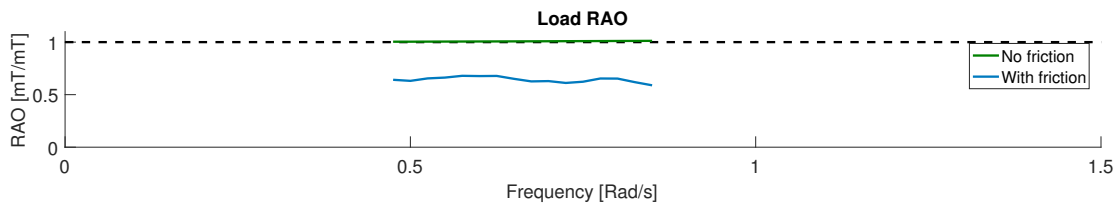
Figure 6.9: RAO between no and with friction

As mentioned earlier identical simulations and calculations are performed for a range of sea states. These are summarized in Figure 6.10. As the input wave spectra were increasing from H_s=1.0m until 3.0m the load fluctuations are also increasing. The standard deviation of the applied load is given in the legend. As the load fluctuation are increasing the force RAO is getting closer to one. This means that the dynamical load measurement is better represented by the load sensor with higher fluctuations. The discontinuities are present due to the a difference in load variance for each case that is considered.
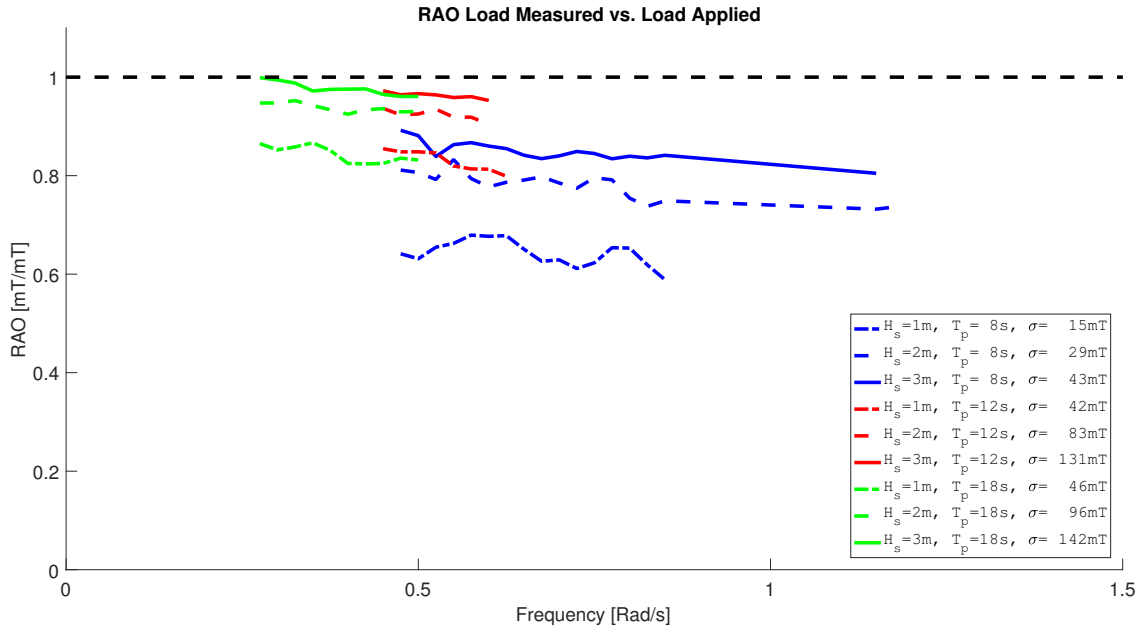
Figure 6.10: RAO for all sea states

In order to visualize it even better better in Figure 6.11 the significant double amplitude 4σ (which statistically approximates the maximum single amplitude that is in a signal) is plotted against the relative error. The relative error is calculated with equation 6.2, where σ is the standard deviation. When keeping the friction factors constant the load measurement in the model is better represented when the load fluctuations are higher. The slip condition is exceeded earlier. The error goes asymptotic to zero for higher load fluctuations.

$$Error = \left(\frac{\sigma_{no\ friction} - \sigma_{with\ friction}}{\sigma_{no\ friction}}\right) * 100\% \tag{6.2}$$
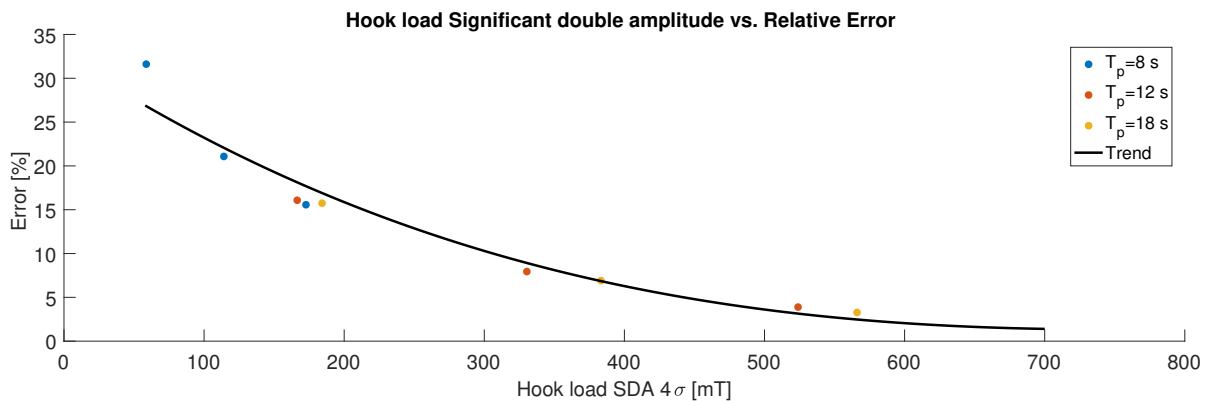
Figure 6.11: Relative error for all sea states

6.2. INFLUENCE OF FRICTION FACTORS

As explained earlier in section 4.7 the static and kinetic friction factors are based on an overall load increase or decrease of the wire force at the measuring sheave of 5%. However there might be an uncertainty for this

percentage. Therefore a sensitivity analysis is performed by varying individual friction factors for a constant environmental condition of H_s = 2.0m and T_p= 12s. This corresponded to a significant double amplitude of 4σ=332 mT. When varying one factor the other one is kept constant. Note that the kinetic friction factor can not exceed the static friction else it would result in an unrealistic situation. Figure 6.12 and Figure 6.13 show both friction factors plotted against the relative error between the variation of no friction and with friction. The relative error is calculated in the same manner as in the equation 6.2. The red dots correspond to the tuned value with a quasi-static friction increase of 5%. The kinetic friction factor has a higher influence on the dynamic load measurement as the error is increasing more rapidly.
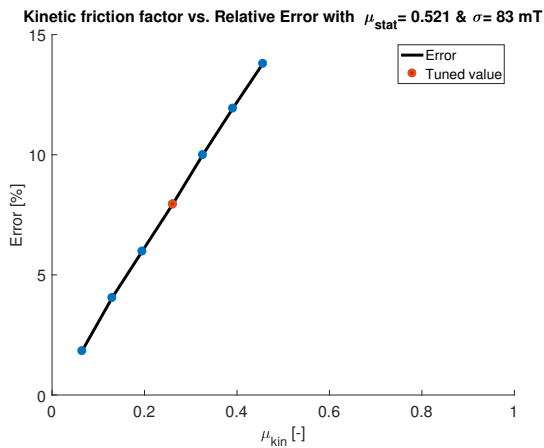
Figure 6.12: Influence kinetic friction μ_{kin}
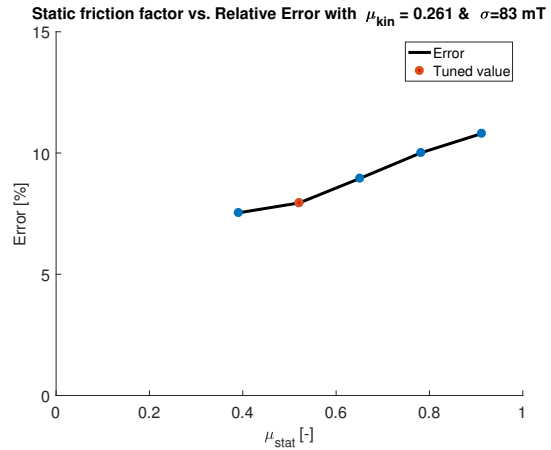
Figure 6.13: Influence static friction μ_{stat}

6.3. COMPARISON IMPOSED MOTION MODEL WITH OFFSHORE MEASUREMENTS

In this section the comparison is made for hook load responses for project A between the imposed motion model and offshore hook loads measurements. The input time traces are the measured vessel motions (heave, roll and pitch) for the free hanging stage of the installation of the topside. The forces in the starboard and port side hoist wires represented as single spring-dashpot elements are the outcomes of the model. There is not yet an integration made with the sheave model, but this is explained in the next section. The output signal of the time domain model is sampled with a rate higher than the offshore measurement sampling rate. In order to compare them equally the signal is filtered with a bandpass filter. The filter passes frequencies within a certain range and rejects frequencies outside that range. The highest frequency that is allowed in the model time trace is equal to the Nyquist frequency or half the offshore sampling frequency. As the crane measurement has a sampling frequency f_s of 1 Hz, energy can only be found above periods of 2 s. Figure 6.14 shows the obtained load fluctuations for the starboard and port side hoist wire force for the first 100 s. High frequency components are visible and with a bandpass filter the signal is reconstructed. This results in Figure 6.15.
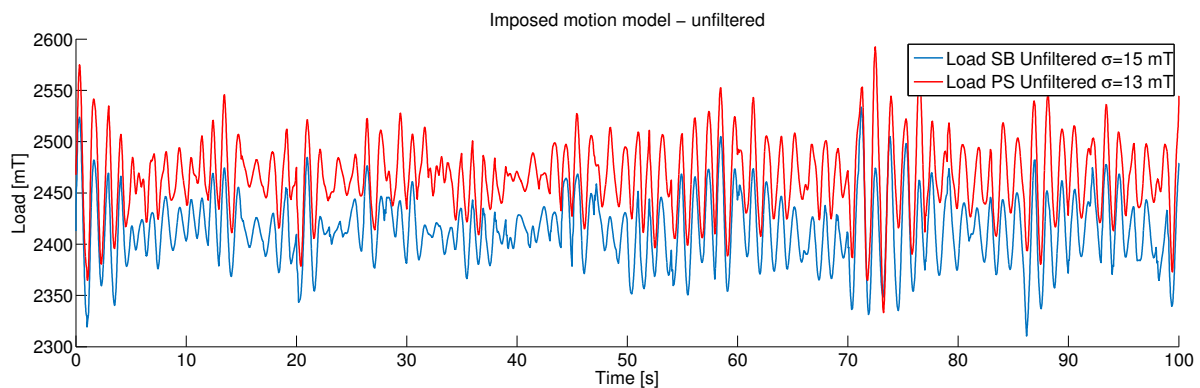
Figure 6.14: Outcome imposed motion model unfiltered
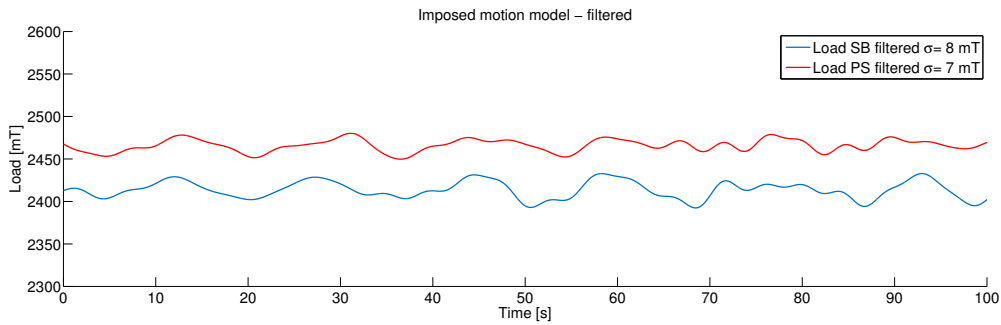
Figure 6.15: Outcome imposed motion model filtered

In Figure 6.16 are the time traces given for the first 100 s of the offshore measurement during the free hanging stage for both cranes. This load measurement is the combination of both sensors for each crane.
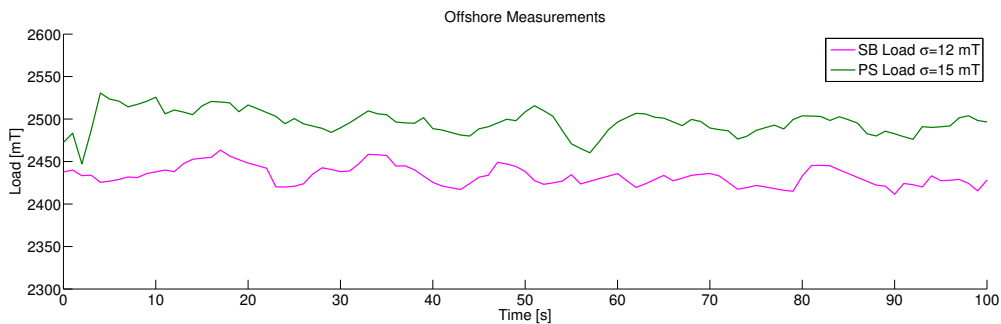
Figure 6.16: Offshore crane measurements

From both the original and filtered time trace a spectral density plot is made which can be found in Figures 6.17 and 6.18 for the starboard crane. This is done for the whole simulation and not for the first 100 s only. It is not expected that the highest frequency components are actively present in reality as well due to the axial hoist wire damping and bending of the wire at the main fall lead-in sheave. To prevent aliasing the load measurement is passing an anti-aliasing filter. An increase of the offshore sampling frequency could observe these high frequency load variation components. The anti-aliasing filter should be adapted then as well. After filtering the simulated load measurement the energy on the left side of the figure at the high frequency components disappears. This also results in a lower variance of the signal. In the spectral density plot the offshore load measurement is also plotted. The same has been performed for the port side crane in Figures 6.19 and 6.20. It is clear that the obtained load fluctuations in the imposed motion are better corresponding with reality for the starboard crane than for the port side crane. A logical reason can not be given for this. A similar analysis should be performed for other installation projects to check their outcomes.
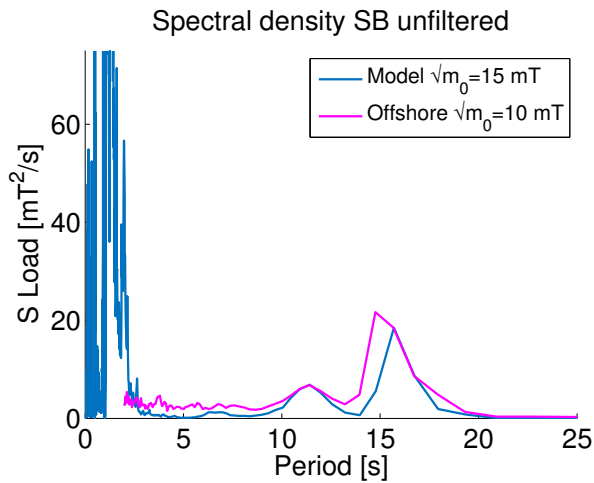
Figure 6.17: Spectrum SB crane unfiltered
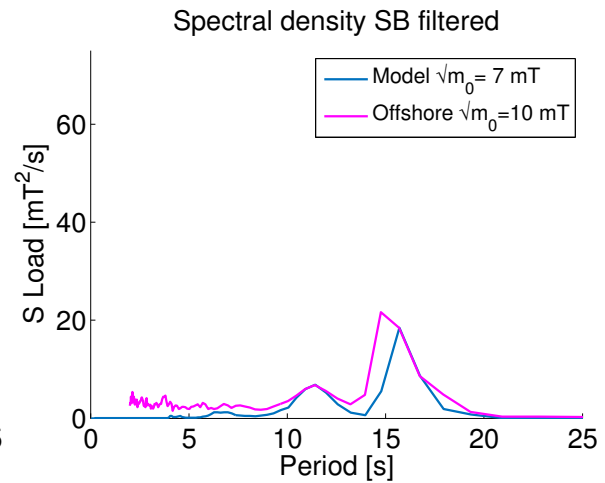
Figure 6.18: Spectrum SB crane filtered
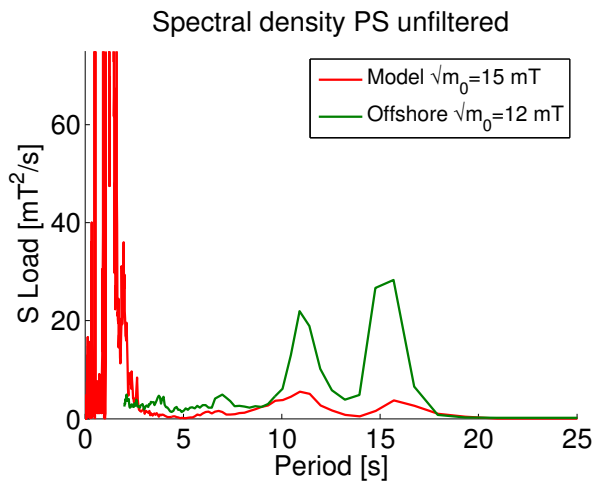
Figure 6.19: Spectrum PS crane unfiltered
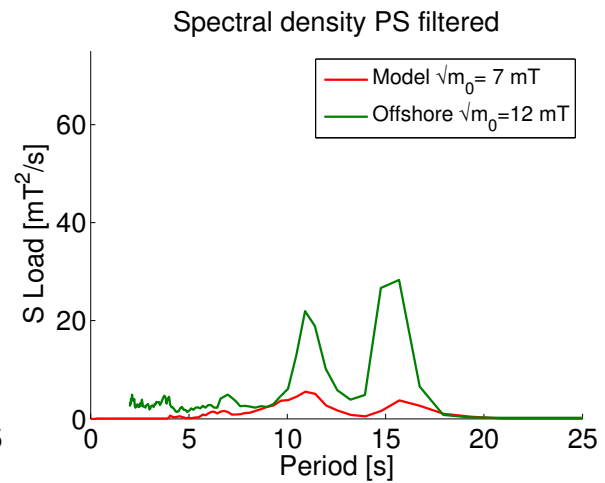
Figure 6.20: Spectrum PS crane filtered

6.4. COMPARISON SPRING ELEMENT AND SHEAVE MODEL

The sheave model is integrated by replacing a linear spring-dashpot element in the imposed motion model by the sheave model. How this coupling is made was earlier explained in section 5.4. The hoist wire spring elements of both cranes are replaced. Figure 6.21 shows the same time trace that was obtained by using a linear spring element together with the force obtained with the sheave model integration. Note that the force in the sheave model is represented by the force in the wire at the measuring sheave. The kinetic μ_{kin} and static μ_{kin} friction factors that are used are the same that were derived from steps in offshore measurements. The factors correspond to a load increase or decrease of 5 % by a lowering or hoisting operation. When taking the friction into account the simulated measurement is again lower which is in line with what was observed in section 6.1.
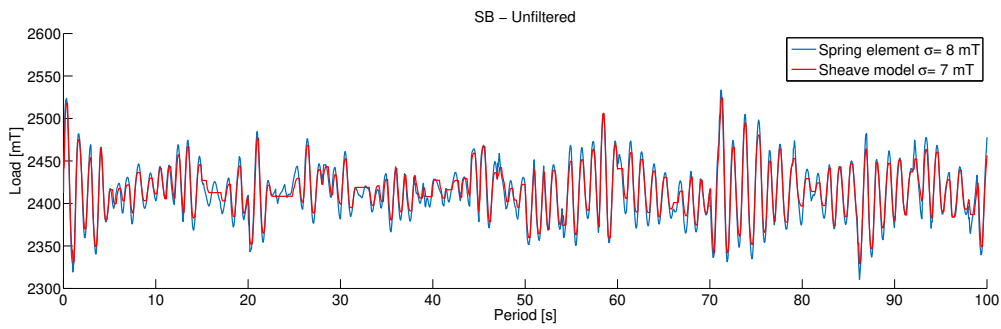
Figure 6.21: Model comparison SB crane unfiltered

The comparison is also made for the port side crane in Figure 6.22. In order to remove the high frequency components the signals are filtered with a bandpass filter again.
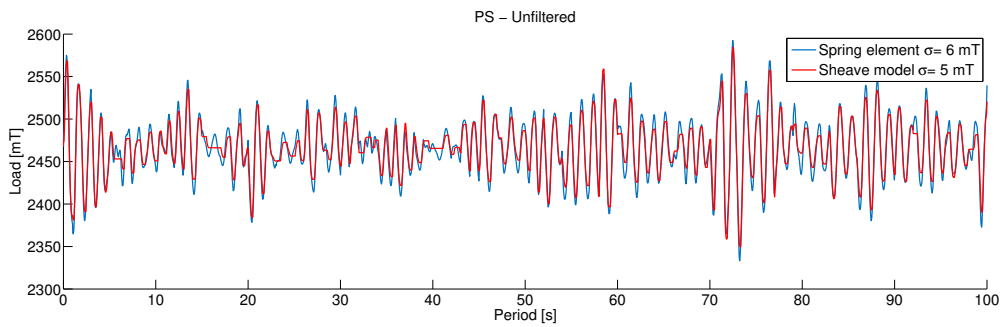
Figure 6.22: Model comparison PS crane unfiltered

After filtering the response results in Figure 6.23 and 6.24. Note that the reconstructed load signals are now composed of regular harmonic components and the nonlinear effects due to the stick-slip motion are not longer visible. Due to the friction the variation of the load is lower in the sheave model compared with using a single spring-dashpot element.
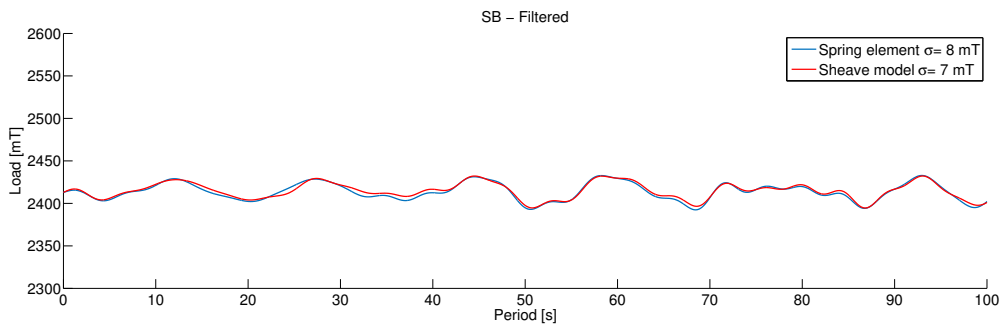
Figure 6.23: Model comparison SB crane filtered
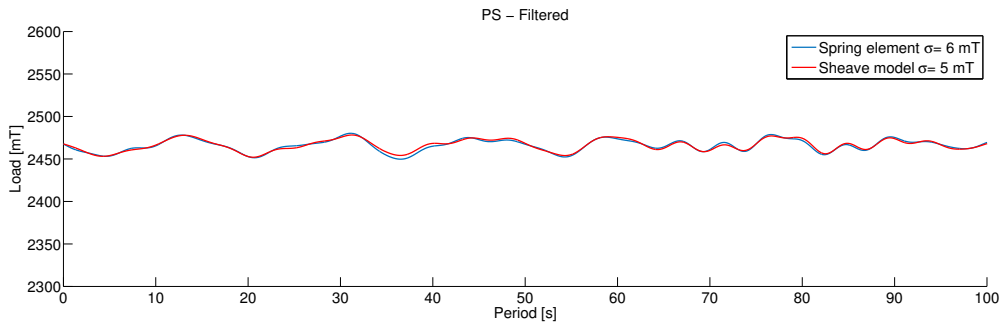
Figure 6.24: Model comparison PS crane filtered

The lower response can also be found in Figures 6.25 and 6.26 where the spectral density is visualized between the spring element in blue and the sheave model in red.
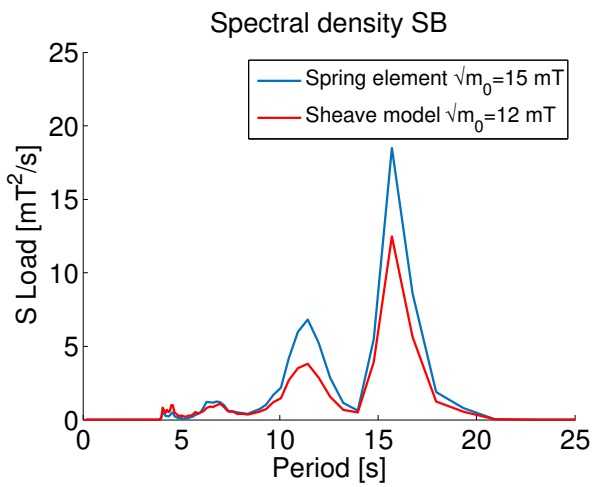
Figure 6.25: Spectral density comparison SB crane
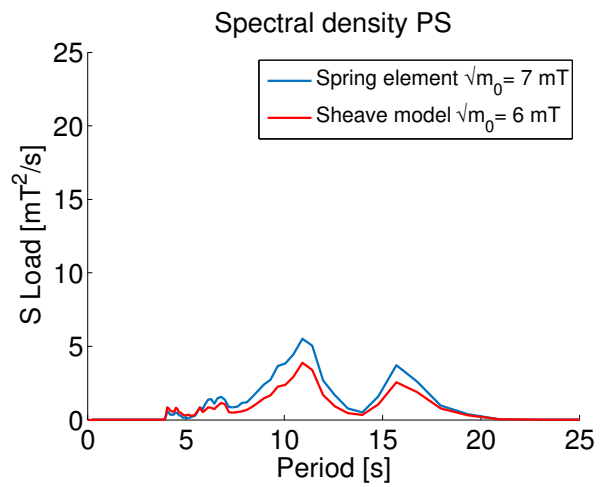
Figure 6.26: Spectral density comparison PS crane

7

Conclusion and recommendations

This chapter gives a summary and interpretation of the results of the research related to the research objectives. Also, recommendations with respect to the assumptions used in the thesis are given. Research methods and models are reviewed and future research points are detailed.

7.1. CONCLUSIONS

FORCES IN INDIVIDUAL CRANE WIRES

A model was created to simulate the behavior of the crane wire reeving. When a load is statically supported by a multiple part wire rope reeving system, the force on each rope part is the total weight divided by the number of wires. When the same load is raised, the stress (and thus the axial force) in each rope part increases progressively from the dead end to the lead line. During a lowering operation the effect is opposite. This increased stress is due to the cumulative effect of friction in the sheave bearings and the internal friction force between the fibers in a wire rope. The sum of the forces in all parts is still equal to the supported weight. With a sensor at the dead-end an increase of load is measured during hoisting and a decrease during lowering. When the operation is ended the force difference still present. When modeling dry friction at the sheave and the resulting stick-slip motion the same effects are observed.

WIRE STIFFNESS

In order to determine the wire rope stiffness an analysis was performed on destruction tests where pieces of stranded wire ropes were elongated to their brake load. Performing these tests was not part of this thesis. From the wire rope tests, a non-linear stiffness was found. The obtained stiffness was increasing while applying a higher axial load for the region between zero and the safe working load. With a low axial force the wire rope experiences a larger extension as all individual wires settle a bit. Due to friction between the individual wires the resistance to extend is increased since there is more contact at a higher stress level. By determining an equivalent stiffness of the crane wire reeving more accurate wire rope elasticity properties were obtained. The stiffness is different for the stages of the installation as the axial force in the wires is not constant. Instead of modeling nonlinear stiffness a quasi-static stiffness is used related to the mean load.

HOOK LOAD SPECTRA

For the load transfer and free hanging stages of the installation hook load spectra for individual load sensors were made and compared with the spectra of the total load. Individual sensors measure an equal force in the load transfer phase, but for the free hanging phase the sensors are experiencing a different amount of energy at certain periods. There is no systematical reason why one sensor is experiencing more load fluctuations as the other sensor. The variance of the total load is not equal to the sum of the variances of the individual sensors which demonstrates an out of phase load measurement.

INFLUENCE OF FRICTION ON DYNAMIC LOAD MEASUREMENT

The hook load at the measuring sheave in the numerical model is lower than the applied hook load when applying sheave friction in the model. Measurements are better represented with higher load fluctuations as the friction is then relatively low and the slip condition is exceeded earlier. When reflecting this to reality the measured offshore hook load fluctuations are lower than the actual hook load variations. A sensitivity

analysis showed that the kinetic friction factor has a higher influence than the static friction factor on the error of the standard deviation.

LOAD CORRECTION FACTORS

For previous topside installation projects the influence of friction of the quasi-static hook load measurement is investigated. It is correctly taken into account in the crane PLC that the correction factors are independent of the topside weight. Observed steps in the load measurement due to crane operations were proportional to the suspended load. The actual correction factors that were calculated from the measurements were both lower for lowering and hoisting operations. Meaning that the real measurement correction is on the conservative side. Even when another reeving arrangement is used the correction factor for the load can be kept the same, because the normal force on each pin then changes with the number of wires.

7.2. RECOMMENDATIONS

MODELING

Offshore load measurements of individual sensors show different phenomenon for the load transfer stage and free hanging stage. The load measurement is in phase in the load transfer stage and (partly) out of phase in the free hanging stage for some projects considered. Linear frequency domain software does not take rotation of the main block into account and it requires further efforts to model this properly. One step might be to extend the sheave wire model with the rotation of the main block. The outcome of the model could also be applied on other reeving arrangements or other crane vessels. An assumption in the model is a constant friction factor for each sheave to solve the equation of motion. Due to uneven wear this assumption might be incorrect. Tuning of the friction factors can be improved by measuring individual wire forces in a test where a wire is bended around a sheave. Another step is to validate the calculated topside motions with offshore measurements. A final step could be to impose the motion of both bodies (vessel and load) simultaneously. A drawback of the imposed motion model is that the vessel motions are not influenced by the behavior of the topside. An improvement could be to incorporate the sheave model in a time domain simulation where wave forces are used as input instead of measured vessel motions and create this interaction. Further improvements could be to reconstruct the imposed motion signals with a smaller step size to have a smooth input signal.

DAMPING

A leading thread through this research was the influence of the damping of steel wires on the model. It is discussed from a theoretical point of view. However practically it is still hard to take the damping correctly into account. It is a fact that viscous damping (due to the internal wire friction) of wire ropes is not constant, but depend on the amplitude, the frequency and the history of the oscillation. However, without a specialized experiment it is hard to predict how big the exact damping influence is. Dedicated tests could performed to determine axial damping of wires as a function of amplitude and frequency. The bending of the wire around a sheave should also be considered here as it could damp out the high frequency response that is found in modeling practices. It is questionable if all frequencies are able to reach the sensors. Modeling an additional damping at the sheave could give a first insight into this. Also dedicated tests could be performed to determine damping for the pendulum motion during a dual crane lift.

STIFFNESS

From analysis of wire rope destruction tests a non-linear stiffness was observed. More research is required to understand how this non-linear stiffness effects the vessel-crane-load system in different installation stages.

HOOK LOAD MEASUREMENT

To have a better understanding of the offshore crane measurement it is an improvement to increase the sampling rate of the sensors. Until now a sampling rate of 1 Hz is used. With a higher sampling rate the Nyquest frequency is increased resulting in capturing higher frequency components. An increase of the sampling rate is recently brought into practice on SSCV Thialf, but the results are not available yet. Another question is how the filtering of outcomes from time domain simulations match with the filter of the crane PLC.

CALIBRATION PROCEDURE

The load measuring pins are calibrated once in a few years with a load equal to the maximum capacity of the crane. The assumption is then made that the strain gauges stretches linearly with the suspended load. During this process the calibration factors are determined by averaging the effect of the crane operation. The calibration process and thereby the load measurement would become better if different loads are used to have more data points between no load and the maximum capacity. This might be possible with a tank that is slowly being emptied from the full crane capacity to completely empty. The calibration process should also be performed more often if it is financially and practically possible.

FUTURE PROJECTS

A similar analysis could be performed for other (future) offshore topside installations. Especially for the load measurement by individual sensors in the free hanging phase, the observed load increase during crane operations and the imposed motion analysis are suitable for this. For the imposed motion analysis the measured motions of the vessel (heave at C.o.G., roll and pitch) and crane load measurements in a stationary phase are required.

Bibliography

[Bridon, 2016] Bridon (2016). Bridon High Performance Offshore Wire Ropes Dyform 6.

[Chaplin, 1991] Chaplin, C. R. (1991). Damping in Wire Rope.

[Cooley and Tukey, 1964] Cooley, J. W. and Tukey, J. W. (1964). An Algorithm for the Machine Calculation of Complex Fourier Series.

[Hartmans, 2016] Hartmans, T. (2016). Hook Load Fluctuations during Offshore Heavy Lifting. Technical report, Delft University of Technology.

[Huisman Special Lifting Equipment BV, 2007] Huisman Special Lifting Equipment BV (2007). Manual Load Measuring Pins.

[Martins et al., 1990] Martins, J. A. C., Oden, J. T., and Simoes, F. M. F. (1990). Recent Advances in Engineering Science - a Study of Static and Kinetic Friction. *International Journal of Engineering Science.*

[Meskers, 2000] Meskers, G. (2000). LiftDyn Theory Manual. Technical report, HMC.

[Ottens, 2016] Ottens, H. (2016). Software Validation Montrose Dynamic Lift. Technical report, HMC.

[Poe, 2000] Poe, J. (2000). Wire Rope Sheave Friction Effects on the Takeup Carriage Belt Tension.

[Raoof and Davies, 2003] Raoof, M. and Davies, T. J. (2003). Simple determination of the axial stiffness for large- diameter independent wire rope core or fibre core wire ropes.

[Schaap, 2017] Schaap, V. (2017). Hoist wire stiffness - destruction tests. Technical report, HMC.

[Spijkers et al., 2005] Spijkers, J. M. J., Vrouwenvelder, A. W. C. M., and Klaver, E. C. (2005). Structural Dynamics CT 4140 Part 1 -Structural Vibrations.

[Sundararajan D, 2001] Sundararajan D (2001). *The Discrete Fourier Transform.*

[Vanderveldt et al., 1973] Vanderveldt, H. H., Chungand, B. S., and Reader W. T. (1973). Some Dynamic Properties of Axially Loaded Wire Ropes. *Experimental Mechanics.*

A

Equations of rigging equipment

To derive the equations of motion for a load connected with slings or grommets between the load and the main block the displacement method is used. This is done for the motions of the topside connected with slings to the main block of the crane. The steel wires are represented as linear spring-dashpot elements with the properties described earlier in section 2.2 and 2.3. The derivation is first performed for a free hanging load with only a translation in x- and z-direction and rotation around the y-axis (3DOF), see section A.1 and later for three translations and three rotations (6DOF), in section A.2.

A.1. EQUATIONS OF MOTION 3DOF

A 2D cross-section of rigging equipment is given in Figure A.1 When considering only one of the two slings, in this case the one on the right, the force of the spring and damper is a function of the motion in the x- and z-direction and a rotation, see Figure A.2. In this figure the dashed line is the original position of the load. The left part of the figure shows the force due to the horizontal displacement, the middle part shows the force due to a vertical displacement and on the right the force due to a rotation around the center of gravity is displayed.
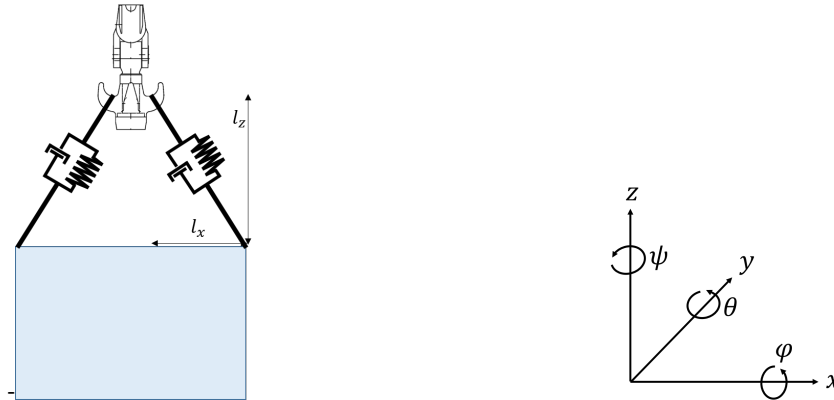
Figure A.1: Rigging configuration for free hanging load 3DOF
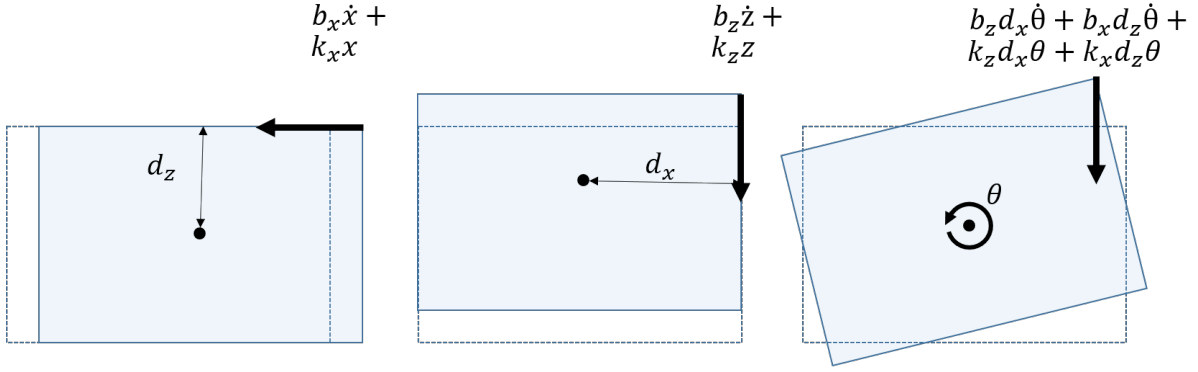
Figure A.2: Displacement method for rigging 3DOF

With the forces from Figure A.2 the equations of motion can be found in equation A.1 for this three degree of freedom system. Where m is the mass and J the mass moment of inertia of the load. In this equation is the stiffness matrix $\mathbf{K_i}$, see equation A.4, and the damping matrix $\mathbf{B_i}$, see equation A.5 composed for each sling. When multiple symmetric slings are added up together some of the terms cancel each other due to contradictory signs. However generally the slings are not symmetrically due to the distribution of the mass and the geometry of the load.

$$
\begin{bmatrix} m & 0 & 0 \\ 0 & m & 0 \\ 0 & 0 & J_{yy} \end{bmatrix} \begin{bmatrix} \ddot{x} \\ \ddot{z} \\ very\ddot{\theta} \end{bmatrix} = \sum_{n=1}^{\#Slings} \mathbf{B}_i \begin{bmatrix} \dot{x} \\ \dot{z} \\ \dot{\theta} \end{bmatrix} + \sum_{n=1}^{\#Slings} \mathbf{K}_i \begin{bmatrix} x \\ z \\ \theta \end{bmatrix}
\tag{A.1}
$$

The stiffness matrix $\mathbf{K}_i$ is the matrix for a single sling represented as a linear spring as a function of the angles α_x (angle between sling and x-axis) and α_z (angle between sling and z-axis).

$$
\alpha_x = \arctan\left(\frac{l_z + z}{l_x + x}\right)
\tag{A.2}
$$

$$
\alpha_z = \arctan\left(\frac{l_x + x}{l_z + z}\right)
\tag{A.3}
$$

The length l_x and l_z are the initial distances between the connection point and the attachment to the block. Because this distance increases or decreases due to a displacement x,z or θ, the angle also differs slight, as can be seen in equations A.2 and A.3, the angle is recalculated every time step and adjusted in the stiffness and damping matrix. The distance d_x and d_z represent the distances between the center of gravity and the connection point of the sling on the load.

$$
\mathbf{K_i} = k \begin{bmatrix} \cos(\alpha_x) & 0 & -d_z\cos(\alpha_x) \\ 0 & \cos(\alpha_z) & d_x\cos(\alpha_z) \\ -d_z\cos(\alpha_x) & d_x\cos(\alpha_z) & d_x^2\cos(\alpha_z) + d_z^2\cos(\alpha_x) \end{bmatrix}
\tag{A.4}
$$

$$
\mathbf{B_i} = b \begin{bmatrix} \cos(\alpha_x) & 0 & -d_z\cos(\alpha_x) \\ 0 & \cos(\alpha_z) & d_x\cos(\alpha_z) \\ -d_z\cos(\alpha_x) & d_x\cos(\alpha_z) & d_x^2\cos(\alpha_z) + d_z^2\cos(\alpha_x) \end{bmatrix}
\tag{A.5}
$$

A.2. EQUATIONS OF MOTION 6DOF

The same as was done for the three degree of freedom system in 2D can be done for six degree of freedom in 3D (Figure A.3). First the displacement method is again used to find the force in a single sling due to the displacements (Figure A.4). The top three figures show the forces due to the translations and the forces due the three rotations are displayed in the bottom ones.

Figure A.3: Rigging configuration for free hanging load 6DOF

$$b_x \dot{x} + k_x x$$

$$b_y \dot{y} + k_y y$$

$$b_z \dot{z} + k_z z$$

$$b_y d_z \dot{\varphi} + b_z d_y \dot{\varphi} + k_y d_z \varphi + k_z d_y \varphi$$

$$b_z d_x \dot{\theta} + b_x d_z \dot{\theta} + k_z d_x \theta + k_x d_z \theta$$

$$b_x d_y \dot{\psi} + b_y d_x \dot{\psi} + k_x d_y \psi + k_y d_x \psi$$
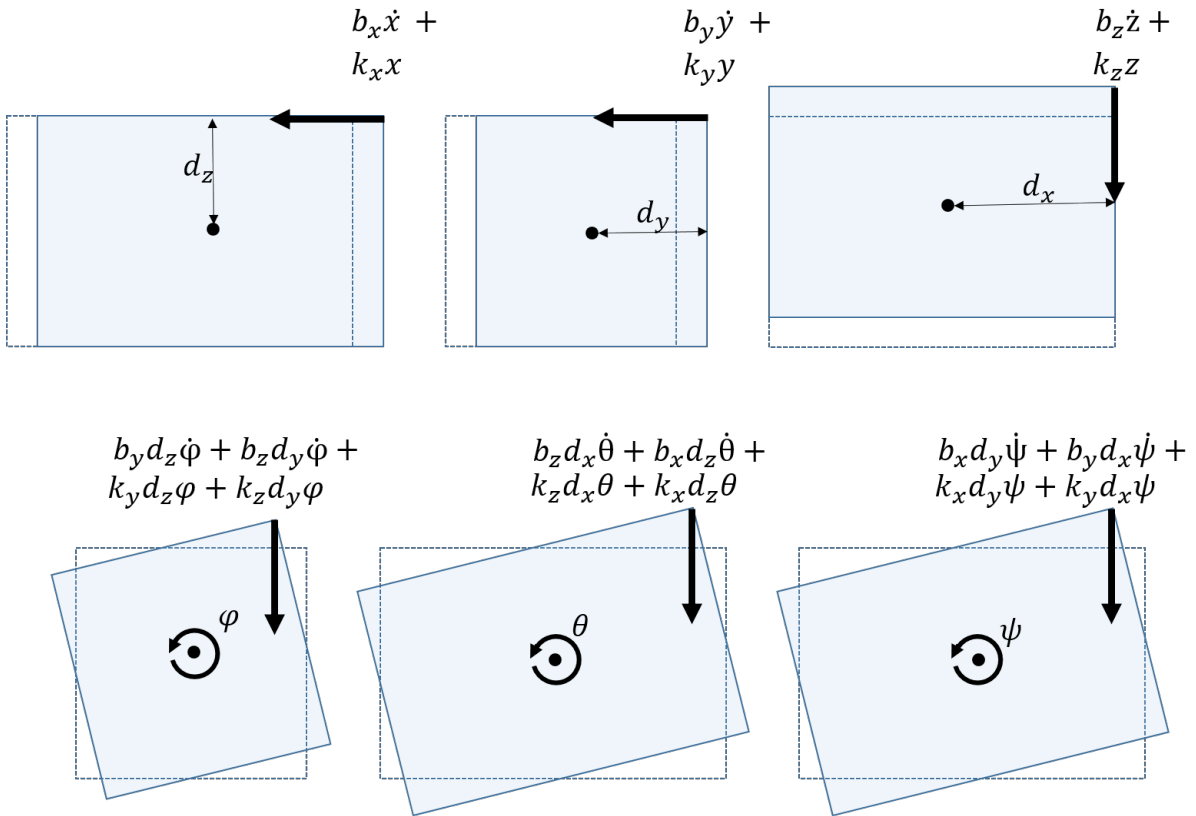
Figure A.4: Displacement method for rigging 6DOF

With the displacement method in 3D equation A.1 can be expanded to in total six displacements, creating a vector with a length of 6 (equation A.6). Again the damping $\mathbf{B}_i$ and stiffness $\mathbf{K}_i$ matrices are constructed for each single sling, see equations A.11 and A.10. The stiffness matrix is a function the three angles the slings makes with the block, see eq. A.7 until A.9.

$$\begin{bmatrix} m & 0 & 0 & 0 & 0 & 0 \\ 0 & m & 0 & 0 & 0 & 0 \\ 0 & 0 & m & 0 & 0 & 0 \\ 0 & 0 & 0 & J_{xx} & 0 & 0 \\ 0 & 0 & 0 & 0 & J_{yy} & 0 \\ 0 & 0 & 0 & 0 & 0 & J_{zz} \end{bmatrix} \begin{bmatrix} \ddot{x} \\ \ddot{y} \\ \ddot{z} \\ \ddot{\phi} \\ \ddot{\theta} \\ \ddot{\psi} \end{bmatrix} = \sum_{n=1}^{\#Slings} \mathbf{B_i} \begin{bmatrix} \dot{x} \\ \dot{y} \\ \dot{z} \\ \dot{\phi} \\ \dot{\theta} \\ \dot{\psi} \end{bmatrix} + \sum_{n=1}^{\#Slings} \mathbf{K_i} \begin{bmatrix} x \\ y \\ z \\ \phi \\ \theta \\ \psi \end{bmatrix}$$ (A.6)

$$\alpha_x = \arctan\left(\frac{\sqrt{(l_y + y)^2 + (l_z + z)^2}}{l_x + x}\right)$$ (A.7)

$$\alpha_y = \arctan\left(\frac{\sqrt{(l_x + x)^2 + (l_z + z)^2}}{l_y + y}\right) \tag{A.8}$$

$$\alpha_z = \arctan\left(\frac{\sqrt{(l_x + x)^2 + (l_y + y)^2}}{l_z + z}\right) \tag{A.9}$$

$$\mathbf{B_1} = b \begin{bmatrix} \cos(\alpha_x) & 0 & 0 & 0 & -d_z\cos(\alpha_x) & d_y\cos(\alpha_x) \\ 0 & \cos(\alpha_y) & 0 & -d_z\cos(\alpha_y) & 0 & d_x\cos(\alpha_y) \\ 0 & 0 & \cos(\alpha_z) & -d_y\cos(\alpha_z) & d_x\cos(\alpha_z) & 0 \\ 0 & -d_z\cos(\alpha_y) & -d_y\cos(\alpha_z) & d_z^2\cos(\alpha_y) + d_y^2\cos(\alpha_z) & 0 & 0 \\ -d_z\cos(\alpha_x) & 0 & d_x\cos(\alpha_z) & 0 & d_x^2\cos(\alpha_z) + d_z^2\cos(\alpha_x) & 0 \\ d_y\cos(\alpha_x) & d_x\cos(\alpha_y) & 0 & 0 & 0 & d_y^2\cos(\alpha_x) + d_x^2\cos(\alpha_y) \end{bmatrix} \tag{A.10}$$

$$\mathbf{K_1} = k \begin{bmatrix} \cos(\alpha_x) & 0 & 0 & 0 & -d_z\cos(\alpha_x) & d_y\cos(\alpha_x) \\ 0 & \cos(\alpha_y) & 0 & -d_z\cos(\alpha_y) & 0 & d_x\cos(\alpha_y) \\ 0 & 0 & \cos(\alpha_z) & -d_y\cos(\alpha_z) & d_x\cos(\alpha_z) & 0 \\ 0 & -d_z\cos(\alpha_y) & -d_y\cos(\alpha_z) & d_z^2\cos(\alpha_y) + d_y^2\cos(\alpha_z) & 0 & 0 \\ -d_z\cos(\alpha_x) & 0 & d_x\cos(\alpha_z) & 0 & d_x^2\cos(\alpha_z) + d_z^2\cos(\alpha_x) & 0 \\ d_y\cos(\alpha_x) & d_x\cos(\alpha_y) & 0 & 0 & 0 & d_y^2\cos(\alpha_x) + d_x^2\cos(\alpha_y) \end{bmatrix} \tag{A.11}$$

B

Crane reeving SSCV Thialf

C
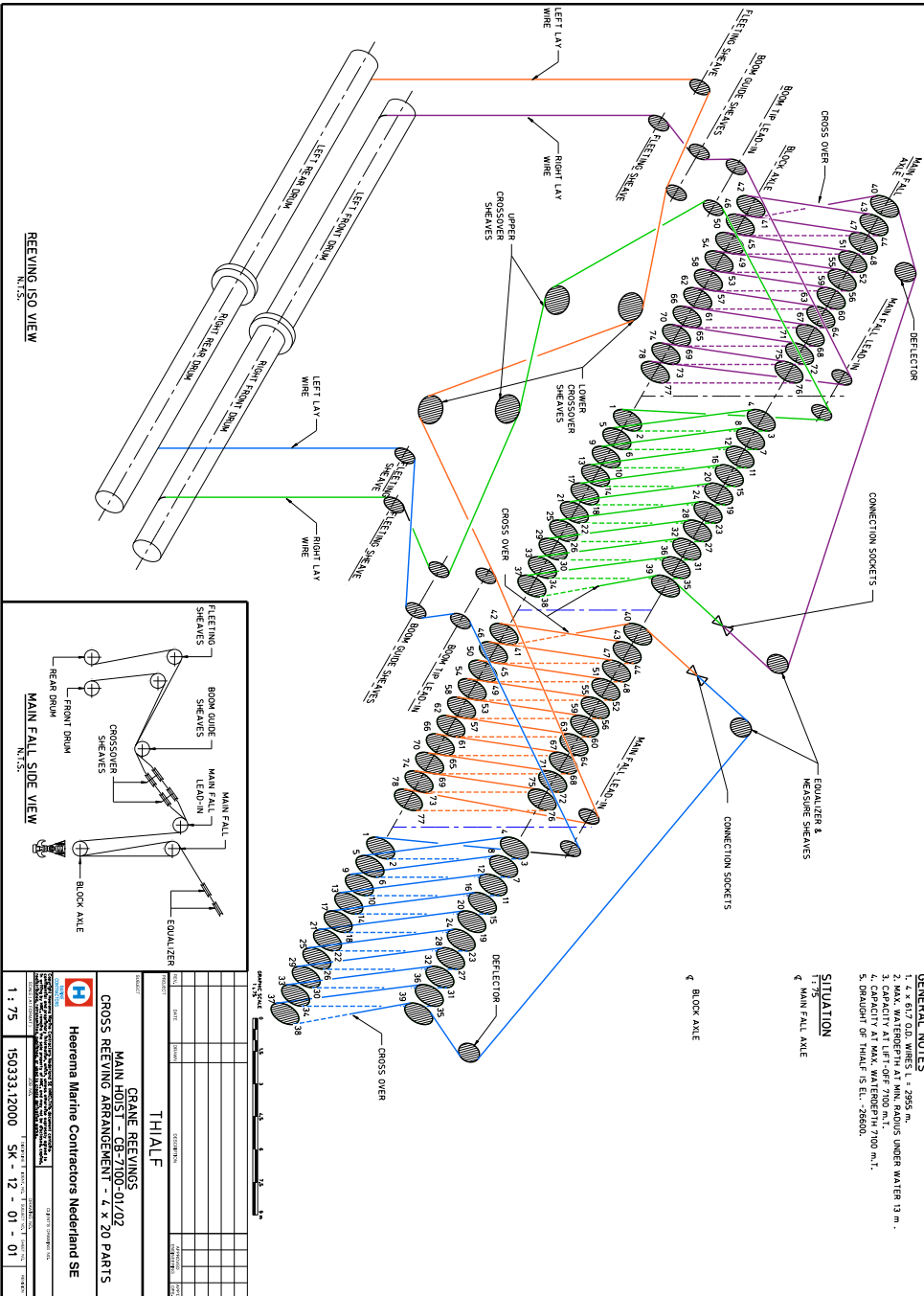
Crane reeving DCV Balder
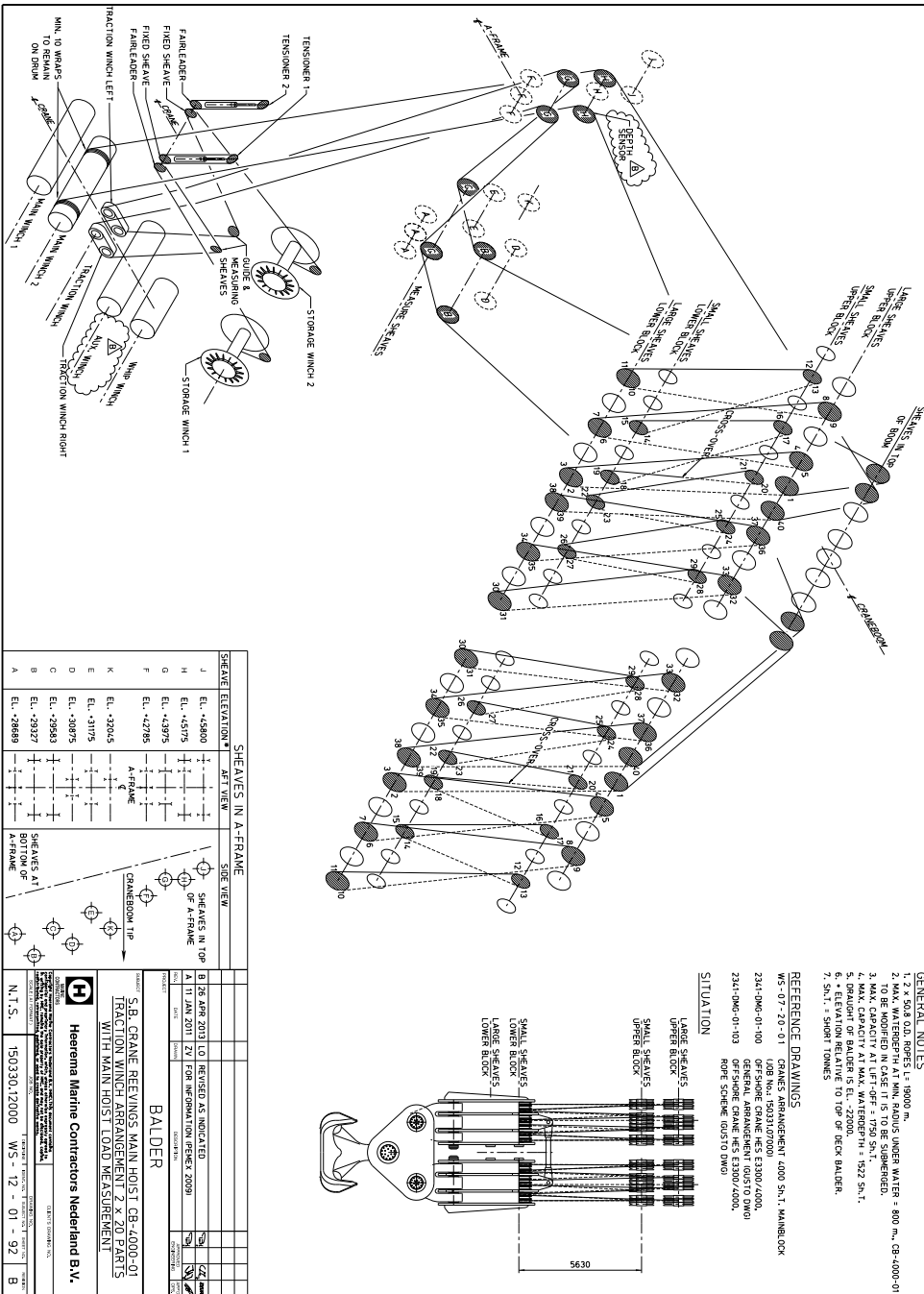
D

Spectral density difference of two sensors

In the following sections the spectral density plots are shown for the free-hanging phase. This is done for all topside installation projects where data was available for measurements of individual load sensors of the crane.The blue lines represent the measurement by sensor 1, the red line the measurement of sensor 2 and the magenta line is the total load measurement (being the sum of sensor 1 and 2).

D.1. PROJECT B
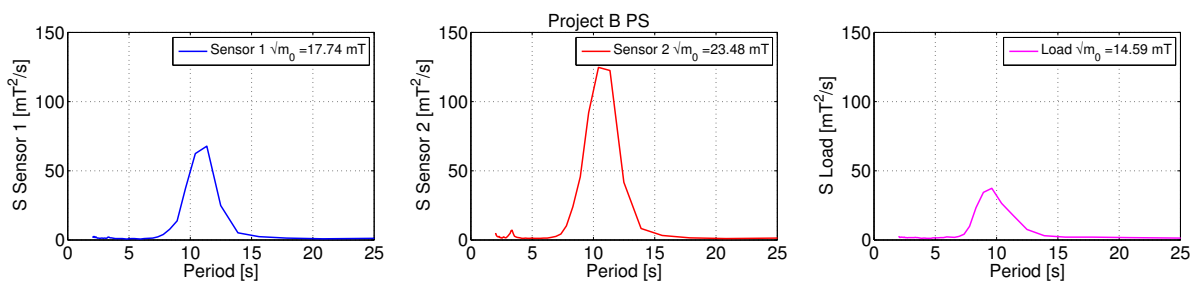
Figure D.1: Load spectrum PS project B
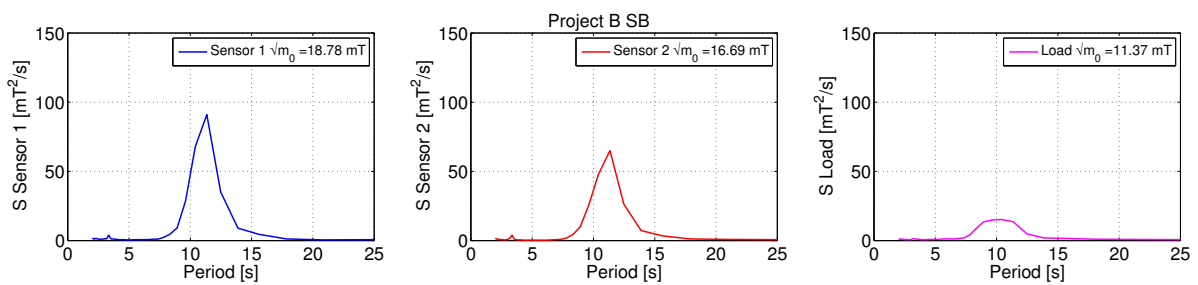
Figure D.2: Load spectrum SB project B

D.2. PROJECT C
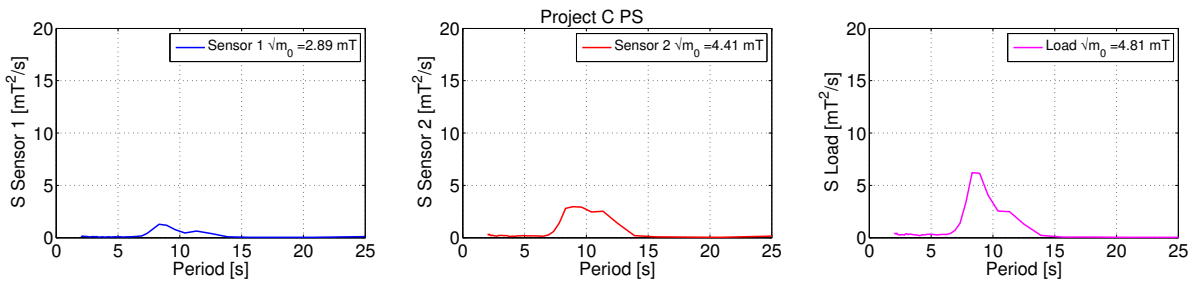
Figure D.3: Load spectrum PS project C
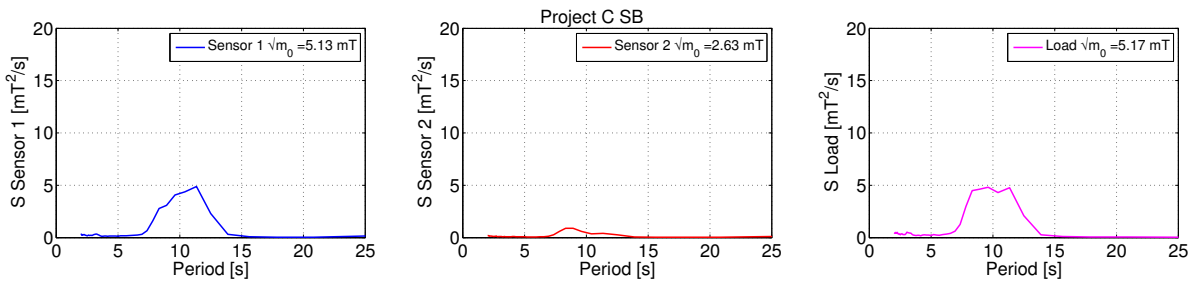
Figure D.4: Load spectrum SB project C

D.3. PROJECT D
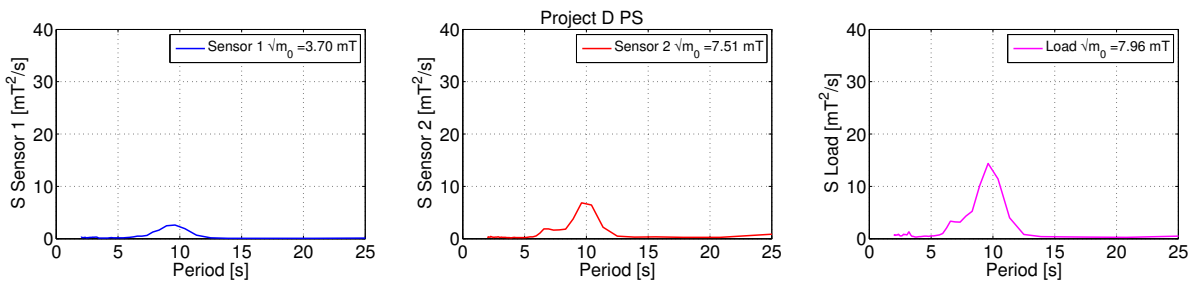
Figure D.5: Load spectrum PS project D
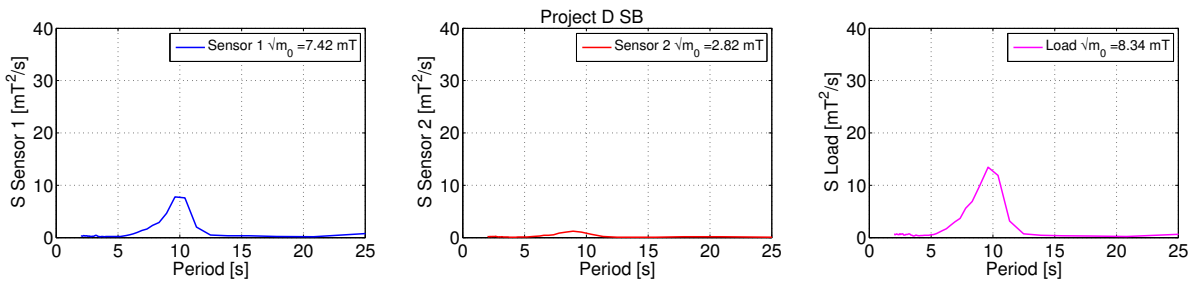
Figure D.6: Load spectrum SB project D

D.4. PROJECT E
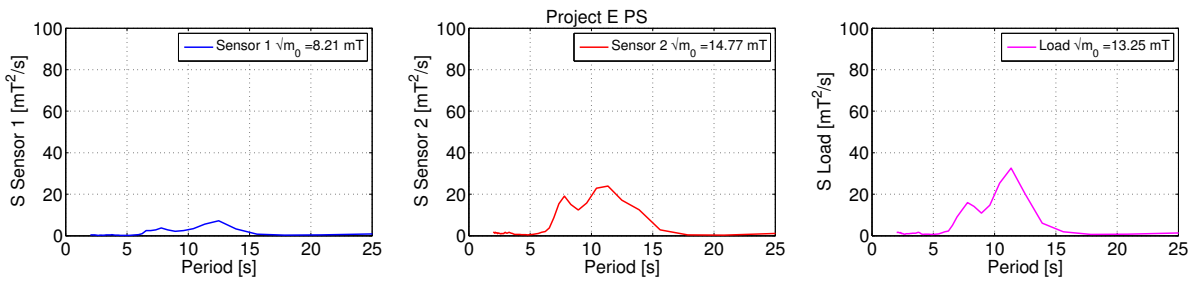
Figure D.7: Load spectrum PS project E
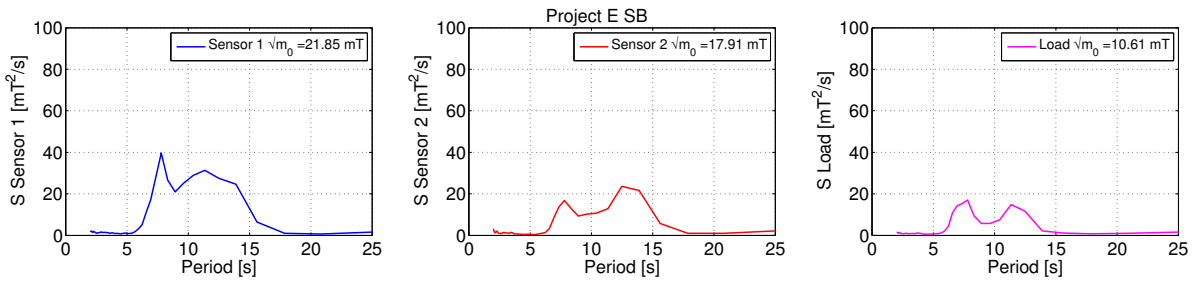
Figure D.8: Load spectrum SB project E

D.5. PROJECT F
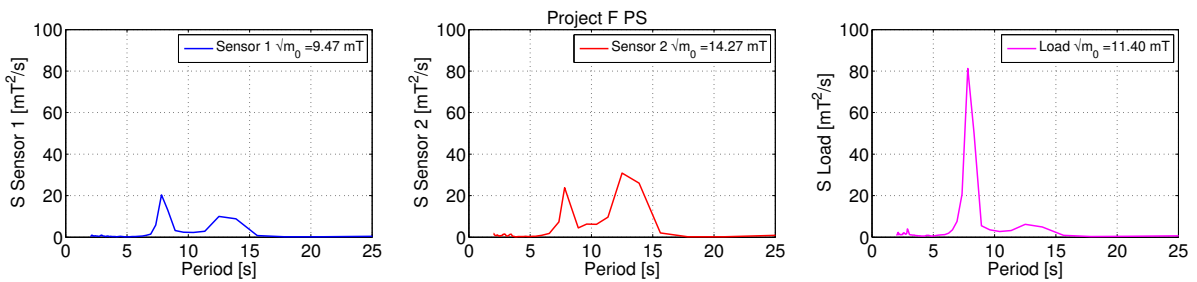
Figure D.9: Load spectrum PS project F
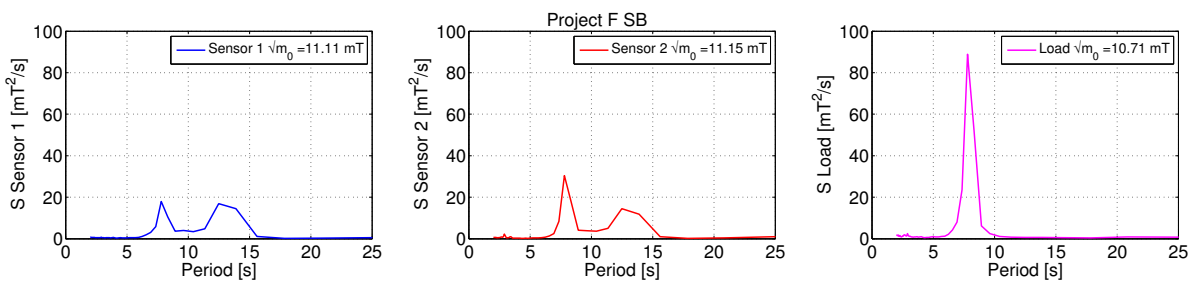
Figure D.10: Load spectrum SB project F

D.6. PROJECT G
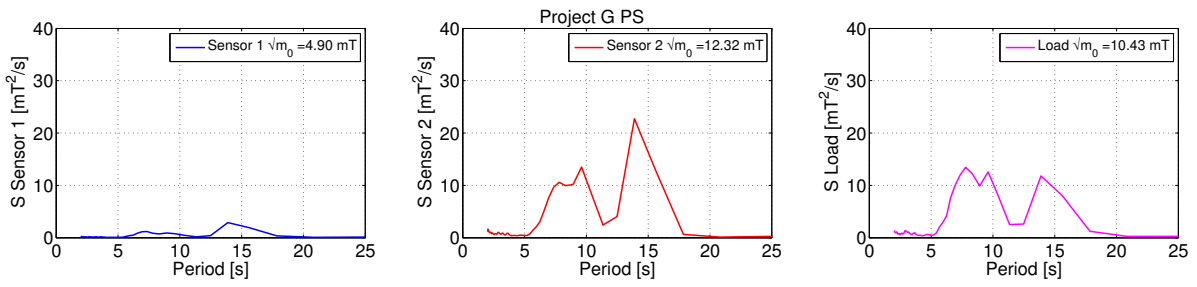
Figure D.11: Load spectrum PS project G
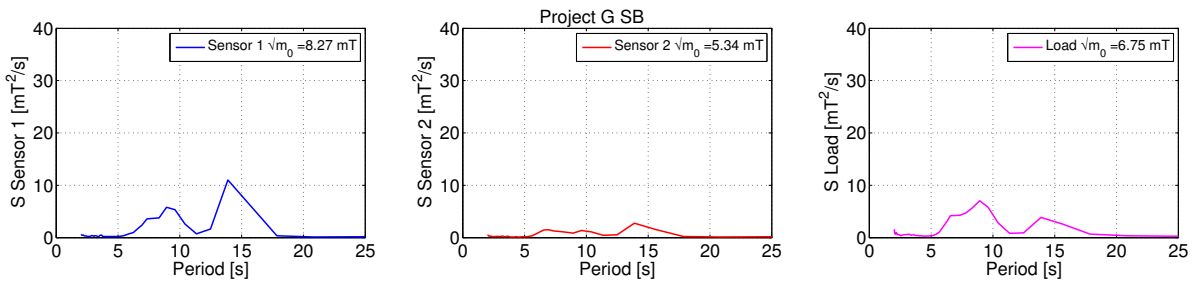
Figure D.12: Load spectrum SB project G

D.7. PROJECT H
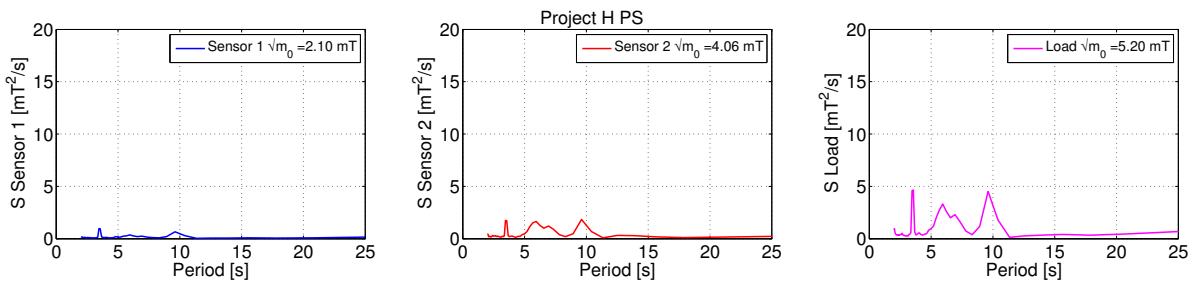
Figure D.13: Load spectrum PS project H
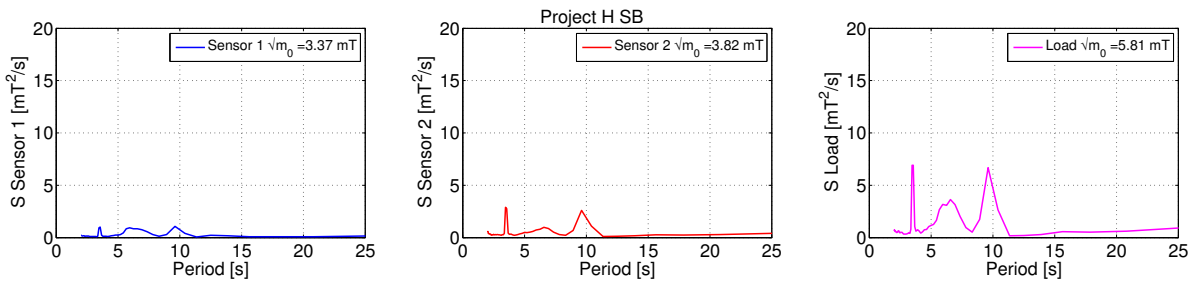
Figure D.14: Load spectrum SB project H

D.8. PROJECT I
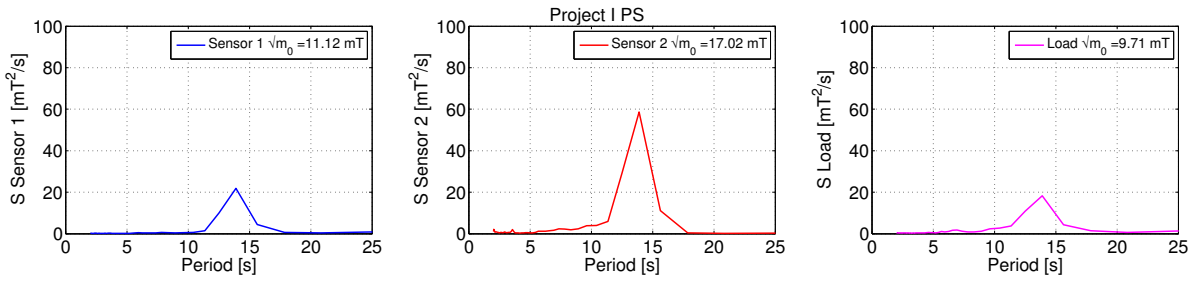
Figure D.15: Load spectrum PS project I
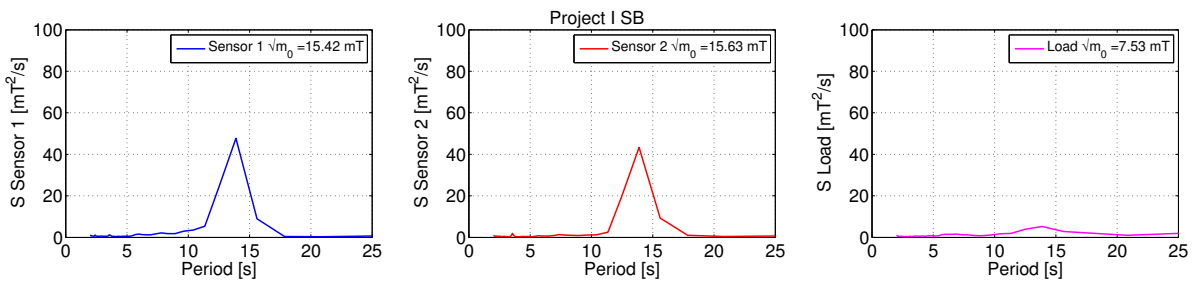
Figure D.16: Load spectrum SB project I

D.9. PROJECT J
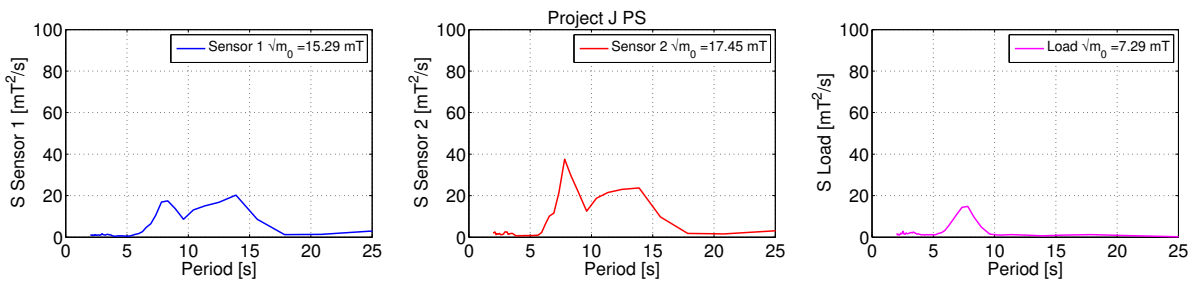
Figure D.17: Load spectrum PS project J

E

Rotation of main block in LiftDyn

From section 3.3 it was found that the spectral density plot of the total hook load measurement is lower than the summation of the spectral density of the individual signals. The conclusion that was drawn is that the load measurement of the individual hoist wires are acting in anti-phase. If they were acting in phase the spectral density of the total load would be higher as the density of an individual sensor. The anti-phase measurements may come from the point that the main block is making a rotational oscillation. The crane hoist wires of a dual heavy lift that are modeled with LiftDyn generally consists of a single connector element (see Figure E.1). All elements join together in a single point. This makes it unable to model the effect of a main block that is rotating and thereby the anti-phase in the measurement. In order to take this effect into account the connector element was replaced by a set of spring elements symmetrically attached to the block (Figure E.2. Also the attachment of the rigging equipment on the prongs was taken into account. After the adaption the Force RAO and phase lead of those two hoist wires elements was computed, see Figure E.3. The mode that should amplify the rotation of the main block is the roll-sway mode (vessel rolls, topside moves in global y-direction), which has its natural period at 12.81 s. When comparing the phase plots of both connector elements the phase lies exactly on top of each other, meaning that the load fluctuations are not canceling out each other.
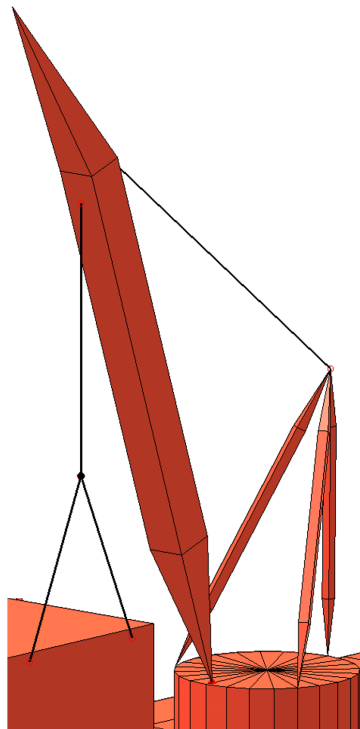
Figure E.1: Original situation   Figure E.2: Situation with rotation of main block
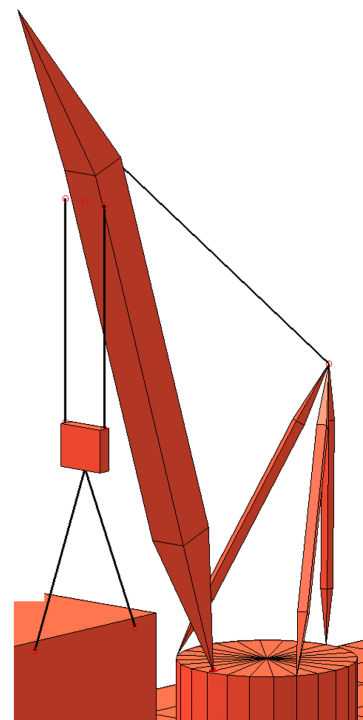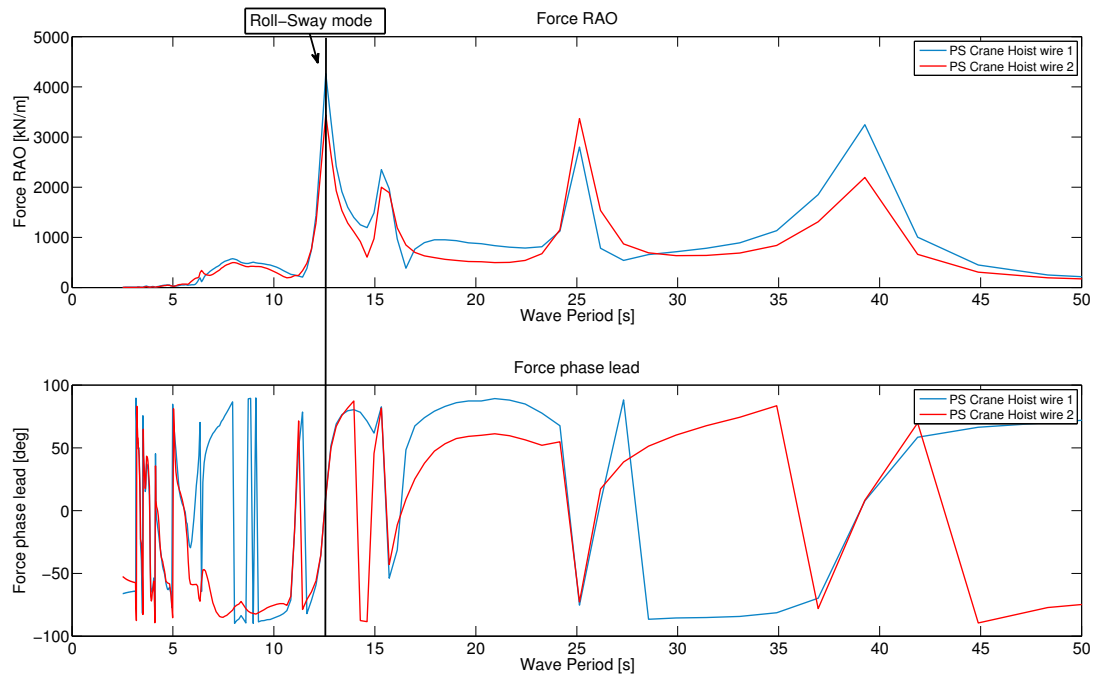
Figure E.3: Force RAO and phase lead of a set of hoist wires on the same crane

F

Simulink crane wire reeving model

This appendix gives an overview of the Simulink model that is created to simulate the rotational motions of the sheaves. It is divided into several sections where firstly an overview is given and later the inside of a block is presented. Prior to the simulation a Matlab file is ran to load all variables and initial conditions. During the simulation all motions of the sheaves are saved and transferred to the workspace in Matlab. After the completion the post-processing takes place where the wire forces are computed and plots are made of the outcomes.

F.1. OVERVIEW OF ALL SHEAVES

The overview of the model is divided into four sections distinguished by four different colors where each block represents one sheave. Inside each block the equation of motion is solved. The output of the sheaves is used where the wire that runs over it is going to or coming from. The letters A until D relate to the four parts of the crane reeving of the SSCV and match with the colors used in B, see Table F.1. The dark shaded blocks correspond to the sheaves at the main fall axle and the light colored ones to the sheaves at the block axle. The cyan blocks correspond to the sheaves between the winches and the main fall lead in. Those sheaves redirect the wire through the structure of the crane. The winches are represented by the four white blocks on the left side of the figure. The white blocks on the right side are being the measuring sheaves and have the task to calculate the hoist wire force.

Table F.1: Thialf wire distinction

A	Purple	Left
B	Green	Center Left
C	Blue	Center Right
D	Orange	Right

F.2. OVERVIEW OF SIMULINK MODEL
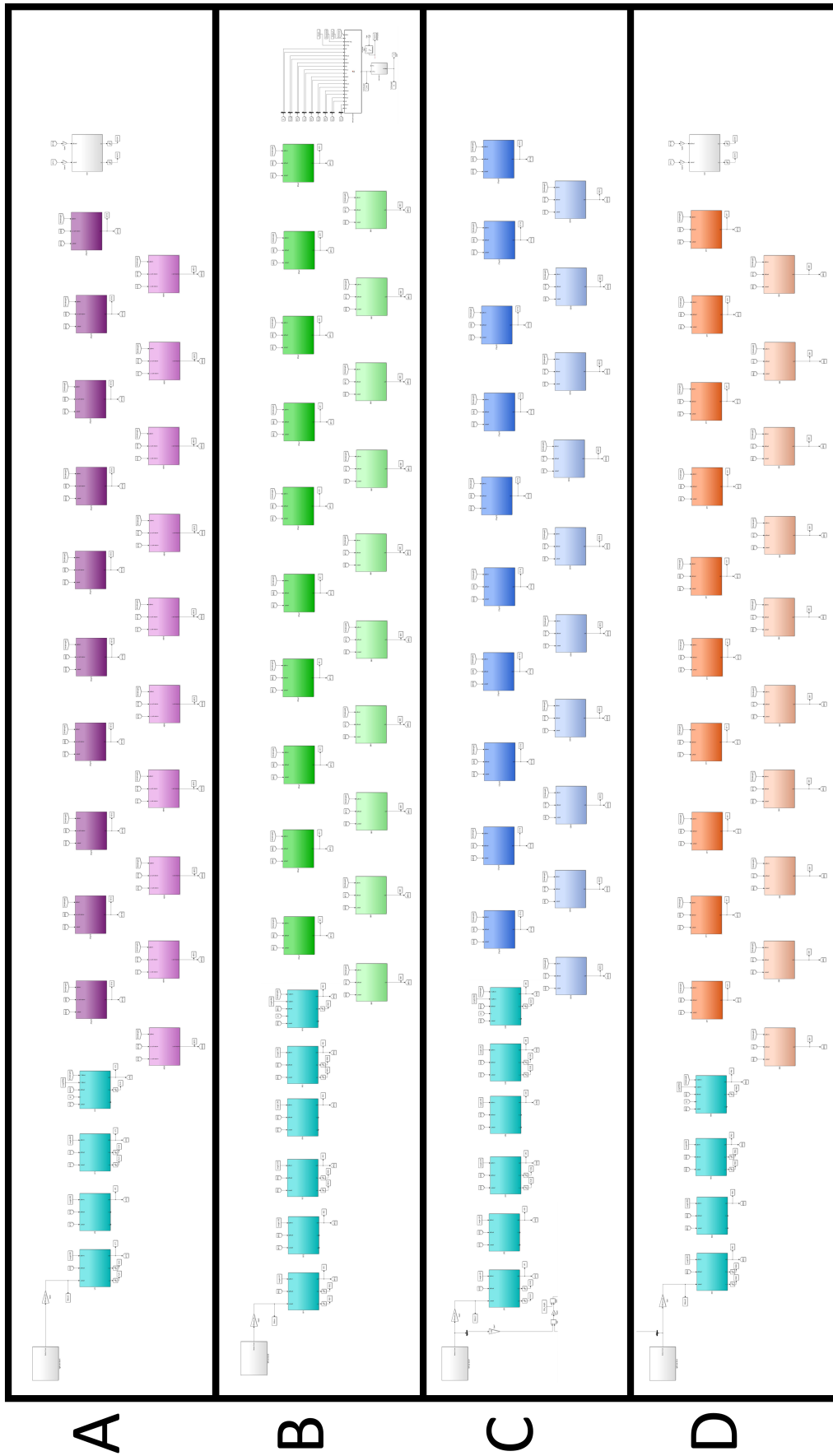
Figure F.1: Simulink model overview

F.3. DETAIL OF PART A

Figure F.2 gives a more detailed overview of how the sheaves in the total model assembly are connected. Each block represents a sheave and inside the block the equation of motion of that particular sheave is solved. The five blocks are in fact part of a longer concatenation of sheaves being visualized by the dashed lines. The red lines show how the sheaves are connected to each other.
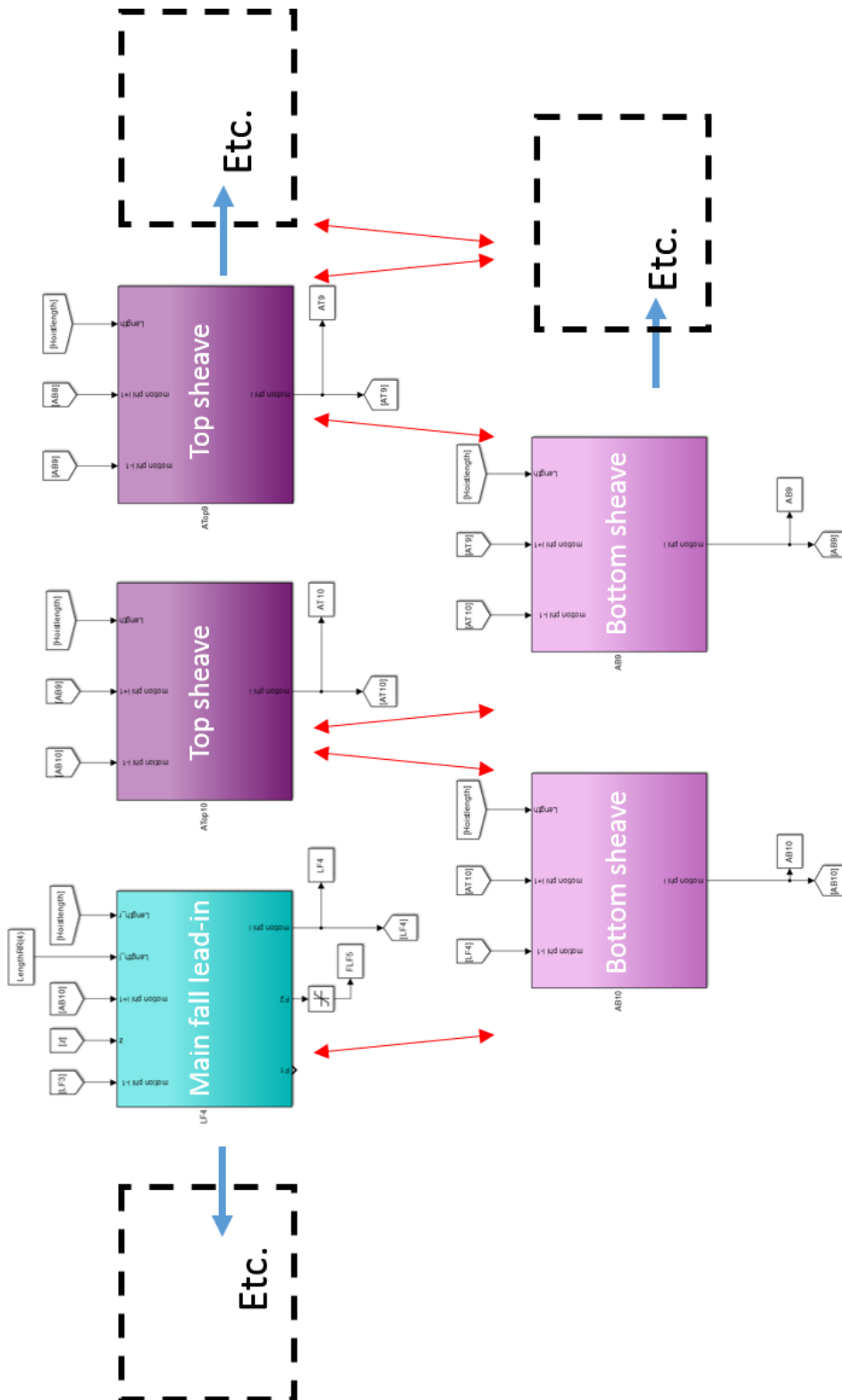
Figure F.2: Detail of part A

Normally in Simulink it is usual to show the connecting between two blocks by an arrowed line, (Figure F.3) however with all the connections made it would be impossible to keep overview. Therefore the blocks 'From' and 'Goto' (Figure F.3) are used to make them invisible, see Figure F.4. If method one or method two is used does not make a difference.
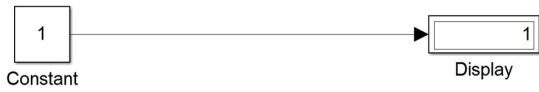
Figure F.3: Method 1: Arrowed connection

Figure F.4: Method 2: From - Goto blocks

F.4. MAIN FALL LEAD-IN SHEAVE BLOCK

Figure F.5 shows the input (top) and output (bottom) of the main fall lead-in sheave of part A. Two of the inputs come from the motions of the sheaves that are before (i-1) and after (i+1) the main fall lead-in (i). Another input motion is the z-motion of the main block. Also the length between the sheave i-1 and i are required as well as the length of the hoist wire in order to calculate the correct stiffness of the steel wires. There are two outputs created, being the wire force and the motion of the sheave itself. The latter is again input for sheave i-1 and i+1.
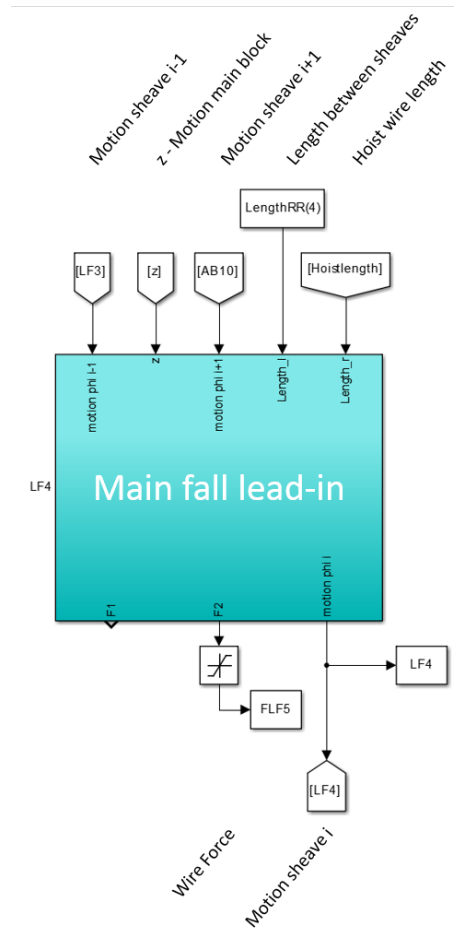
Figure F.5: Main fall lead-in sheave block of part A

F.5. TOP SHEAVE BLOCK

Figure F.6 shows the input (top) and output (bottom) of a top sheave of part A. This block looks similar to the block in Figure F.5 but is more simple. Again two of the inputs comes from the motions of the sheaves that are before (i-1) and after (i+1) the sheave that is being solved(i). The z-motion of the main block is not longer required. They are canceled out when calculating the corresponding force and has no influence on the calculation of the moment of the sheave.The length of the hoist wire is required to calculate the stiffness of the steel wires as it might increase or decrease due to crane operations. There is one output created, being the motion of the sheave itself and is input for sheave i-1 and i+1 positioned next to it.
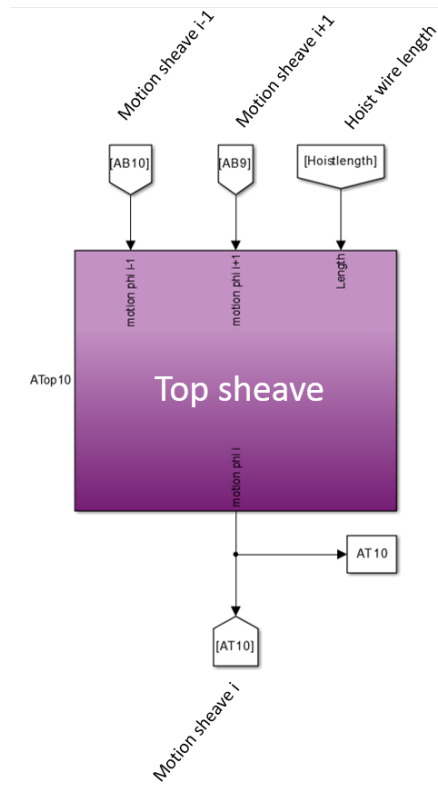
Figure F.6: Top sheave block

F.6. DETAIL OF TOP SHEAVE BLOCK

Figure F.7 shows the inside of a sheave block as was given in Figure F.6. On the top left side the inputs are shown which are routed to a Matlab function block which calculates the moment based on the motions of sheave i-1, i & i+1 and properties like the stiffness coefficient k, the damping coefficient b, the sheave radius R and the hoist wire length. The calculated moment goes to a memory block in order for the friction model to work properly in terms of selection and instability of an ODE solver. The friction block itself is marked red and further details on this block can be found in Figure F.8 in the next section. The friction moment M_{fric} of the friction model is added to the moment calculated earlier. The rotational acceleration of the sheave is calculated by dividing the moment by the mass moment of inertia J. Once integrated gives the rotational velocity and twice integrated the rotational displacement which are processed as outputs of the sheave block.
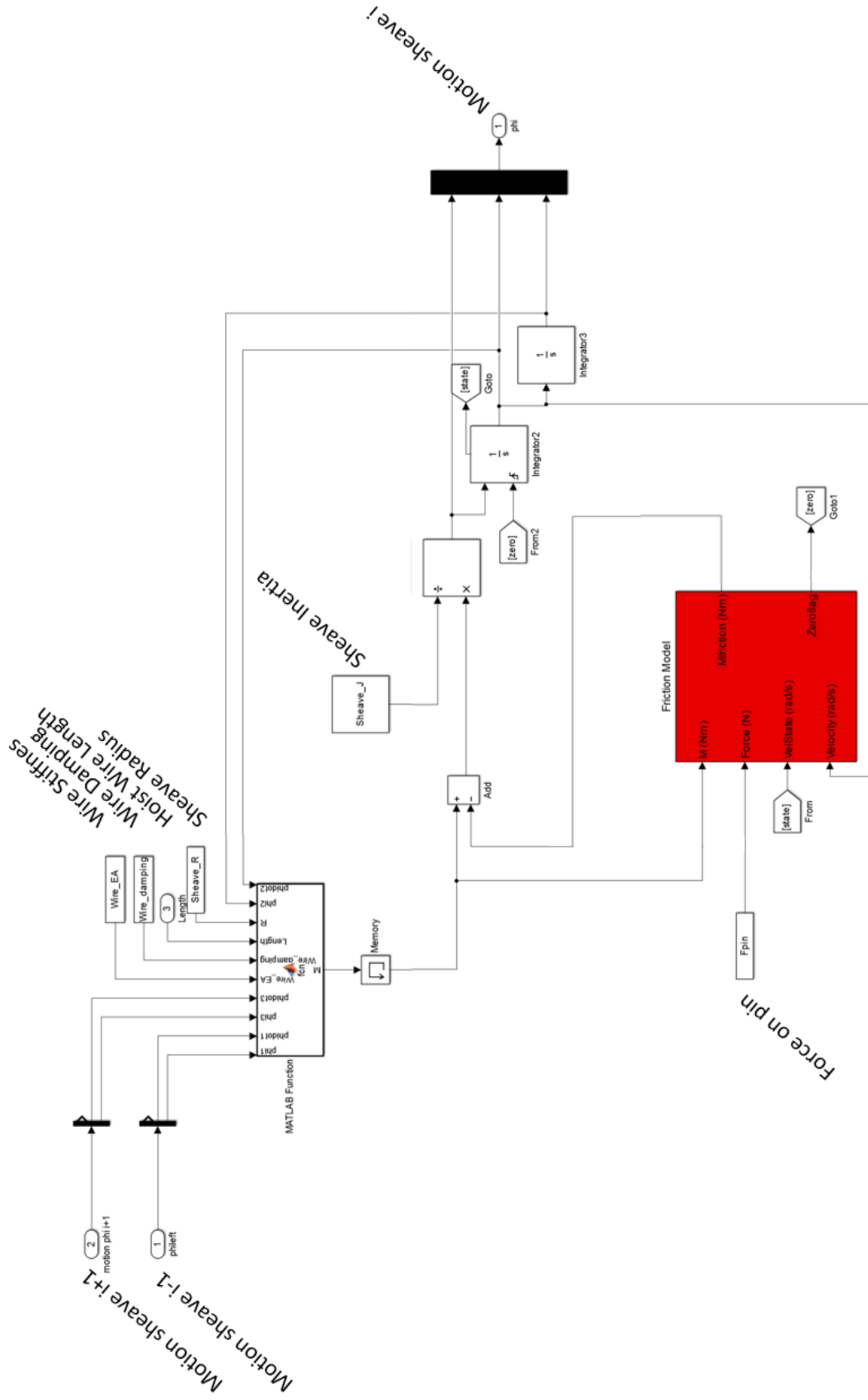
Figure F.7: Detail of top sheave block of part A

F.7. DETAIL OF FRICTION BLOCK

As part of a sheave block a friction block determines the amount of friction that is counteracting the motion and resulting in force differences between individual wires. The friction model is also taking care of the stick-slip effect. Inputs of the friction model are the force on the pin of the sheave, the resulting moment that is calculated earlier in the sheave block, the velocity, the state of the velocity (being positive, negative or zero) and the friction factors μ_{stat} and μ_{kin}. Every time the velocity of the sheave is crossing the zero it is checked whether the external moment is still higher than the static friction. If this is not the case the sheave quits rotating else it keeps oscillating. Obviously during the simulation it is checked whether the external moment is increasing to start a motion again. The friction moment is either zero when there is no rotation or equal to the kinetic friction moment.
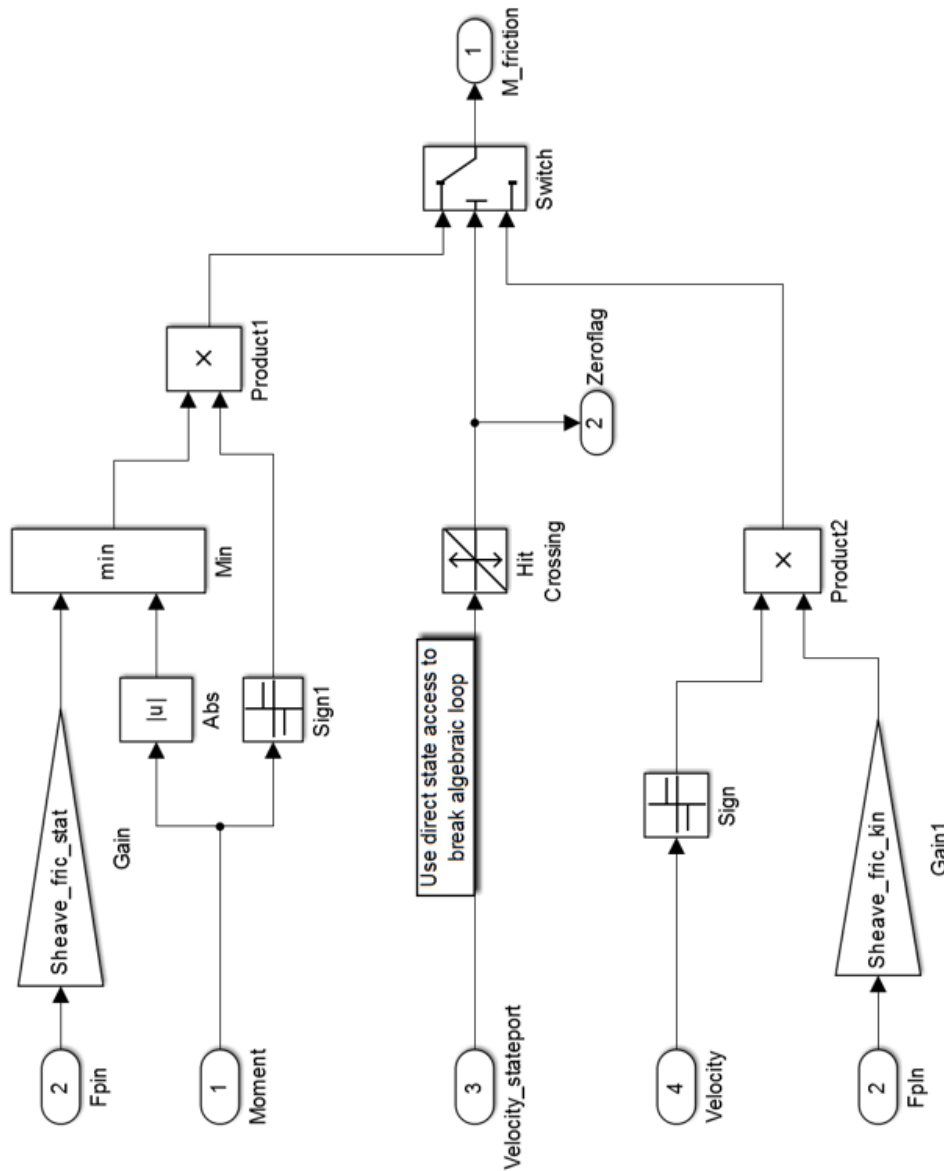
Figure F.8: Detail of friction model

F.8. DETERMINATION OF THE HOIST WIRE FORCES

One part of the post-processing is the calculation of the hoist wire forces by determining the elongation of the wire from the sheave motions. The hoist wire forces are also required during the simulation to compute the vertical motion of the topside. This is done by using the motion of particular sheaves as input, see Figure F.9. The reason that not all sheave motions are required is that a lot are being canceled out, making the simula-

tion faster and it leads to the same result. The calculation of the hoist wire force as a total is performed in the matlab function block. Finally this force is transferred to the block on the bottom where the z-displacement of the topside is being calculated by integrating the acceleration twice. The acceleration is known by dividing the external force by the mass.
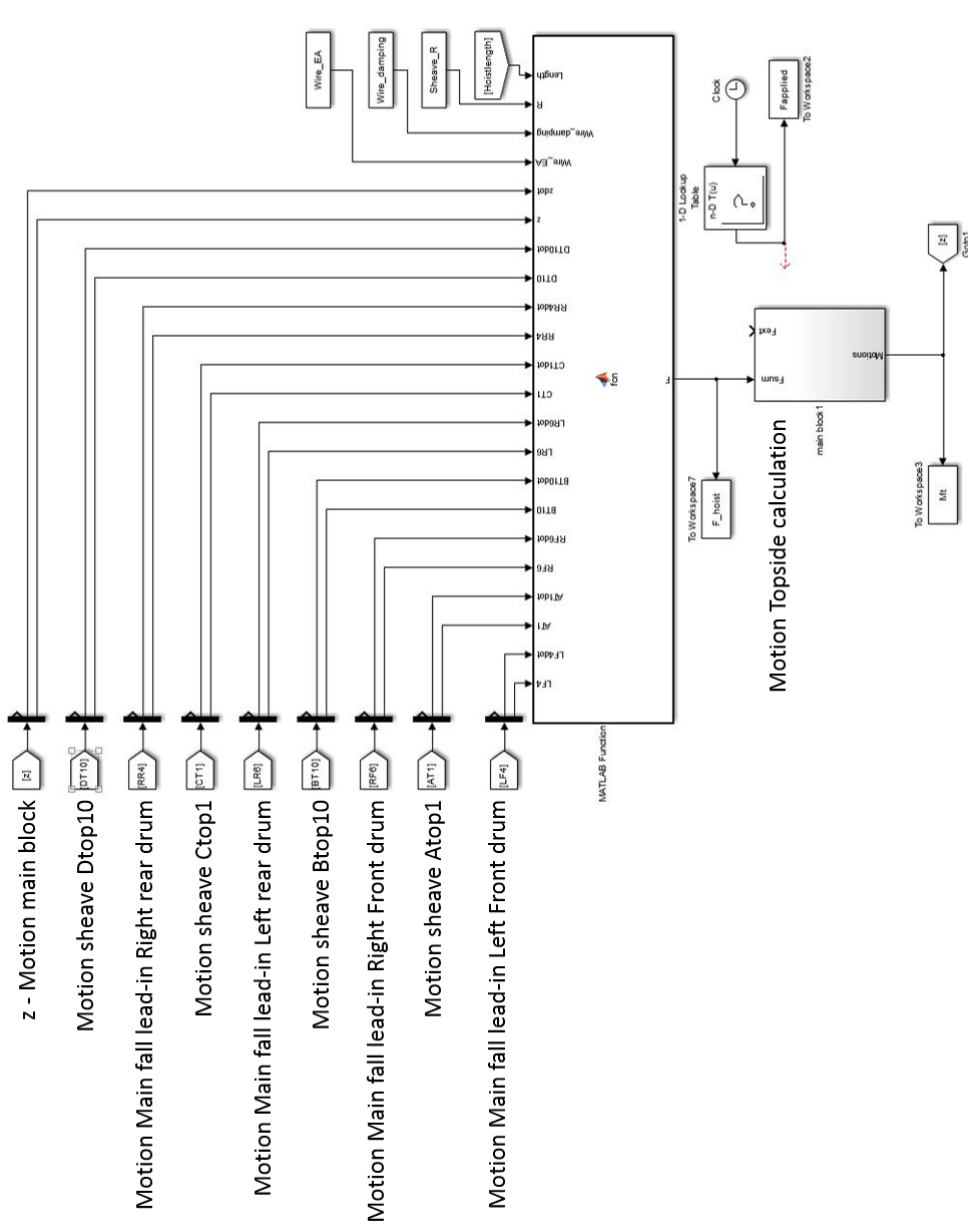
Figure F.9: Determination of total hoist wire force

G

Sheave rotations

G.1. SHEAVE ROTATION DURING LOWERING
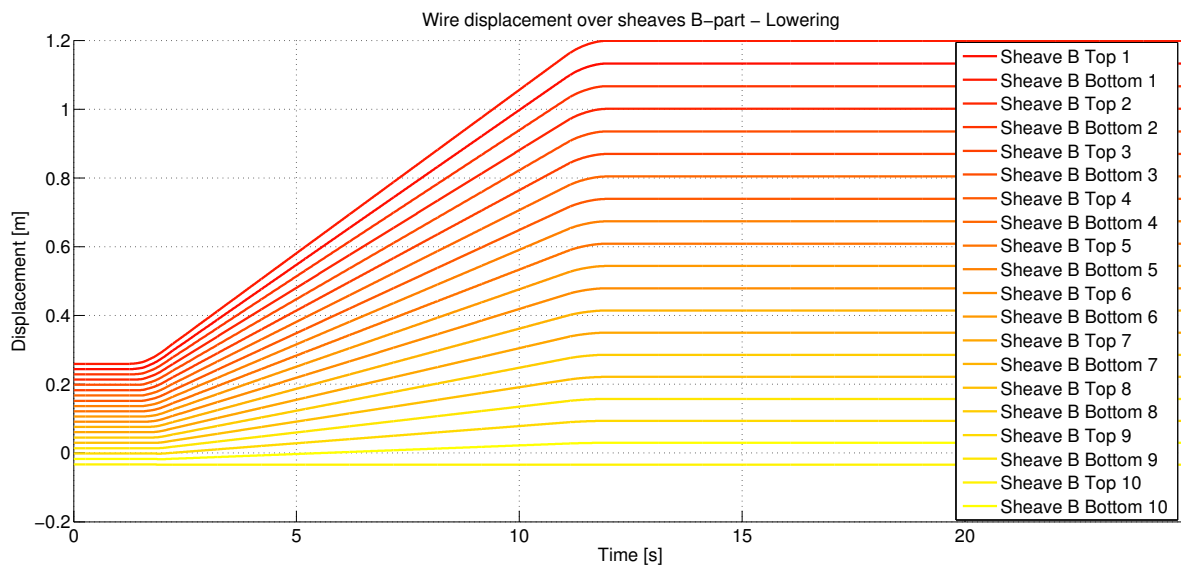
Figure G.1: Wire displacement over sheaves in part B (green) during lowering
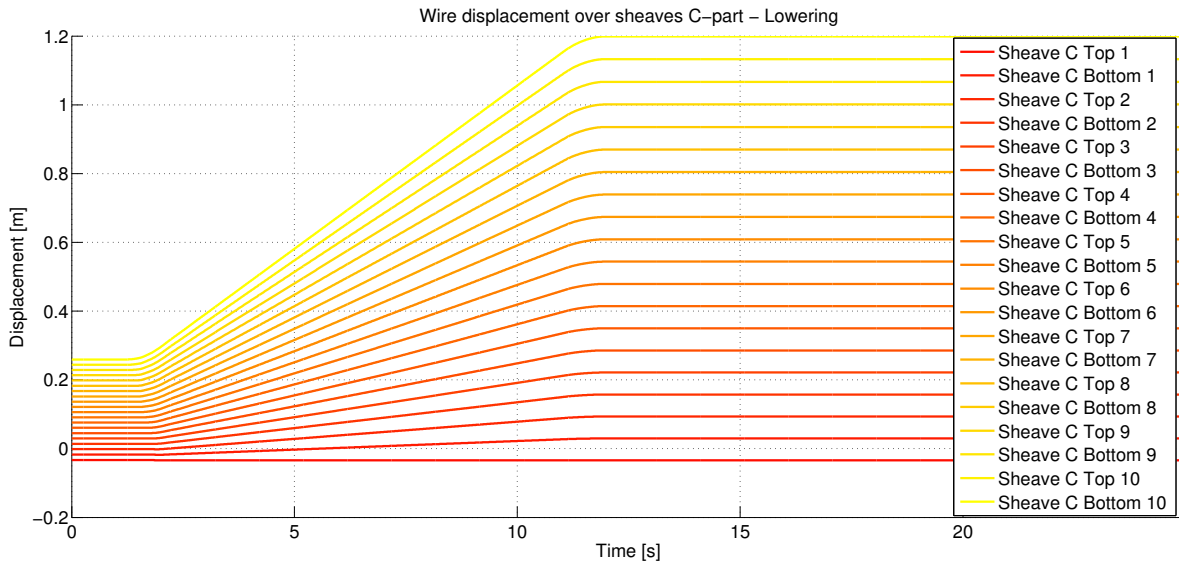
Figure G.2: Wire displacement over sheaves in part C (orange) during lowering
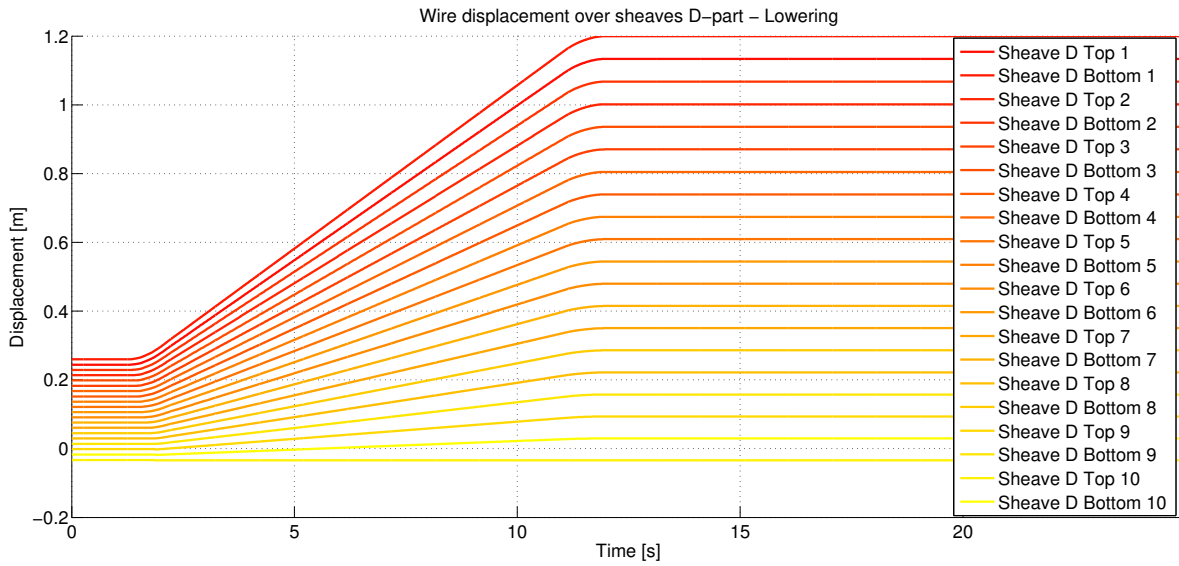
Figure G.3: Wire displacement over sheaves in part D (blue) during lowering

G.2. SHEAVE ROTATION DURING HOISTING
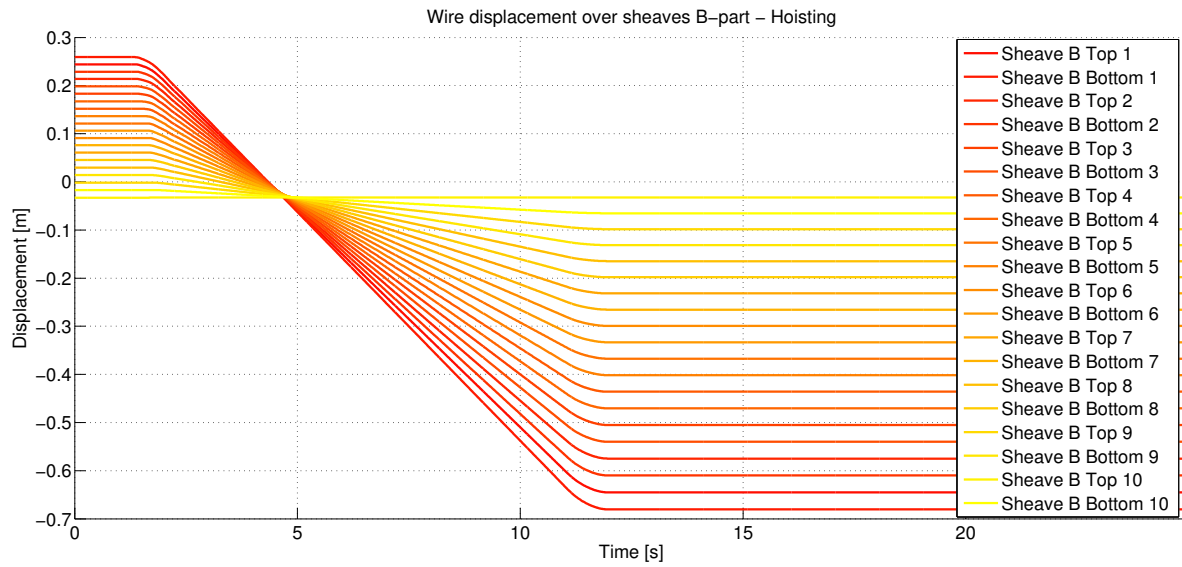
Figure G.4: Wire displacement over sheaves of part B (green) during hoisting
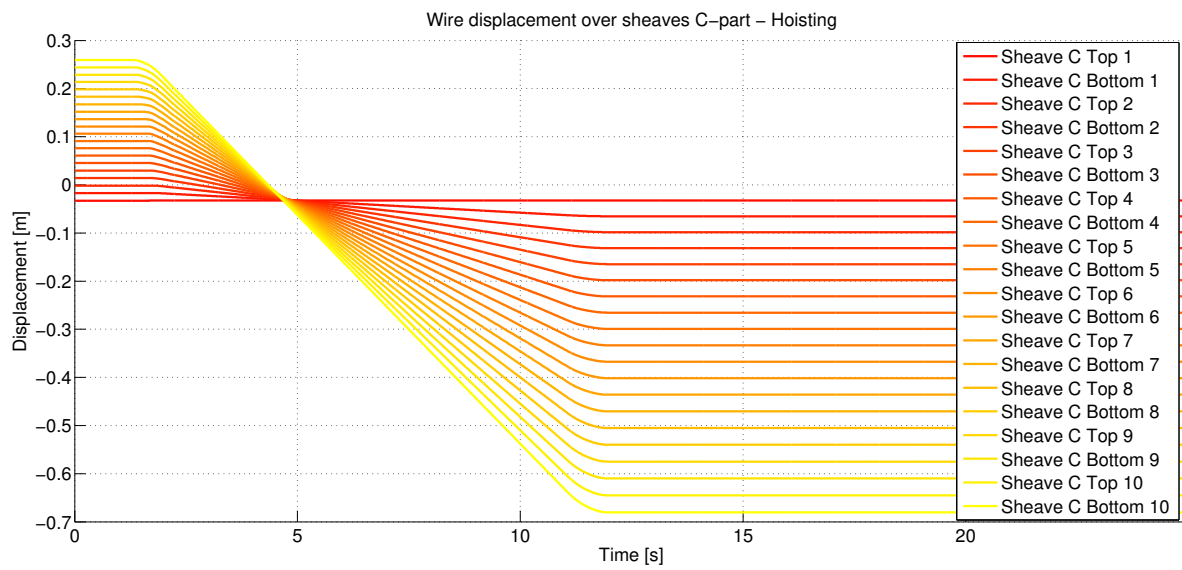
Figure G.5: Wire displacement over sheaves of part C (orange) during hoisting
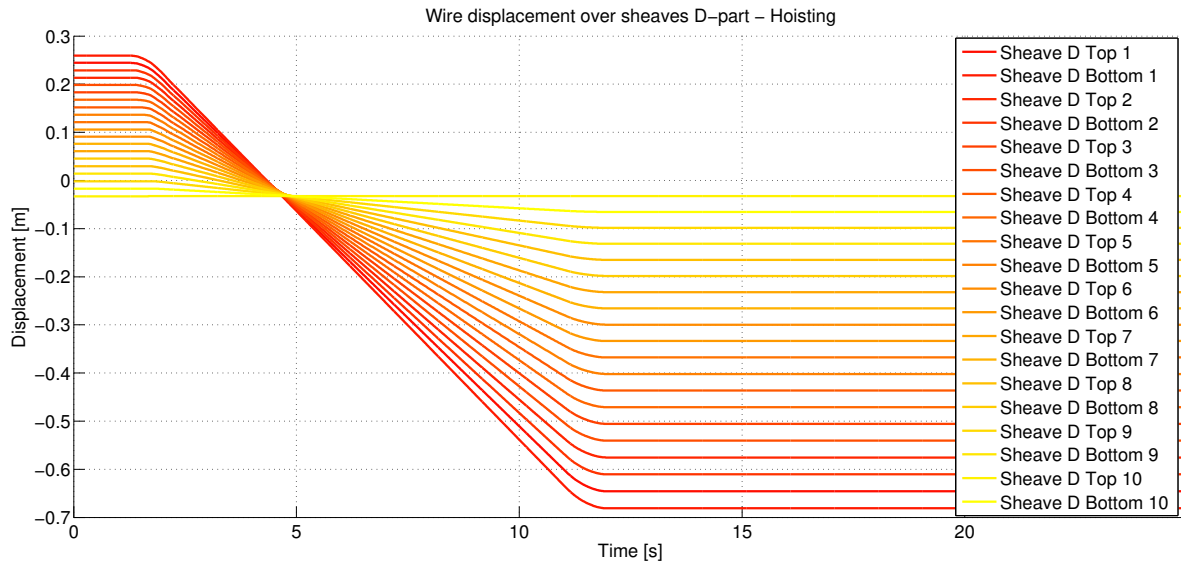
Figure G.6: Wire displacement over sheaves of part D (blue) during hoisting

H

Wire forces

H.1. FORCES DURING HOISTING
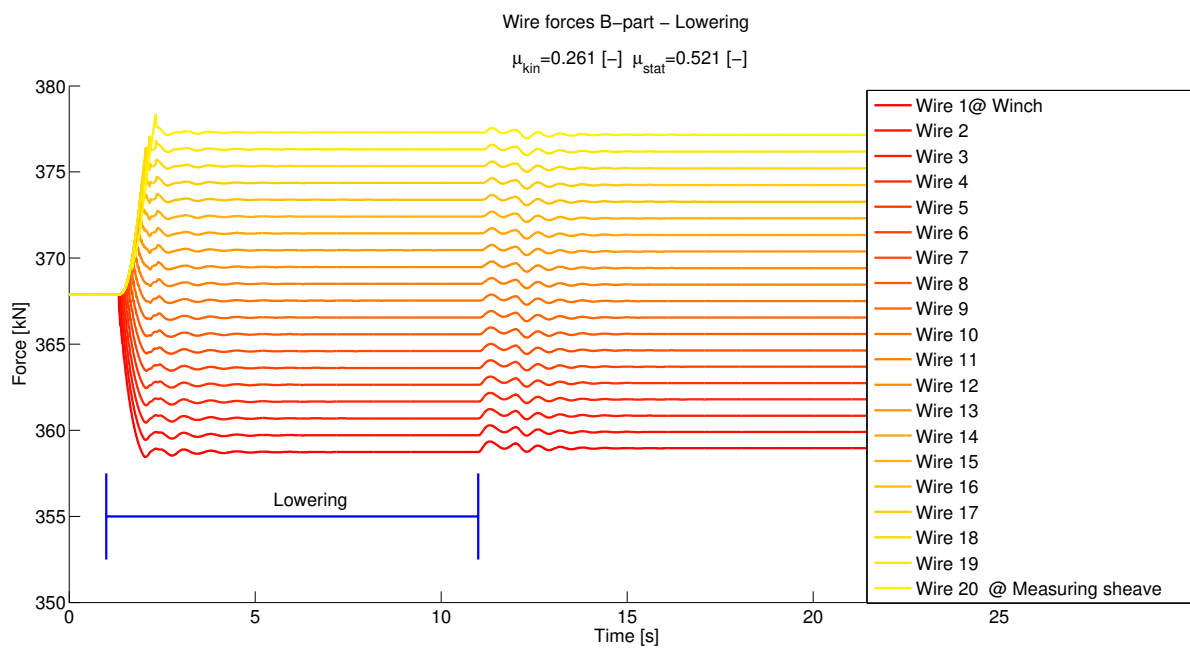
Figure H.1: Wire forces of part B (green) of crane reeving during lowering
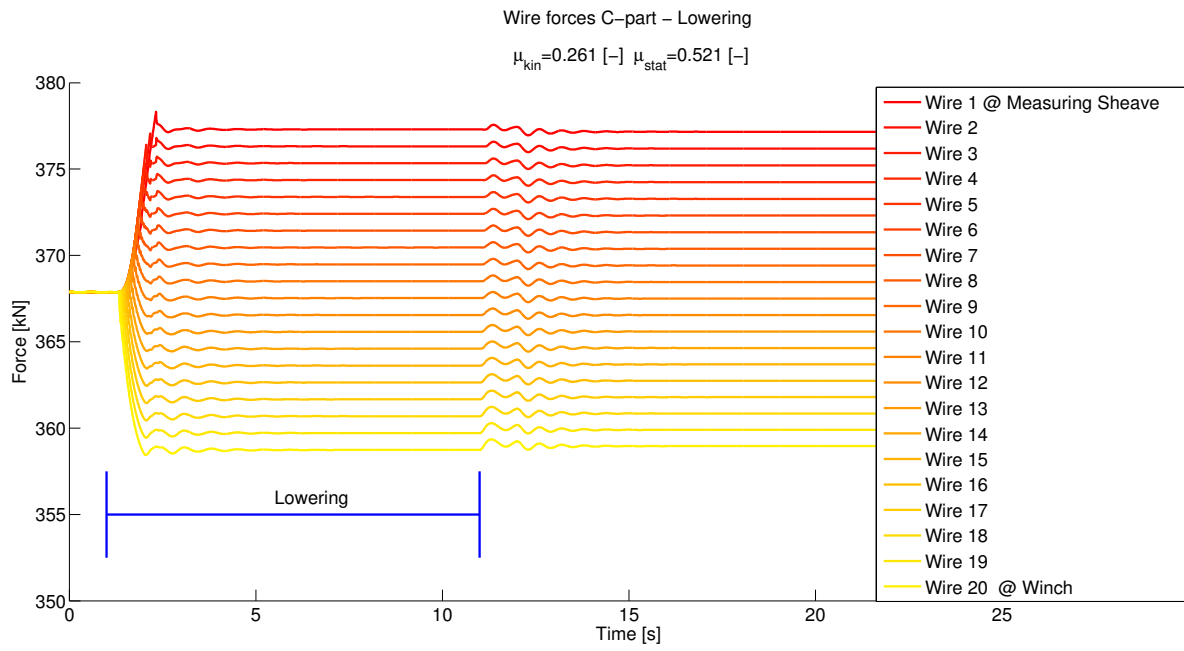
Figure H.2: Wire forces of part C (orange) of crane reeving during lowering
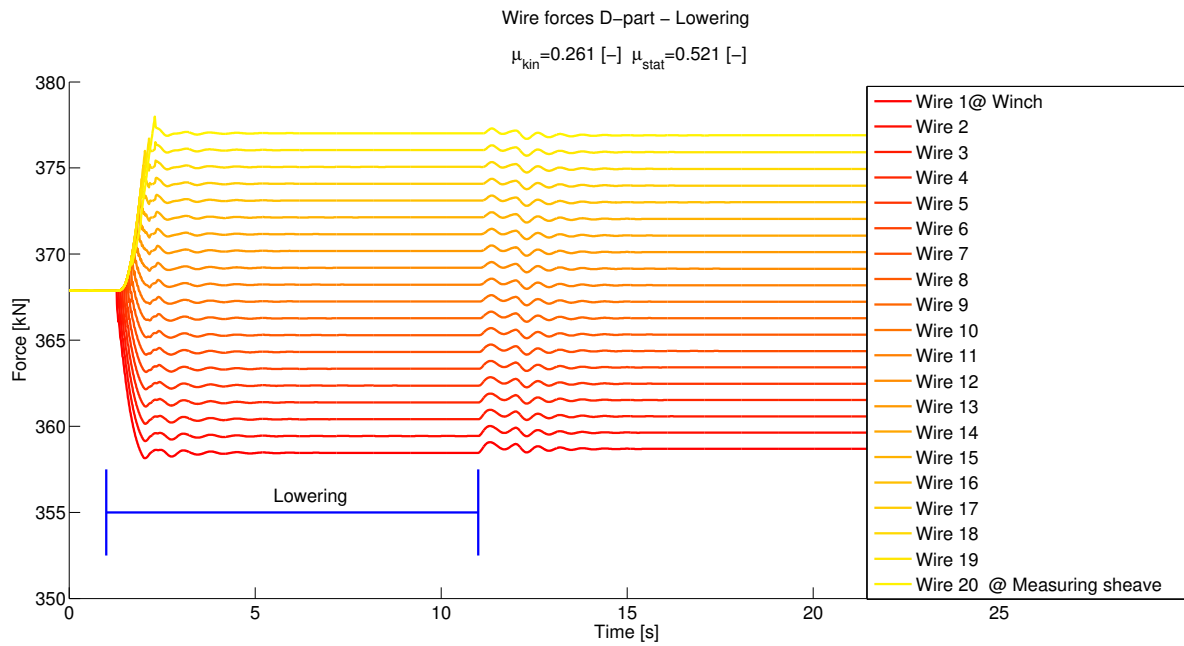
Figure H.3: Wire forces of part D (blue) of crane reeving during lowering

H.2. FORCES DURING HOISTING
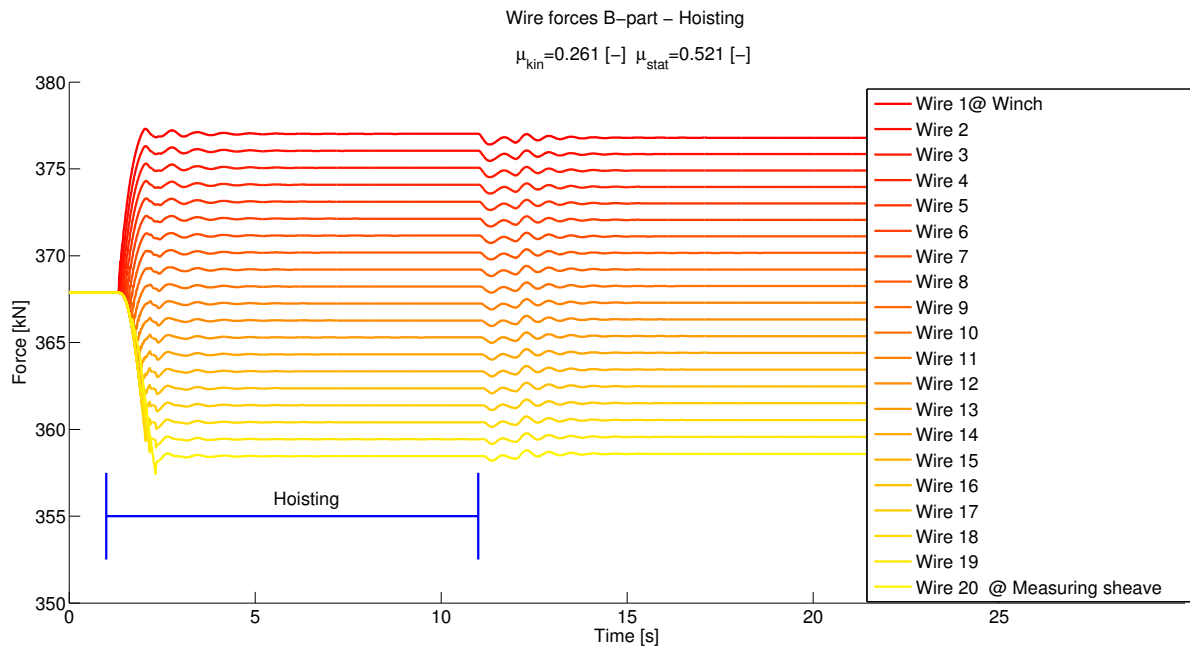
Figure H.4: Wire forces of part B (green) of crane reeving during hoisting
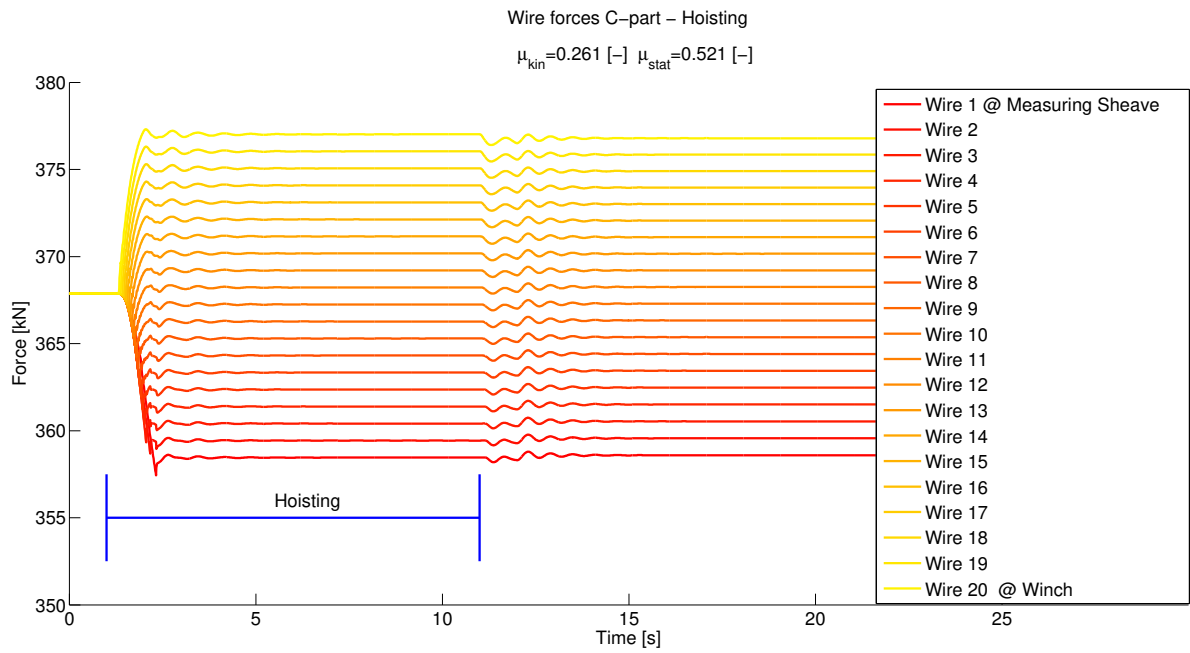
Figure H.5: Wire forces of part C (orange) of crane reeving during hoisting
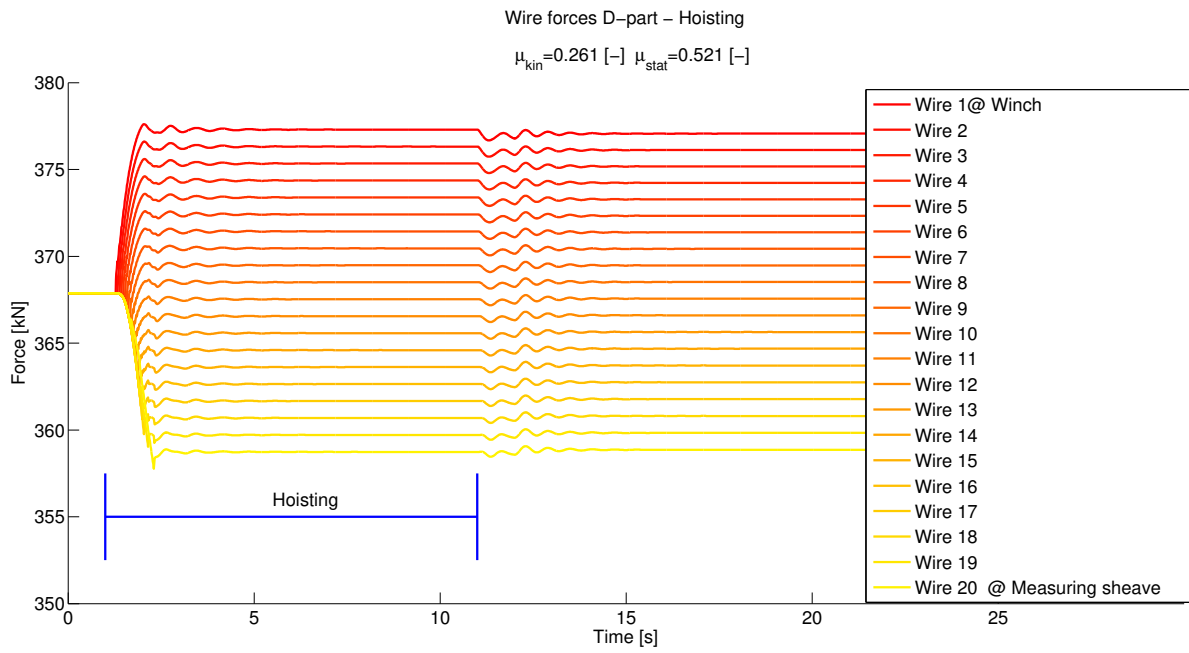
Figure H.6: Wire forces of part D (blue) of crane reeving during hoisting

Imposed motion with Lagrangian

This appendix is divided into two parts: the first part consist of a spring pendulum with a fixed suspension point and the second part with a suspension point that is able to translate in three directions. The translation of the suspension point corresponds to the motion of the crane tip.

Consider the setup with a point mass m on the end of a spring of natural length r_0 and spring constant k in 3D, see Figure I.1. The position of the mass can be described in a Cartesian coordinate system by three translations being x, y, z. Firstly this location is written as a function of the generalized coordinates r, θ and ϕ, see equations I.1.
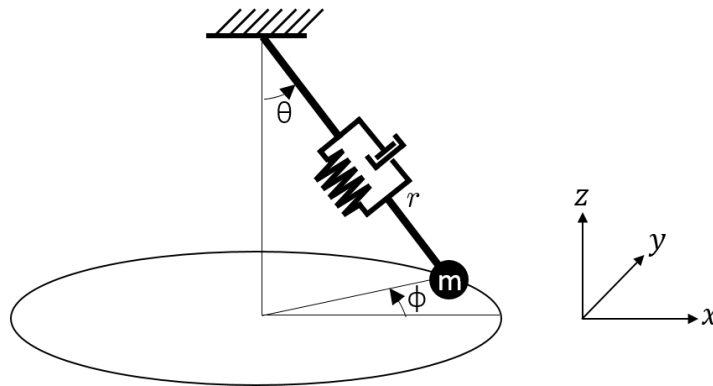
Figure I.1: 3D spring Pendulum

Location description of point mass m.

$$
\begin{aligned}
x &= r(t)\sin\theta(t)\cos\phi(t) \\
y &= r(t)\sin\theta(t)\sin\phi(t) \\
z &= -r(t)\cos\theta(t)
\end{aligned}
\tag{I.1}
$$

First, the kinetic energy K is given by the motion of the mass in equation I.2.

$$
\begin{aligned}
K &= 0.5m(\dot{x}^2 + \dot{y}^2 + \dot{z}^2) \\
&= 0.5m(r(t)^2\dot{\phi}(t)^2\sin(\theta(t))^2 + r(t)^2\dot{\theta}^2 + \dot{r}^2)
\end{aligned}
\tag{I.2}
$$

The potential energy P (equation I.3 is composed of two parts: the gravitational part mgh and the elastic spring part $0.5(\Delta L)^2$.

$$
\begin{aligned}
P &= mgz + 0.5k(r(t) - r_0)^2 \\
&= mg(-r(t)\cos(\theta(t)) + 0.5k(r(t) - r_0)^2
\end{aligned}
\tag{I.3}
$$

If the mass keeps rotating or the spring length keeps increasing and decreasing infinite long would be an unrealistic response. Therefore a damping term, or a dissipation of energy in other words, is added to the Lagrangian by the expression R (equation I.4). There is a damping factor b for each generalized coordinate.

$$R = 0.5b_r \dot{r}(t)^2 + 0.5b_\theta \dot{\theta}(t)^2 + 0.5b_\phi \dot{\phi}(t)^2 \tag{I.4}$$

After taking the Lagrangian derivatives and rewriting the outcome for each generalized coordinate an equation of motion can be derived. Equations I.5 to I.10 gives pairs of derivatives and equations of motion. Note that these equations are not linearized.

For coordinate r:

$$\frac{d}{dt}\frac{\partial K}{\partial \dot{r}} - \frac{\partial K}{\partial r} + \frac{\partial P}{\partial r} + \frac{\partial R}{\partial r} = 0 \tag{I.5}$$

$$\ddot{r} = r\dot{\phi}^2 \sin(\theta)^2 + r\dot{\theta}^2 + g\cos(\theta) - \frac{kr}{m} + \frac{kr_0}{m} - \frac{b_r \dot{r}}{m} \tag{I.6}$$

For coordinate θ:

$$\frac{d}{dt}\frac{\partial K}{\partial \dot{\theta}} - \frac{\partial K}{\partial \theta} + \frac{\partial P}{\partial \theta} + \frac{\partial R}{\partial \theta} = 0 \tag{I.7}$$

$$\ddot{\theta} = \frac{-2\dot{r}\dot{\theta}}{r} + \dot{\phi}^2 \sin(\theta)\cos(\theta) - \frac{g\sin(\theta)}{r} - \frac{b_\theta \dot{\theta}}{mr^2} \tag{I.8}$$

For coordinate ϕ:

$$\frac{d}{dt}\frac{\partial K}{\partial \dot{\phi}} - \frac{\partial K}{\partial \phi} + \frac{\partial P}{\partial \phi} + \frac{\partial R}{\partial \phi} = 0 \tag{I.9}$$

$$\ddot{\phi} = \frac{-2\dot{\theta}\dot{\phi}\cos(\theta)}{\sin(\theta)} - \frac{2\dot{r}\dot{\phi}}{r} - \frac{b_\phi \dot{\phi}}{mr^2 \sin(\theta)^2} \tag{I.10}$$

Until now the spherical pendulum is attached to a fixed point and thus there is no imposed motion possible. However the previous calculation can also be performed for a slightly different setup where the suspension point of the spring is able to follow a prescribed displacement, see Figure I.2. In this case the top displacement is represented by the motion of the crane tip. These local motions come from the global motions of the vessel (heave, roll and pitch). They are translated by a transformation matrix which relates the motions at the COG of the vessel to the motion at a point of interest, in this case the crane tip. Again for this system the position of the mass can be written with the generalized coordinates now including the imposed x, y, z-motion.
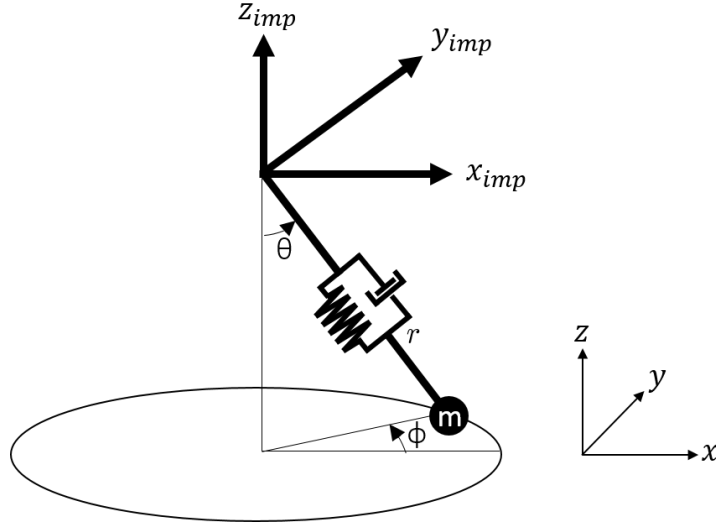
Figure I.2: 3D spring Pendulum with imposed motions

$$x = x_{imp}(t) + r(t)\sin\theta(t)\cos\phi(t)$$
$$y = y_{imp}(t) + r(t)\sin\theta(t)\sin\phi(t) \tag{I.11}$$
$$z = z_{imp}(t) - r(t)\cos\theta(t)$$

Together with the relation of the position of the mass from equation I.11 relations for the kinetic and potential energy can be made. As the method is clear now these are not included in this report. After taking the Lagrangian derivations the equations of motion of the mass are derived. Clearly additional terms (depending on the acceleration of hinge point) have come along due to the imposed motion compared to the previous situation, see equations I.12 until I.14.

$$\ddot{r} = r\dot{\phi}^2\sin(\theta)^2 + r\dot{\theta}^2 + g\cos(\theta) - \frac{kr}{m} + \frac{kr_0}{m} - \frac{b_r\dot{r}}{m} - \ddot{x}_{imp}\sin(\theta)\cos(\phi) - \ddot{y}_{imp}\sin(\theta)\sin(\phi) + \ddot{z}_{imp}\cos(\theta) \tag{I.12}$$

$$\ddot{\theta} = \frac{-2\dot{r}\dot{\theta}}{r} + \dot{\phi}^2\sin(\theta)\cos\theta - \frac{g\sin(\theta)}{r} - \frac{b_\theta\dot{\theta}}{mr^2} - \frac{\ddot{x}_{imp}\cos(\theta)\cos(\phi)}{r} - \frac{\ddot{y}_{imp}\cos(\theta)\sin(\phi)}{r} - \frac{\ddot{z}_{imp}\sin(\theta)}{r} \tag{I.13}$$

$$\ddot{\phi} = \frac{-2\dot{\phi}\dot{\theta}\cos(\theta)}{\sin(\theta)} - \frac{2\dot{r}\dot{\phi}}{r} - \frac{b_\phi\dot{\phi}}{mr^2\sin(\theta)^2} - \frac{\ddot{x}_{imp}\cos(\phi)}{r\sin(\theta)} - \frac{\ddot{y}_{imp}\cos(\phi)}{r\sin(\theta)} \tag{I.14}$$

J

Simulink model imposed motions dual lift

This part of the appendix goes into detail of the model that is created to solve the imposed motion model together with the sheave model. The overview of the model consists of three main parts (see Figure J.1). The red part is the input from the model were the motions are multiplied by their influences in the mass, damping and stiffness matrices. See Figure J.2 and J.3 for the detail of this block. This block exports a force vector. This force vector is transferred to the purple part. Here is the equation of motion solved (see Figure J.4 and J.5. The equation is governed by the total stiffness, damping and stiffness matrix excluding the contributions of the hoist wire force. This contribution is calculated in the green part of the model (J.6 and J.7. Here the motion of the main block and the crane block are used as inputs and where an elongation is determined. This elongation is then used to determine to hoist wire forces for both cranes with the sheave model. The sheave model is described earlier in section **??** and is inside the green block of Figure J.7. The force is added to the force vector and the model can be solved for each time step.
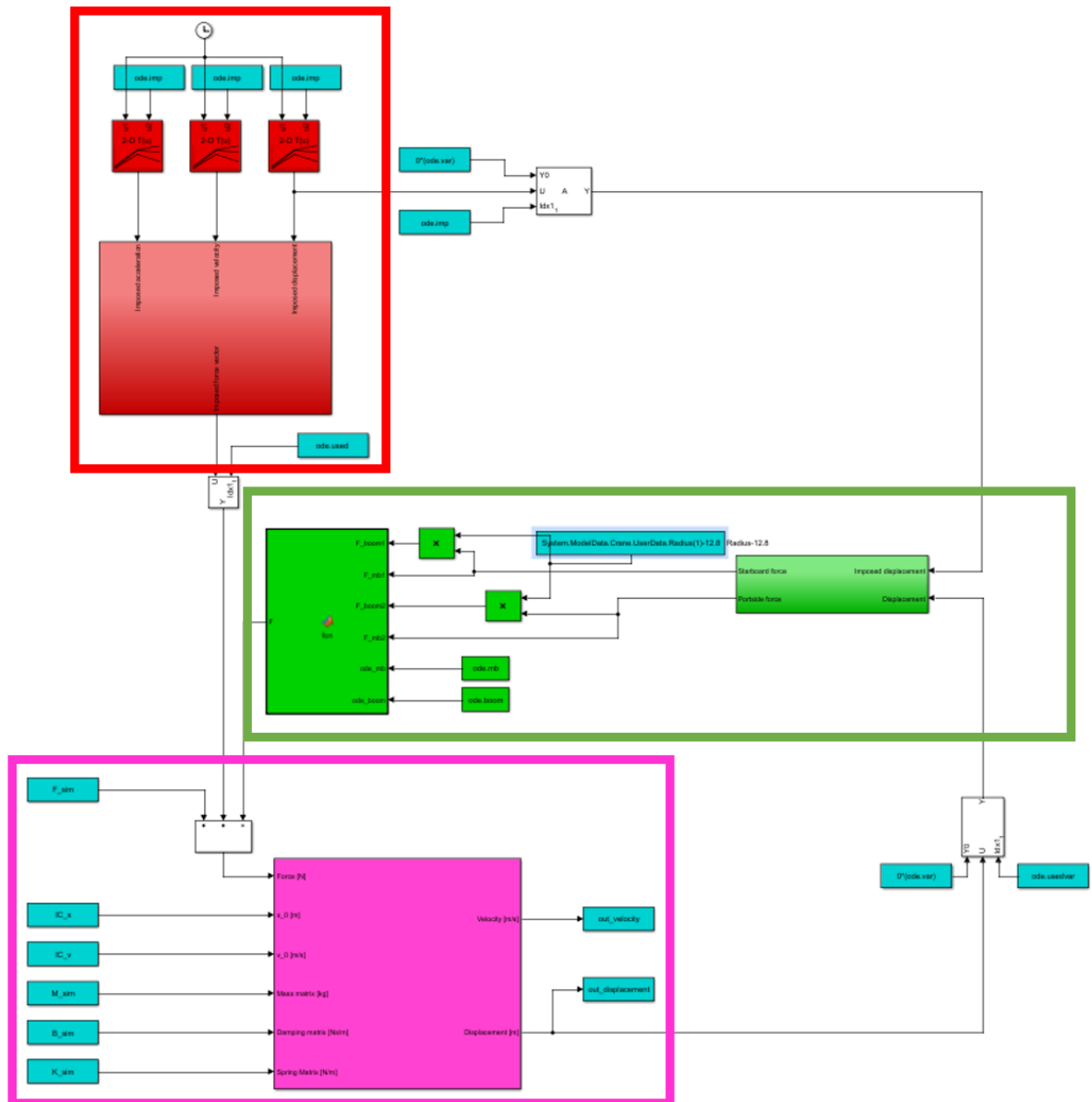
Figure J.1: Overview
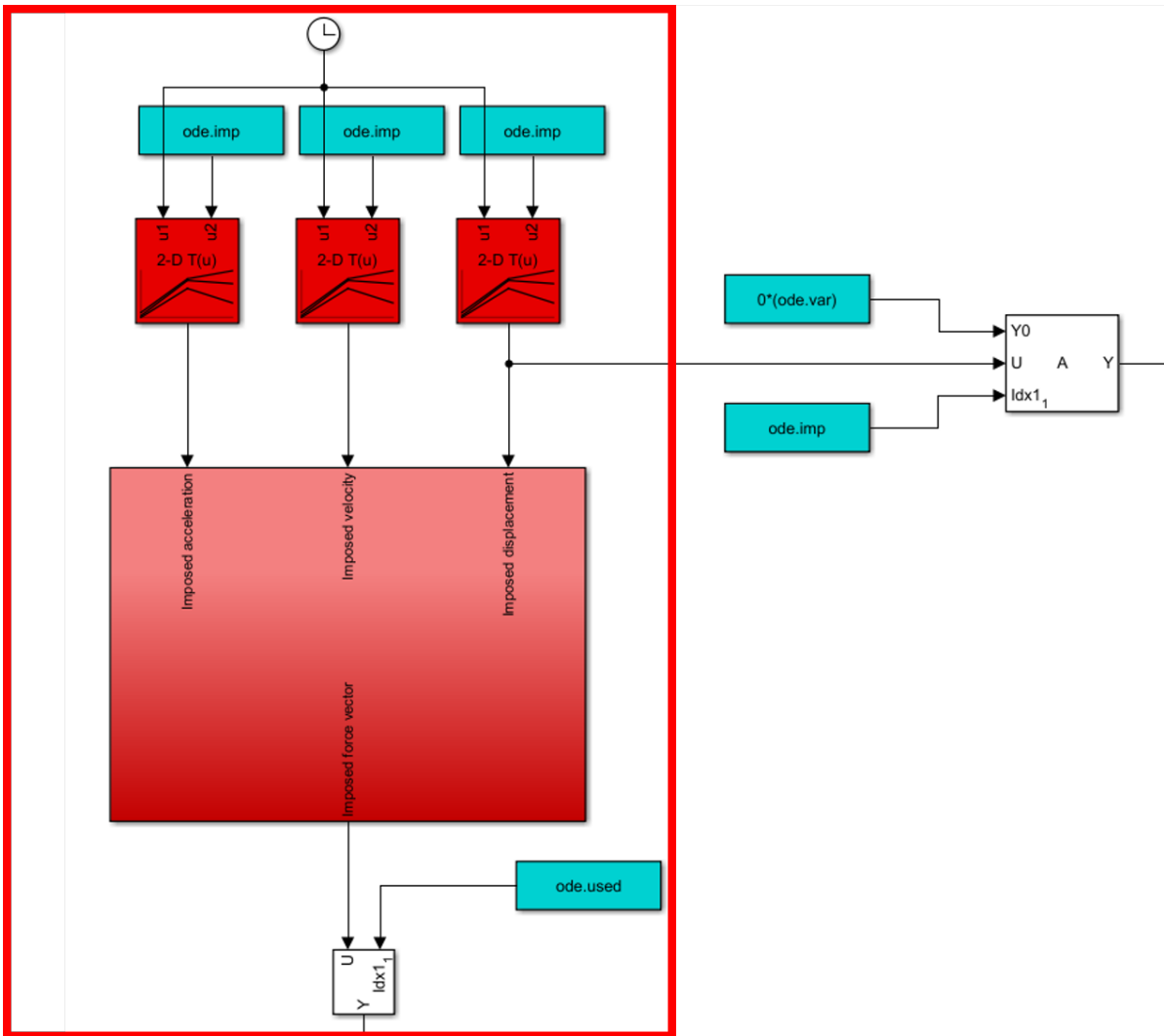
Figure J.2: External force due to imposed motion detail
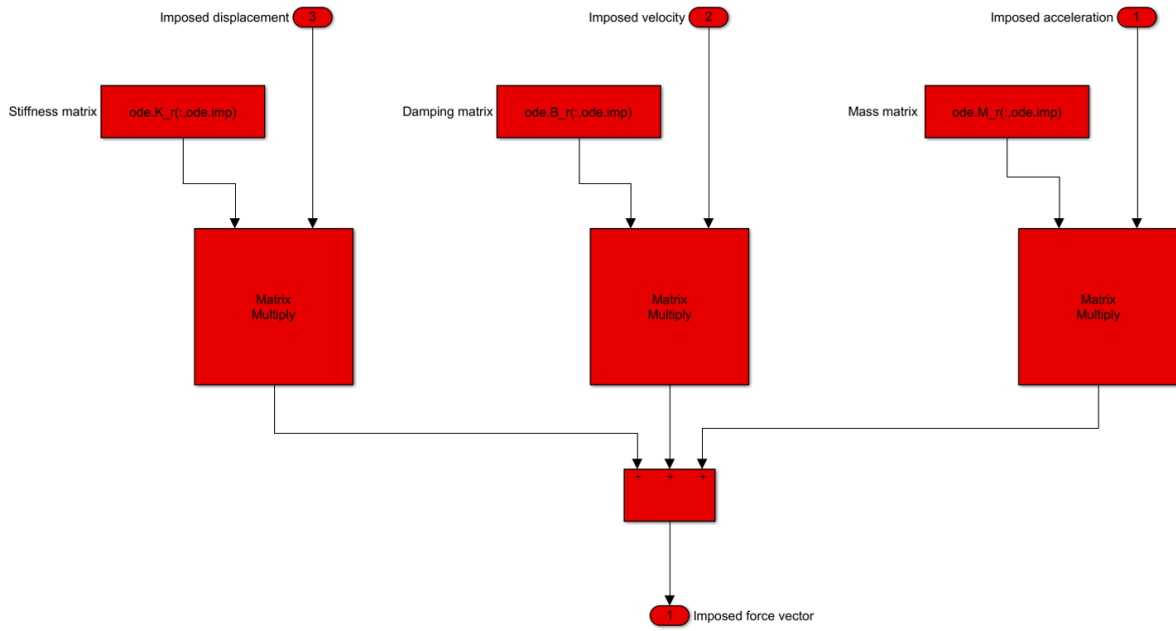
Figure J.3: Imposed motion block
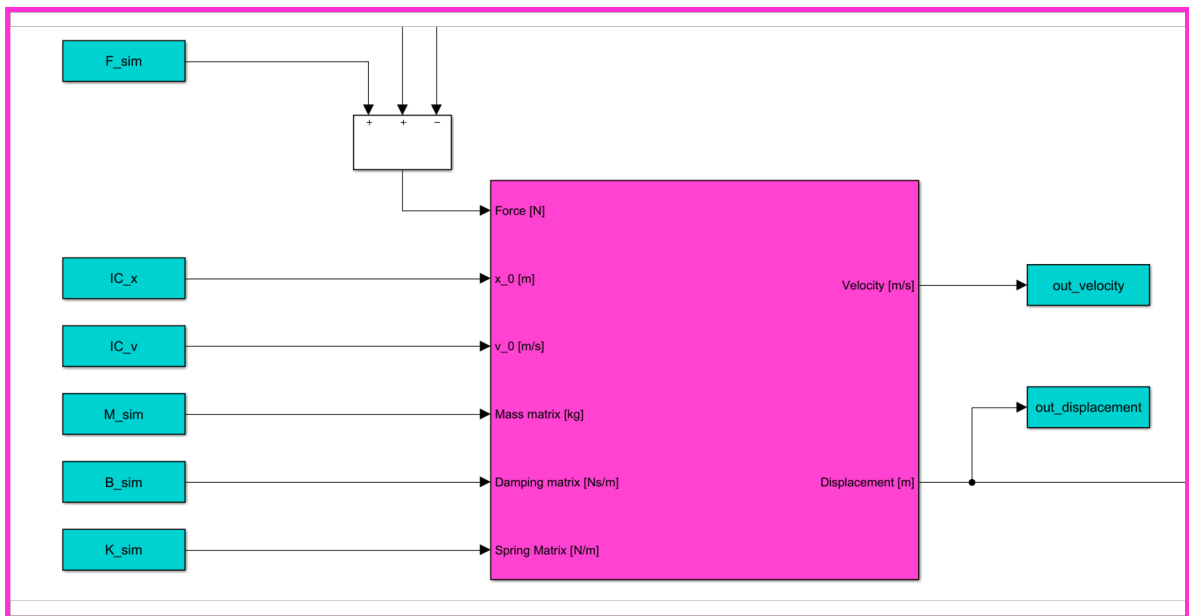
Figure J.4: Solving equation of motion matrices detail
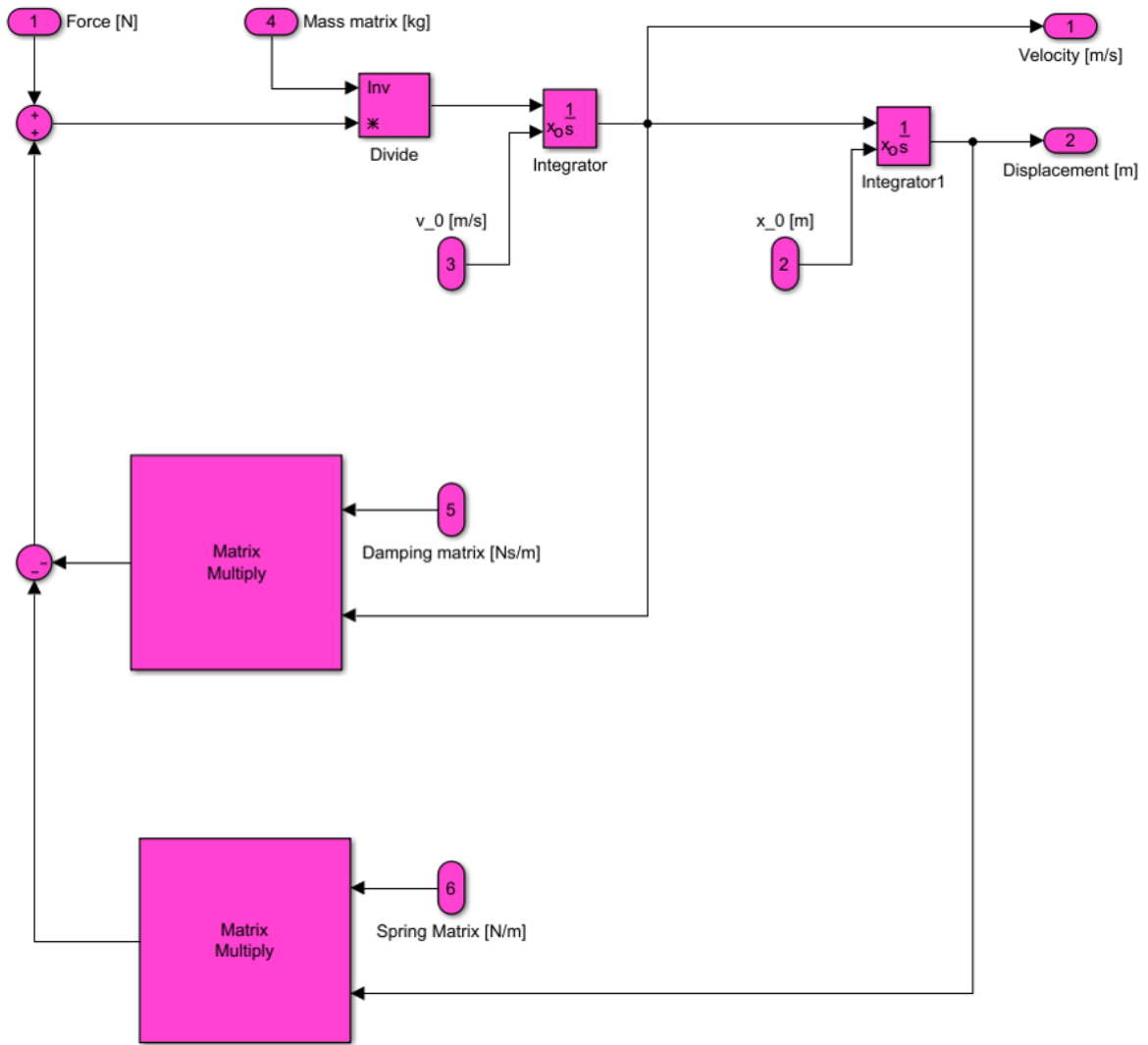
Figure J.5: Solving equation of motion matrices block
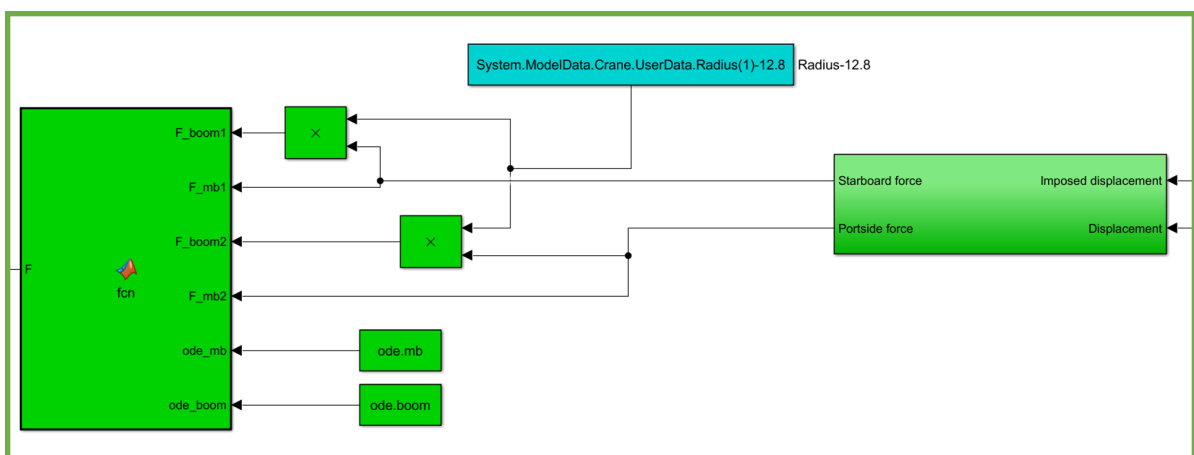
Figure J.6: Calculation of hoist wire force from sheave model detail
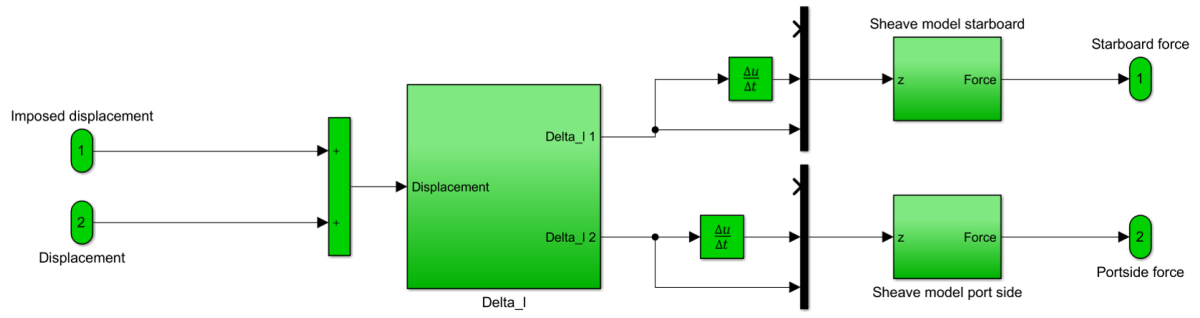
Figure J.7: Hoist wire force block

K
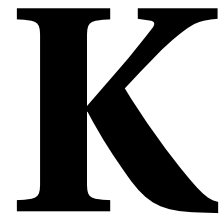
Project properties

			Project A
Vessel	Mass	[mT]	169687
	C.o.G.	[m,m,m]	[75.6, 0.0, 21.2]
	Radii of Gyration	[m,m,m]	
SB Crane	Mass	[mT]	1005
	Radii of Gyration	[m]	36.1
	Boom Angle	[deg]	67
	Slew Angle	[deg]	161
	Load	[mT]	2401
	Hoist wire stiffness k	[kN/m]	180820
	Boom wire stiffness EA	[kN]	8875657
	Suspended Length	[m]	59.2
PS Crane	Mass	[mT]	1005
	Radii of Gyration	[m]	36.071
	Boom Angle	[deg]	67
	Slew Angle	[deg]	199
	Load	[mT]	2643
	Hoist wire stiffness k	[kN/m]	166859
	Boom wire stiffness EA	[kN]	12984934
	Suspended Length	[m]	59.2
Load	Mass	[mT]	4944

L

Imposed motion responses

The sections below show the obtained responses for the imposed motion model. In order to verify the model 4 cases were studied which is described in section 5.3. In this appendix the remaining responses can be found that were not given in the aforementioned section. These are the motion responses of the load, main block and crane tip for the heave, roll and pitch cases. The natural modes that correspond to the natural periods can be found in Table L.4.

L.1. IMPOSED HEAVE MOTION
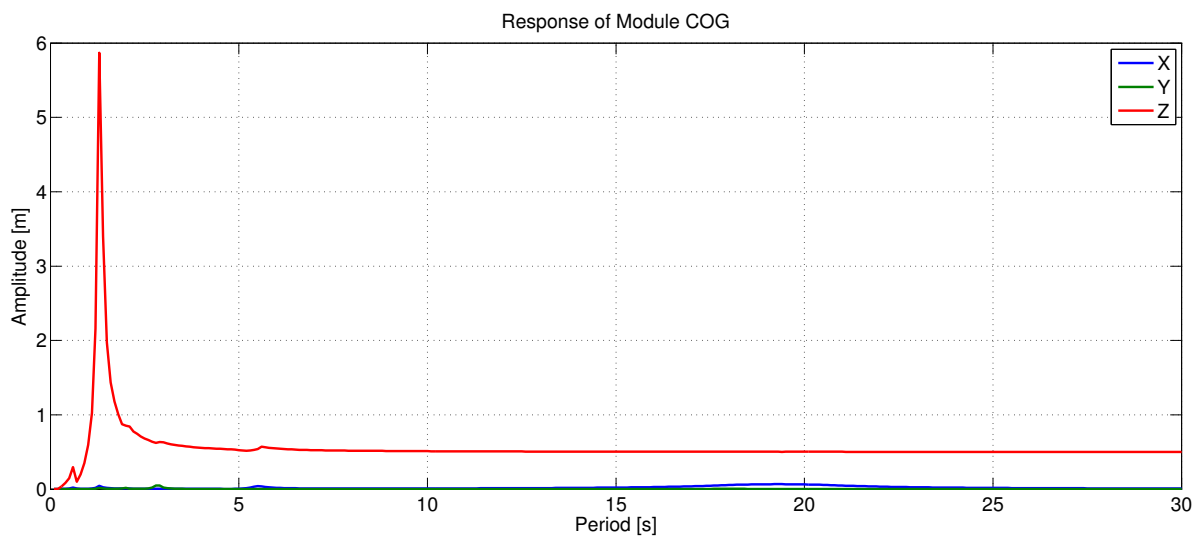
Figure L.1: Module response due to sinusoidal heave motion
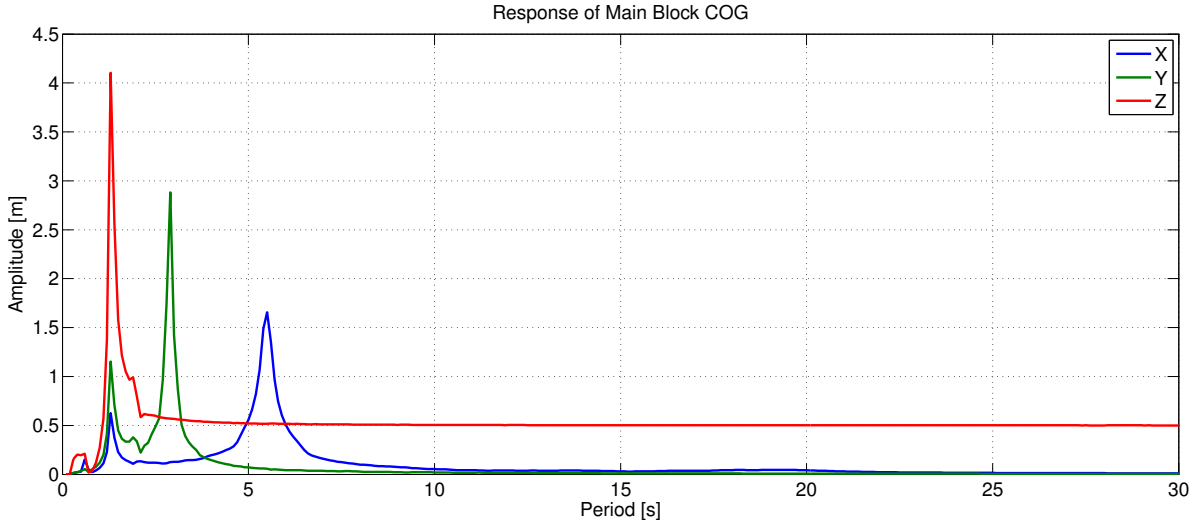
Figure L.2: Main block response due to sinusoidal heave motion
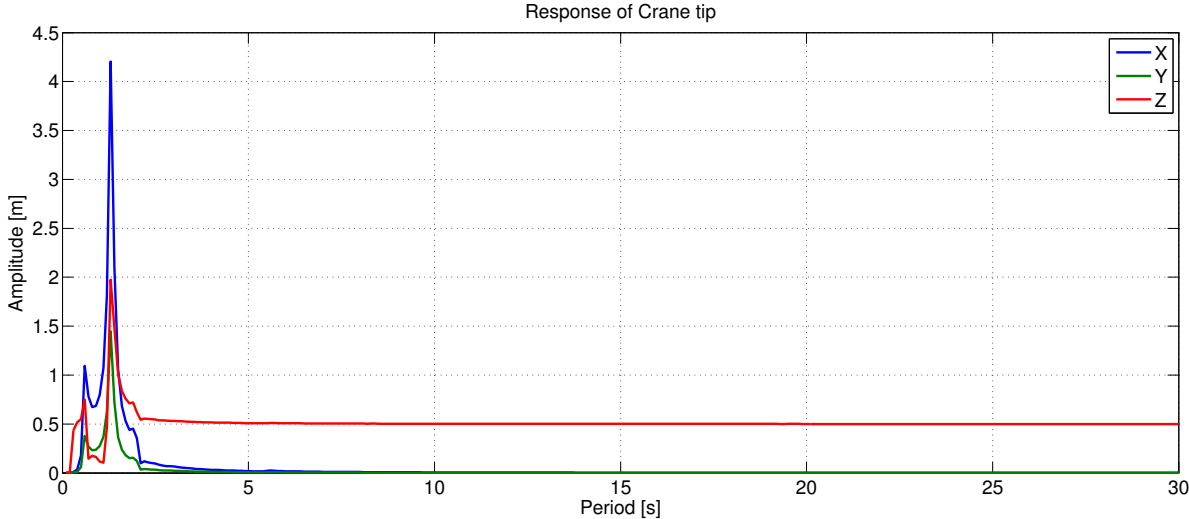
Figure L.3: Crane tip response due to sinusoidal heave motion

L.2. IMPOSED ROLL MOTION
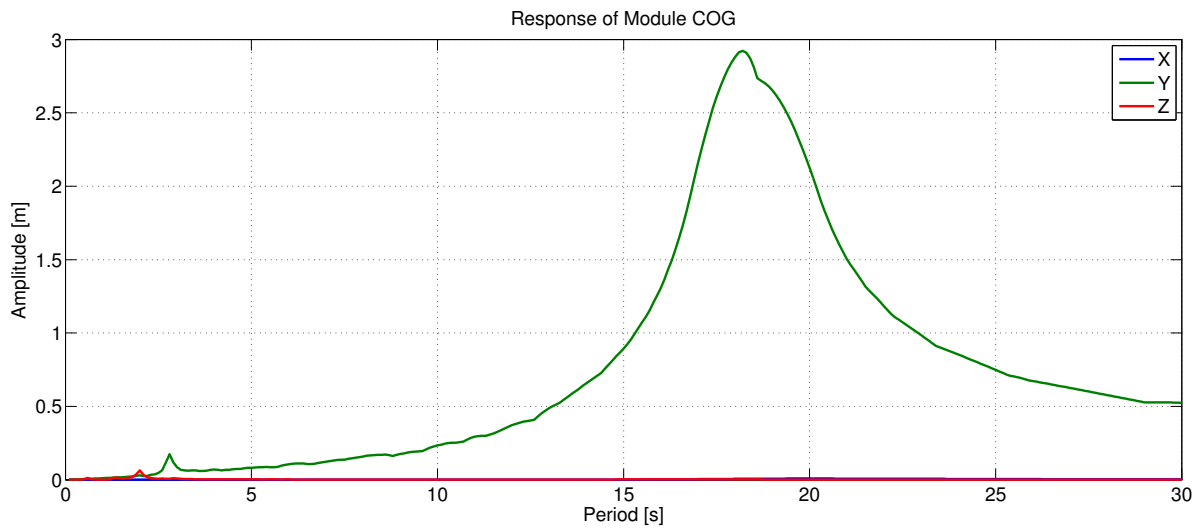
Figure L.4: Module response due to sinusoidal roll motion
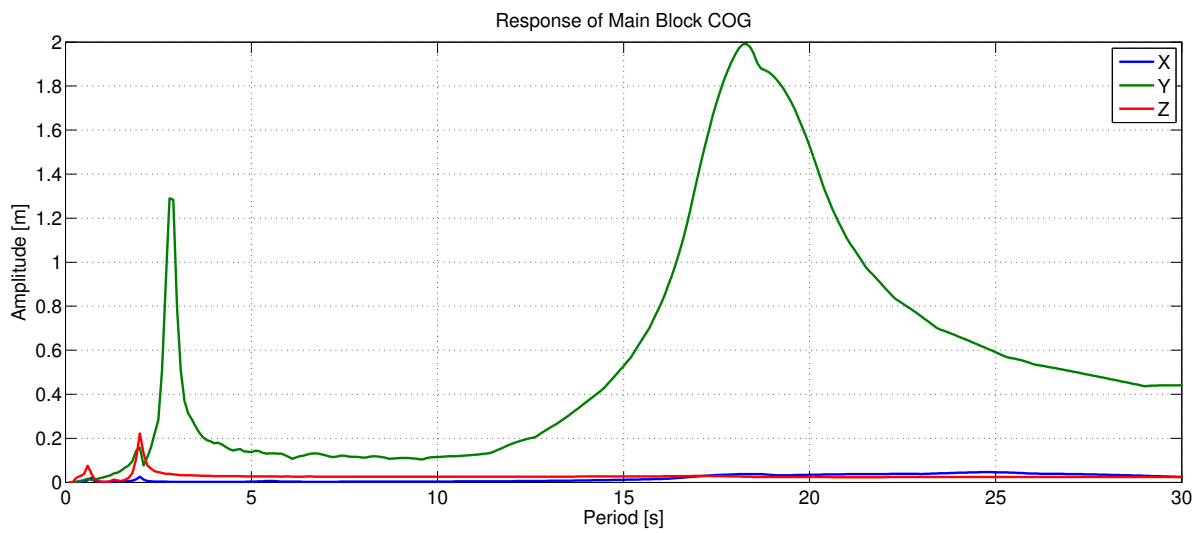
Figure L.5: Main block response force due to sinusoidal roll motion
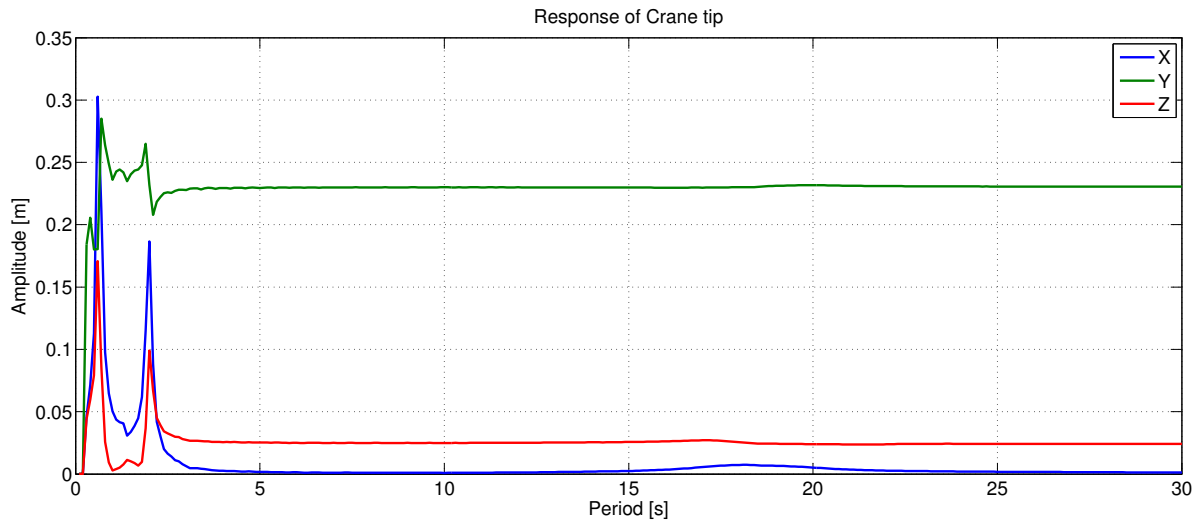
Figure L.6: Crane tip response force due to sinusoidal roll motion

L.3. IMPOSED PITCH MOTION
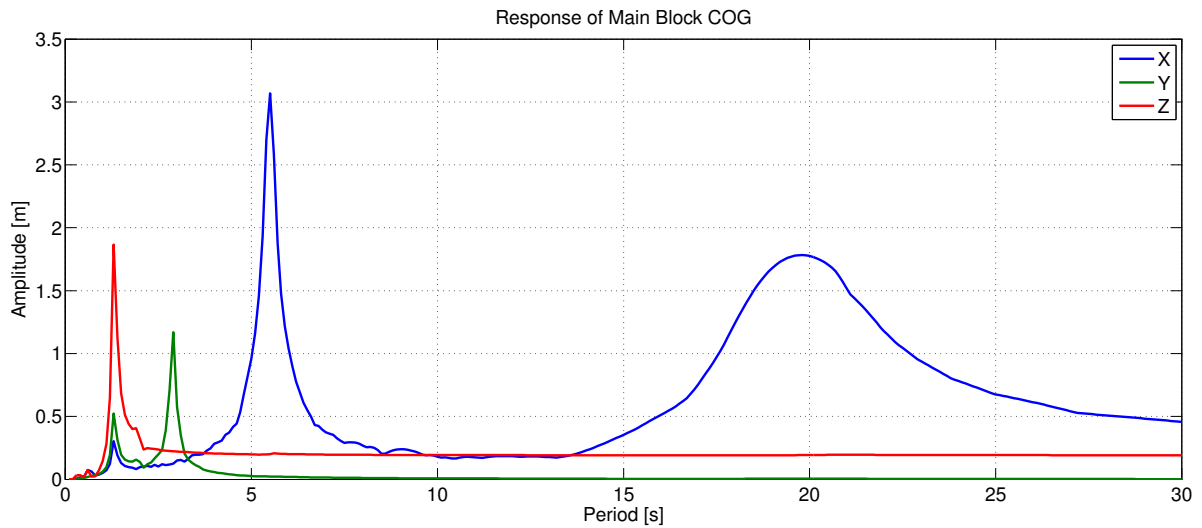
Figure L.7: Module response due to sinusoidal pitch motion
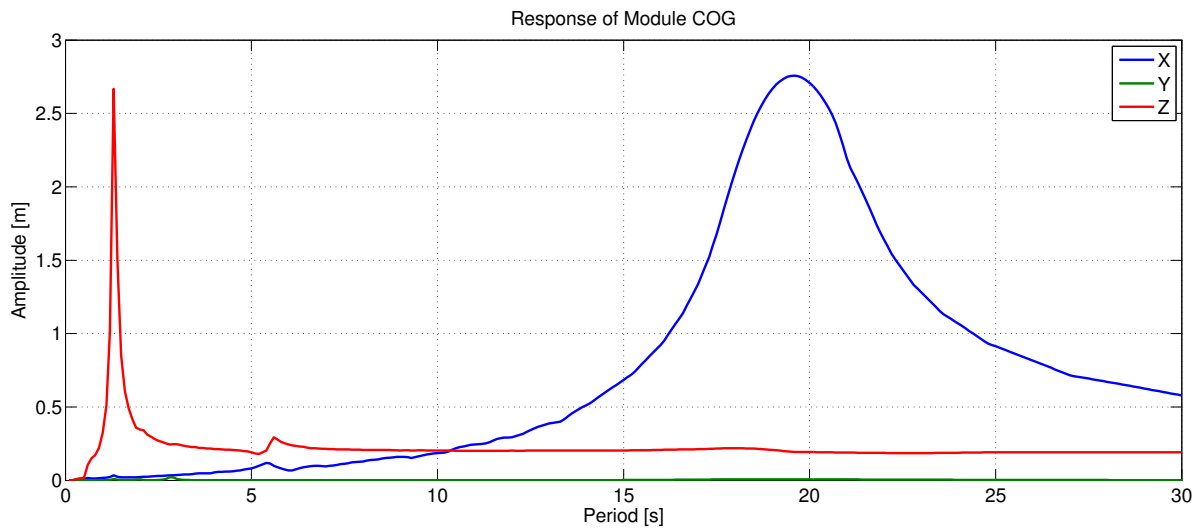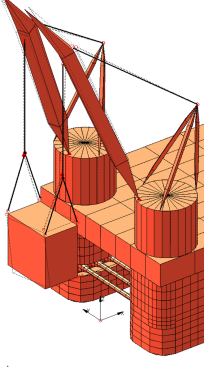
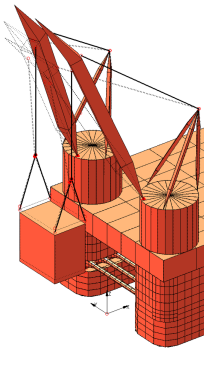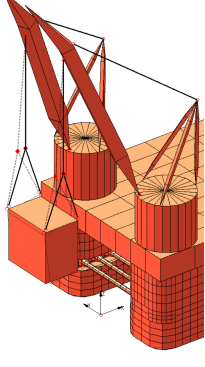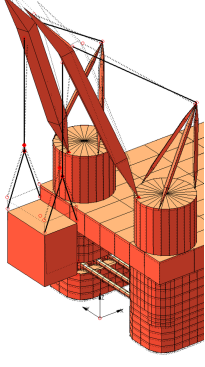Figure L.8: Main block response due to sinusoidal pitch motion
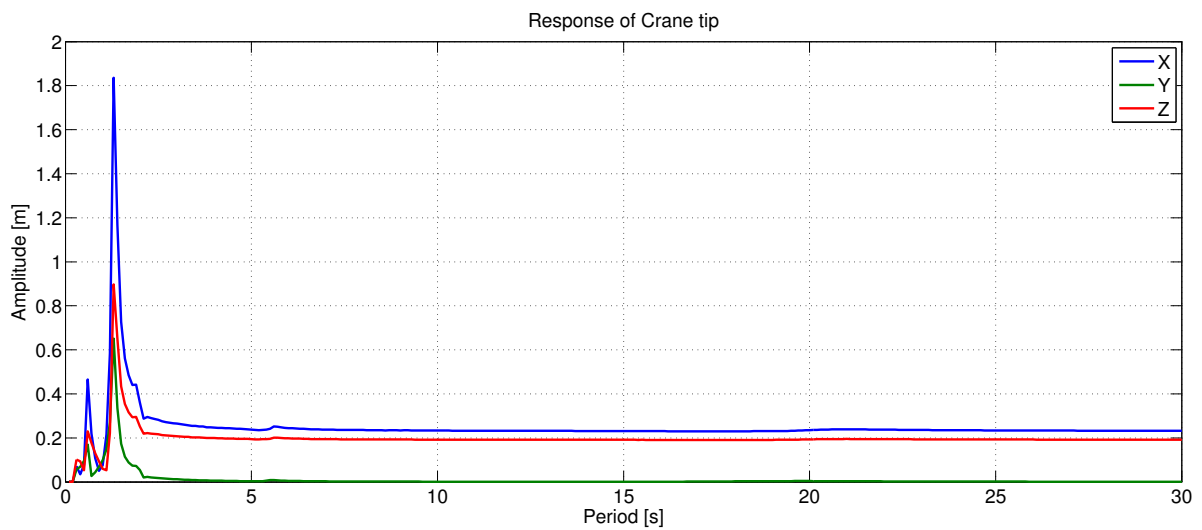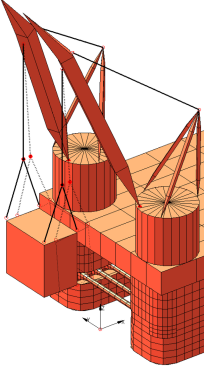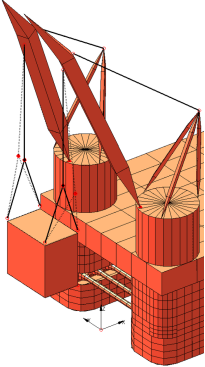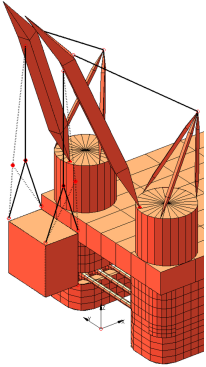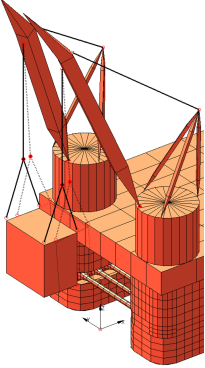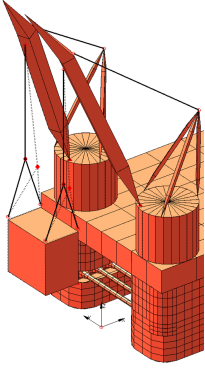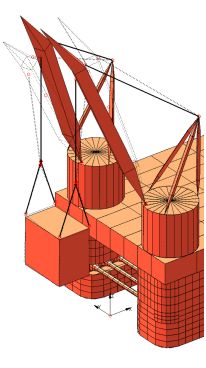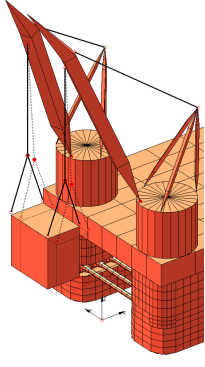
Figure L.9: Crane tip response force due to sinusoidal pitch motion

L.4. NATURAL MODES

Table L.1: Natural periods

Natural period	Mode	Natural period	Mode	Natural period	Mode
25.4 s		5.5 s		1.2 s	
19.4 s		2.9 s		0.7 s	
18.3 s		2.8 s		0.6 s	
16.2 s		2.0 s		0.6 s	